

Propositions

Associated with the dissertation **Studies on the Flow Induced by an Oscillating Airfoil in a Uniform Flow**, by Zeguang Wang

1). The 'memory effect' of shed vortices in the wake of an oscillating airfoil should be $1-C(k)$, instead of $C(k)$ as stated in Ashley and Landahl's book *Aerodynamics of Wings and Bodies*. Here, k is the reduced frequency, and $C(k)$ Theodorsen's function.

2). It can be shown rigorously that Maskell's conjecture on the flow at the trailing edge of a moving airfoil with variable circulation yields a continuous pressure at the vortex wake line. The flow then leaves the airfoil tangentially to either the upper- or the lower-surface, while the free vorticity at the trailing edge has a non-zero finite velocity.

[Basu & Hancock, 1978, *JFM*. Vol. 87, Pt. 1, pp. 159-178.]

3a). A flow which satisfies the Kutta-Joukowski condition evolves from a strong viscous-inviscid interaction, though in an established steady state weak and mild interactions take place.

3b). Without viscosity of the air, modern flight would not be possible.

4). The correctness of the solution to a (boundary value) problem depends on the correctness of modelling in the field, and on correctly posed boundary conditions. In this sense, D'Alembert's paradox and the Kutta-Joukowski condition suggest the same thing, though they end up quite differently.

5). A singularity is an important tool in mathematics. But in the field of continuum mechanics, singularities are difficult to accept. To resolve a mathematical singularity in continuum mechanics requires either a certain magnification with a proper scale, or formulation of a realistic physical hypothesis.

6). Programming is not too much of a difficulty, iff the programmer knows precisely what he wants to do.

7). Hot-wire technique for velocity measurement may be a derivative of the Dutch *natte vinger* method.

8). 'No one believes the analytical results (except for the modeller), and everyone believes the test data (except for the experimentalist)' [MSC/NASTRAN Dynamic Seminar Notes, London, 1993]. This is a legitimate complaint.

9). Human behaviour generally tends to be viscous.

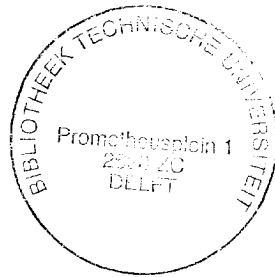
**TR diss
2343**

Studies on the Flow Induced by an Oscillating Airfoil in a Uniform Stream

Studies on the Flow Induced by an Oscillating Airfoil in a Uniform Stream

PROEFSCHRIFT

Ter verkrijging van de graad van doctor
aan de Technische Universiteit Delft,
op gezag van de Rector Magnificus,
prof. ir. K.F. Wakker,
in het openbaar te verdedigen
ten overstaan van een commissie
aangewezen door het College van Dekanen
op dinsdag 8 maart 1994 te 16.00 uur



door

Zeguang Wang

civiel ingenieur
geboren te Penlai, Shandong, China

Delft University Press/1994

Dit proefschrift is goedgekeurd door de promotor:
prof. dr.ir. J.A. Steketee
Toegevoegd promotor: dr.ir. R. Coene

Published and distributed by:

Delft University Press
Stevinweg 1
2628 CN Delft
The Netherlands

Telephone +31 15 783254
Fax +31 15 781661

ISBN 90-6275-963-7 / CIP

Copyright © 1994 by Z.Wang

All rights reserved.

No part of the material protected by this copyright notice may be reproduced or utilized in any form or by any means, electronic or mechanical, including photocopying, recording or by any information storage and retrieval system, without permission from the publisher: Delft University Press, Stevinweg 1, 2628 CN Delft, The Netherlands.

Printed in The Netherlands

*To:
my wife Gui Lai,
my parents,
and my grandmother.*

Table of Contents

Chapter 1. Introduction	1
1.1 The Classical Unsteady Airfoil Theory	1
1.2 Statement of the Problem	4
1.3 Plan of the Present Thesis	5
Chapter 2. Two-dimensional Potential Flow Around Oscillating Airfoils	7
2.1 Introduction	7
2.2 Statement of the Problem	9
2.3 The Governing Equation and the Determinant Conditions	10
2.3.1 The Governing Equation	10
2.3.2 The Boundary Conditions	11
2.3.3 The Kutta-Joukowski Condition	14
2.3.4 The Conservation of Circulation	15
2.4 Thin Airfoil Oscillating in a Uniform Flow	18
2.4.1 The Non-circulatory Solution	18
2.4.2 The Circulatory Solution	22
2.5 The Kutta-Joukowski Condition	29
2.6 Discussion	31
Chapter 3. The Unsteady Flow Around an Airfoil in a Real Fluid	33
3.1 Introduction	33
3.2 The Scales	36
3.3 The Boundary Layer and the Wake	39
3.4 The Triple-deck Structure	42
3.5 The Kutta-Joukowski Condition	49
3.6 Turbulent Boundary Layer and the Near Wake	52
3.7 Discussion	54

Chapter 4. The Experimental Studies	56
4.1 Introduction	56
4.2 The Experiment	61
4.3 The Study of the Near Wake for an Airfoil at Zero Angle of Incidence	65
4.4 Experimental Study of the Periodic Flows	73
4.4.1 Calibration of the Motion of the Airfoil	74
4.4.2 The Spectra of the Signals	78
4.4.3 The First Harmonic Velocity Perturbation	80
4.5 The Viscous Effect on Vorticity Convection	85
4.5.1 Some Consideration of the Flow Conditions	86
4.5.2 The Viscous Effect on Vorticity Convection	87
4.5.2.1 The difference in the Perturbation Behaviour at Larger Distance from the Trailing Edge	94
4.5.2.2 The Difference in the Position Where the Minima Occur	95
4.5.2.3 The Difference in the Depth of the Dip	96
4.6 Concluding Remarks	101
Chapter 5. Numerical Studies	103
5.1 Introduction	103
5.2 The Panel Method	105
5.3 The Governing Equations and the Discretization	108
5.3.1 The Governing Equations	108
5.3.1.1 The Boundary Conditions	108
5.3.1.2 The Conservation of Circulation	109
5.3.1.3 The Kutta-Joukowsky Condition	110
5.3.1.4 The Integration	113
5.3.2 The Discretization	115
5.3.2.1 The Panels	115
5.3.2.2 The Process	116

5.3.2.3	The Distribution of Vorticity	117
5.3.2.4	The Discretization of the Governing Equations	117
5.3.2.5	The Numerical Calculations	119
5.4	Results and Discussion	121
5.4.1	The 3/4 Chord Point	121
5.4.2	The Bound Circulation and the Related Force	124
5.4.3	The Distribution of Bound Vorticity	129
5.4.4	The Velocity Perturbation in Space	136
5.4.5	Modification due to Retardation in Vorticity Convection	139
5.5	Concluding Remarks	145
Chapter 6.	Summary and Conclusions	148
6.1	Conclusions	150
6.2	Recommendations	152
Appendix A.		154
A.1	The Velocity Components on the Boundaries in the Two Planes	154
A.2	Tangential Velocity Component on the Circle due to the Source-Sink Distribution	155
A.3	Tangential Velocity Component on the Circle due to a Vortex Pair	157
Appendix B.	Derivation of the Vorticity Equation	159
Appendix C.	Design of the Airfoil	161
Appendix D.	The Mean Velocity in an Unsteady Wake	164
Appendix E.	Green's Identity	166
Appendix F.	Induced Velocity at a Collocation Point due to the Vortex Elements	169
F.1	Normal Perturbation Velocity Component due to the Singular Distribution of the Bound Vorticity	169

F.2	Normal Perturbation Velocity Component due to the Linear Distribution of the Bound Vorticity on a Panel	170
F.3	Normal Perturbation Velocity Component due to a Wake Vortex Element	171
Appendix G.	The Perturbation Velocity in Space	172
G.1	Induced x-wise Velocity Component due to the Singular Vorticity Distribution $\gamma = A/x^{1/2}$	173
G.2	Induced x-wise Velocity Component due to Linear Bound Vorticity Distribution on a Panel	175
G.3	Induced x-wise Velocity Component due to Shed Vorticity Distribution	176
List of Major Symbols		178
Bibliography		180
Abstract		183
Samenvatting		184
Acknowledgements		185
Curriculum Vitae		186

Chapter 1

Introduction

Wings are essential for the flight of an aircraft. They produce the lift to keep the aircraft in the air. Naturally, many studies have been directed at the theory of wings. In the present study, we are dealing with a case where the flight speed is substantially lower than the speed of sound, so that the air can be regarded as incompressible. In agreement with daily experience, we consider the air to be inviscid except in the regions of boundary layers and wake. The flow in the inviscid region is considered to be irrotational. We shall concentrate here on two-dimensional wings (airfoil), i.e. the spanwise dimension of the wing is very large with respect to the dimension in the chordwise direction.

The lift force arises from the circulation bound to the airfoil. The bound circulation is there because otherwise there would be a singularity in the flow velocity at the trailing edge of the airfoil, which is physically unacceptable. To eliminate this difficulty a circulation of proper magnitude and sign is imposed such that the flow leaves the trailing edge smoothly, as observed in experiments (Prandtl and Tietjens [27]). The smooth off-flow requirement is referred to as the Kutta-Joukowski condition.

1.1 The Classical Unsteady Airfoil Theory

Airplanes do not always fly smoothly. Sometimes they encounter gusts, at other times the wings may oscillate. In all these cases the angle of attack changes continuously. This gives rise to the unsteady airfoil problem. Theodorsen and other researchers studied these problems in the 1930's. Corresponding theories were developed. In view of the historical importance we call it the classical theory.

Within the scope of the present study we consider the problem in Theodorsen's formulation—an airfoil performing small amplitude oscillations of a certain kind in a steady uniform flow. The oscillation can be assumed to be harmonic without loss of generality, thanks to the superposition principle and the Fourier transformation.

In the same way as in the steady airfoil problem, the Kutta-Joukowski condition has to be met at each moment of the unsteady motion. Consequently, a continuous change of bound circulation takes place. In view of the law of conservation of total circulation in the whole flow field, corresponding to the change of bound circulation counter vortices must be continuously shed into the wake.

In potential theory the wake is usually considered to be of zero thickness. It represents a vortex sheet across which the tangential velocity component is discontinuous. The local strength of the vortex sheet (circulation per unit length) is equal to the velocity discontinuity.

In the case of two-dimensional flow without viscosity, conservation of circulation is conceived with material fluid particles, i.e. vortices moving with the local velocity of the flow. In the classical airfoil theory which is within the framework of potential flow, the shed vortices move with the uniform flow velocity[†]. Therefore, when the airfoil is performing a harmonic motion, a sinusoidal distribution of shed vorticity would be found in the wake. Clearly, in this context, the wave length is $\lambda = U_0 T$, where U_0 is the uniform flow velocity and T is the period of the oscillation of the airfoil. In unsteady airfoil theory the wave structure is represented with a dimensionless parameter, the reduced frequency, defined as $k = \omega c / 2U_0$, where c is the chord length of the airfoil and ω the angular frequency of the oscillation.

[†] If otherwise, the vortex sheet would be subject to a non-zero pressure difference across it. Being with zero mass per unit length, which is implied by its zero thickness, the vortex sheet would be set into an infinite acceleration in the lateral direction which is physically unacceptable.

The influence of the shed vortices may not be neglected since they will induce a perturbation velocity to the flow field at the airfoil (the upwash field) so that the angle of incidence of the airfoil is modified (Steketee [30]). The influence of a shed vortex in the wake upon the up-wash field depends on its relative position with respect to the airfoil—in the two-dimensional case the influence is inversely proportional to the distance. In view of the fact that shed vortices are not convected away to infinity in negligible time, so that it is clear that in the due course of their being carried away, they keep perturbing the flow field. Focusing at an individual shed vortex, it would be seen that the influence becomes weaker and weaker. As a whole, the perturbation is a sum of the contribution of all the vortices in the wake. In view of their phase differences, the extent of the influence on the up-wash field depends on the wave structure. In some of the cases it can amount to 50 % in terms of the lift force (Theodorsen [34]). The influence of the shed vortices in the wake constitutes one of the major features of the unsteady airfoil problem.

One of the important applications of unsteady airfoil theory concerns the stability of the structures that undergo vibrations in a stream. The stability problem of a vibration arises because in some cases when the oscillatory motion and the reaction of the air stream are in phase, the forcing from the flow does positive work on the structure such that there is a net energy input to the structural vibration. The vibration will then be divergent. In fact, Greidanus [16] has performed such calculations for a combined small amplitude rotational and translational oscillation of a rigid airfoil. Taking account of the influence of the shed vorticity and omitting the structural damping, he was able to find that unfavourable combination of amplitude ratio and phase difference of the two would result in divergent oscillation of the airfoil.

Besides the flutter of airfoils in the aeronautical field, suspension bridges subject to lateral wind, pipelines in a cross stream are good examples of this type of problem in civil engineering (Fung [13]). Though the vortex shedding in these cases is not determined by the Kutta-Joukowski condition, the wake vortices exert their influence in a similar way.

1.2 Statement of the Problem

The classical unsteady airfoil theory reveals the essential mechanisms of the flow accompanying the unsteady motion of an airfoil. Within the framework of potential flow the solution is consistent.

However, flights take place in an actual flow, where the fluid has a certain viscosity. For the practical interest of airfoil theory, the flow is of high Reynolds' number. In this circumstance, the flow field can be distinguished into two parts. In the major part of the field the flow is effectively inviscid as described in the potential flow. In the other part, i.e. the boundary layer and the wake, however, the flow is viscous. The lateral dimension of the viscous regions is small with respect to that in the streamwise direction. The flow in the viscous region is characterized by a velocity defect (with respect to the flow outside). Also, vorticity, both bound on the surface and shed in the wake, is contained in these viscous regions.

In view of what is described above, the classical treatment of the problem gives rise to an inconsistency. Recognizing the fact that free vortices have to move with the local flow velocity, we would expect that the convection of the shed vorticity in an actual flow is retarded with respect to what is assumed in the classical theory because of the velocity defect in the wake. Consistent with the viscous flow theory, we would expect that the convection velocity of the shed vorticity would be small near the trailing edge of the airfoil. As the distance from the trailing edge is increased the convection velocity develops, approaching the value of the outer flow velocity asymptotically.

In a way similar to the boundary layer theory, the local interaction theory, established by Stewartson [31,32] and others, studies the case where streamwise change of the flow condition happens in a singularly fast rate. Flow near the trailing edge falls in this category. Boundary layer flow from upstream is constrained by the solid surface. Upon leaving the wall the constraint is suddenly released, which gives a large acceleration of the flow in the streamwise direction. In such a case the usual assumption adopted in

boundary layer theory (which states that large gradients occur only in the normal direction but not in the streamwise direction) is not true. The abrupt change of the boundary condition induces the flow to have a kind of layered structure in the neighbourhood of the trailing edge. After Stewartson, this structure is named the *triple deck*, since according to the physical property of the flow the structure can be distinguished into three layers. These layers extend into the near wake where convection of shed vorticity takes place. In view of this we expect that the convection of the shed vorticity in the near wake would also be conceived in a layered structure. With regard to the important role the shed vortices play in unsteady airfoil theory, the investigation of shed vorticity convection is one of the chief interests in the present study.

The study in the classical theory is mainly for the concern of aeroelasticity. The results are presented in terms of aerodynamic loadings, such as lift force and moment. The kinematics of the flow, however, is not discussed explicitly in the literatures. Therefore, in the present study we shall focus on this aspect. The other reason why we emphasize the study of the kinematics of the flow is because we approach the investigation of the shed vorticity convection from this point of view.

1.3 Plan of the Present Thesis

The thesis is organized in the following way. In chapter 2 a review of the classical unsteady airfoil theory is given. In this theory the airfoil is assumed to be thin and rigid. It performs a certain kind of small amplitude oscillation in an uniform flow. This review is aimed at clarifying the physical background of the theory. To this end, the problem is studied in terms of the velocity potential, rather than by the method of acceleration potential which provides another way of approach (Fung [13]). This review serves as a theoretical basis for the numerical calculation in the later chapters. A survey of viscous flow structure is presented in chapter 3. Through this, we put forward the hypothesis that convection of shed vorticity is actually retarded, and further speculate

that the convection is likely to be conceived in a kind of layered structure. Experimental studies are described in chapter 4. The experimental study consists of two parts, namely, experimental measurements and numerical calculations based on a panel method which is discussed in detail in chapter 5. The outcome of the numerical calculation serves as a reference in the interpretation of the experimental results. Chapter 4 accounts for the study of a steady near wake, and the unsteady velocity perturbations in the outer flow due to the shed vortices in the viscous wake. In chapter 5 numerical studies based on a panel method are presented. Convection of shed vorticity in the numerical models is assumed to be of two forms, namely, no retardation and retarded convection at the centerline velocity of a wake. This chapter is directed at two objectives, namely, the study of the flow kinematics and an elucidation of the numerical calculation employed in chapter 4. Conclusions are summarized in chapter 6.

Chapter 2

Two-dimensional Potential Flow Around Oscillating Airfoils

2.1 Introduction

In this chapter the classical linearized potential flow formulation is presented for cases with small amplitude harmonic oscillations of an airfoil. The objective here is to obtain some physical insight of the problem. This is essential for the experimental study and the numerical modelling to be presented in chapters 4 and 5. In doing so, we make the assumption that the fluid is inviscid and incompressible. A motion of the fluid of this nature is completely described by the conservation of mass and momentum. In view of the small density of air, in which the motion of airfoils takes place, the gravity effect will be neglected.

Assuming a coordinate system $\mathbf{x}=\mathbf{x}(x,y,z)$ fixed in space, the conservation of mass can be expressed with the following equation

$$\frac{\partial \rho}{\partial t} + \nabla \cdot (\rho \mathbf{v}) = 0, \quad (2.1)$$

where ρ is the density of the fluid, $\mathbf{v}=\mathbf{v}(\mathbf{x},t)$ is the flow velocity at point \mathbf{x} and time t . For an incompressible fluid the density is a constant, so that equation (2.1) can be reduced to

$$\nabla \cdot \mathbf{v} = 0. \quad (2.2)$$

The equation for the momentum relates the rate of change of momentum of a fluid element to the sum of all the forces acting on it. With the assumptions we have made, it can be written

$$\frac{\partial \mathbf{v}}{\partial t} + (\mathbf{v} \cdot \nabla) \mathbf{v} = -\frac{1}{\rho} \nabla p, \quad (2.3)$$

Vorticity of the fluid is defined as $\boldsymbol{\omega} = \text{curl } \mathbf{v}$. By Stokes's theorem we have the relation

$$\begin{aligned} \Gamma &= \oint_c \mathbf{v} \cdot d\mathbf{x} \\ &= \int_A (\nabla \times \mathbf{v}) \cdot \mathbf{n} dA, \end{aligned} \quad (2.4)$$

where c is a simple, closed curve in the fluid, spanned by a surface A with unit normal \mathbf{n} . In equation (2.4), Γ is the circulation round c , positive clockwise. The circulation is equal to the strength of $\boldsymbol{\omega}$ over a surface bounded by c . Here we define the circulation yielded by integrating along a circuit that encloses an airfoil as the bound circulation. The bound circulation represents the strength of the vortices bound to the airfoil. So that the circuit has to be chosen such that it does not enclose the free vortices.

Kelvin's theorem, or the law of conservation of circulation, states that for an inviscid, barotropic flow (which is applicable in our case), the circulation round a material circuit moving with the fluid does not change with time. Based on this, it is further stated in Landau and Lifshitz [18] that if $\boldsymbol{\omega} = 0$ at any arbitrary point on a certain streamline, then $\boldsymbol{\omega} = 0$ at all the points on that streamline. It is to be noticed that this statement is not true for streamlines in contact with a solid body. A uniform flow is irrotational. We know, therefore, that when it streams past a solid body, $\boldsymbol{\omega}$ keeps to be zero on all the streamlines except the ones in contact with the body surface.

If $\text{curl } \mathbf{v} = 0$ everywhere in a flow, the flow is said to be irrotational. For irrotational flow a velocity potential ϕ can be defined by

$$\phi = \int_O^P \mathbf{v} \cdot d\mathbf{x}, \quad (2.5)$$

where O is an arbitrary fixed point, and P is the point at which the potential is to be determined. Partial differentiation of equation (2.5) gives

$$\mathbf{v} = \nabla\phi. \quad (2.6)$$

In fact, the vector identity $\text{curl grad } \phi = 0$ implies that a potential flow is necessarily irrotational.

Taking the curl of equation (2.3), with some vector manipulation on the term $(\mathbf{v} \cdot \nabla)\mathbf{v}$, it is found that the equation for conservation of momentum is satisfied automatically by irrotational flow. To satisfy the conservation of mass, we substitute equation (2.6) into equation (2.2). This gives the Laplace equation for the velocity potential

$$\nabla^2\phi = 0. \quad (2.7)$$

Using equation (2.6) it follows that the (x,y,z) velocity components also satisfy the Laplace equation.

2.2 Statement of the Problem

Throughout this thesis, we are dealing with two-dimensional airfoil problems. When not specially mentioned, the discussions will be limited to the two-dimensional case. Consider a thin, symmetric, rigid airfoil of chord $c=2b$, with its mid-chord point at the origin of a set of Cartesian coordinates (x,y) . The x -axis is parallel to the uniform flow at infinity, and points in the direction of the flow. The velocity of the uniform flow is U_0 . The airfoil, with its mean position on the x -axis at $[-b,b]$, is performing a small

amplitude simple harmonic oscillation at not too high frequency[†] in the direction perpendicular to the uniform flow (figure 2.1). We are to study the reaction of the flow to the unsteady motion of the airfoil described above.

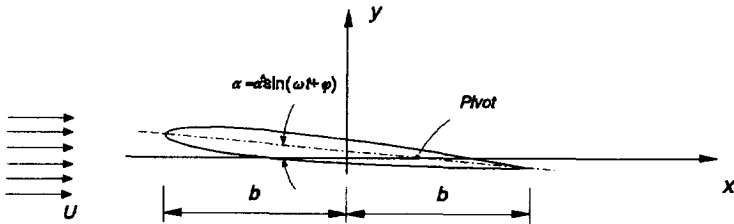


Figure 2.1 A thin symmetrical airfoil undergoing small amplitude oscillation and the coordinate system.

2.3 The Governing Equation and the Determinant Conditions

2.3.1 The Governing Equation

As mentioned in the introduction, the potential flow problem is governed by the Laplace equation. In the two-dimensional case this reads

$$\frac{\partial^2 \phi}{\partial x^2} + \frac{\partial^2 \phi}{\partial y^2} = 0. \quad (2.8)$$

In this circumstance, the problem can be represented with a complex potential

$$w(z) = \phi + i\psi, \quad (2.9)$$

where ψ is the stream function, $u = \partial\psi/\partial y = \partial\phi/\partial x$, $v = -\partial\psi/\partial x = \partial\phi/\partial y$; $i^2 = -1$; z is a complex number $z = x + iy$. Both ϕ and ψ in equation (2.9) satisfy the Laplace equation. Velocity components are related with the complex potential such that

[†] More precisely, the magnitude of the frequency is limited such that its product with the amplitude of the oscillation is small with respect to U_0 .

$$\frac{dw}{dz} = u - iv = \frac{\partial\phi}{\partial x} + i \frac{\partial\psi}{\partial x}. \quad (2.10)$$

For two-dimensional problems complex function theory is often used to construct solutions of flow past more complicated configurations in a physical plane (z -plane) from solutions at a simpler level in a mathematical plane (ζ -plane). The two planes are related with a certain mapping function. For our problem, the Joukowski transformation

$$z = \zeta + \frac{b^2}{4\zeta}, \quad (2.11)$$

will be used. It maps a circular cylinder of radius $b/2$ with center at the origin of the ζ -plane to a plate at $-b \leq x \leq b, y=0$ on the z -plane (figure 2.2).

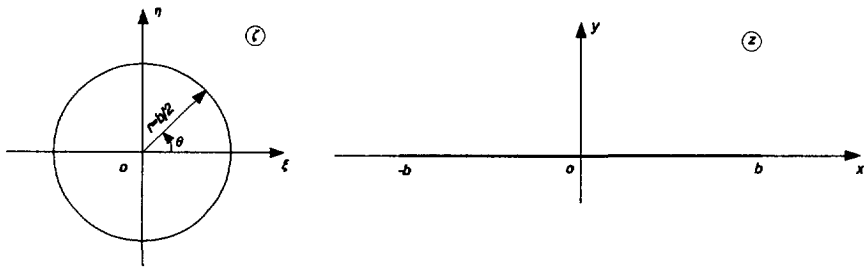


Figure 2.2 Transformation from a flat plate to a circle by $z = \zeta + b^2/4\zeta$.

2.3.2 The Boundary Conditions

In section 2.2 we have assumed that the airfoil is thin, the amplitude of the oscillation is small, and the frequency of the oscillation is not too high. The implication of these assumptions is that the dimension of the airfoil in the y -direction is small with respect to that in the x -direction which we assume of order of unity, and the magnitude of the perturbation velocity \mathbf{v} is small with respect to $U_0 \propto O(1)$. While this is generally true

over the major part of the airfoil, it is not quite so at the nose of the airfoil where dy/dx is not a small quantity. Fortunately, this violation is only very local. The properties mentioned above allow a series of linearizations which simplify the problem.

First of all, with these assumptions, the velocity perturbation \mathbf{v} due to the airfoil can be separated into two parts, namely, a symmetric and an anti-symmetric perturbation. The symmetric part, with

$$\mathbf{u}_1(x,y,t) = \mathbf{u}_1(x,-y,t), \quad \mathbf{v}_1(x,y,t) = -\mathbf{v}_1(x,-y,t), \quad (2.12)$$

is the perturbation due to the thickness of the airfoil. It has no direct consequence for the aerodynamic loadings, instead it gives rise to a potential wake as we shall see later. This is often referred to as the *thickness problem*.

The anti-symmetric part, with

$$\mathbf{u}_2(x,y,t) = -\mathbf{u}_2(x,-y,t), \quad \mathbf{v}_2(x,y,t) = \mathbf{v}_2(x,-y,t), \quad (2.13)$$

is the perturbation due to the anti-symmetry of the configuration with respect to the plane $y=0$. In the present case, where the airfoil is uncambered, the anti-symmetry is due to the angle of incidence of the airfoil. This part gives rise to the lift force and moment on the airfoil, and is referred to as the *lift problem*.

In equations (2.12) and (2.13) $\mathbf{v}_1 = i\mathbf{u}_1 + \mathbf{j}v_1$, $\mathbf{v}_2 = i\mathbf{u}_2 + \mathbf{j}v_2$ represent the symmetric and anti-symmetric part of the perturbation velocity respectively. The total perturbation is $\mathbf{v} = \mathbf{v}_1 + \mathbf{v}_2$. For detailed derivation in this respect the reader is referred to Steketee [30].

Since only the lift problem has a direct consequence on the aerodynamic loadings, we shall concentrate on this part. In what follows, we replace the thin, symmetric airfoil with a flat plate.

The boundary condition for a flow past an impermeable solid body requires that on the surface of the body the normal component of the flow velocity with respect to the

surface must be zero. This is sometimes referred to as the *flow-tangency condition*. Let the flat plate be described by $Y = Y(x, t)$, we define a quantity $F(x, y, t) = y - Y(x, t)$. It has to remain zero for any particular fluid particle in contact with the surface. It follows that the material time derivative of F (DF/Dt) is equal to zero

$$\frac{\partial F}{\partial t} + (\mathbf{V} \cdot \nabla) F = 0, \quad \text{on } -b \leq x \leq b, y = Y(x, t) \quad (F=0, \text{ equivalently}). \quad (2.14)$$

where $\mathbf{V} = iU_0 + \mathbf{v}$ is the flow velocity. On the argument that the oscillation is of small amplitude, equation (2.14) can approximately be written on $-b \leq x \leq b, y=0$, if we expand it in a Taylor series at $y=0$ and neglect the quadratic and higher order terms of Y .

Recognizing that

$$\frac{\partial F}{\partial t} = -\frac{\partial Y}{\partial t}, \quad (U_0 + u) \frac{\partial F}{\partial x} = -(U_0 + u) \frac{\partial Y}{\partial x}, \quad (2.15)$$

and the term $u \partial F / \partial x$ is small by an order with respect to $U_0 \partial F / \partial x$, on the assumptions made above ($u \ll U_0$), the boundary condition can be written

$$v_b = \frac{\partial Y}{\partial t} + U_0 \frac{\partial Y}{\partial x}, \quad \text{on } -b \leq x \leq b, y=0. \quad (2.16)$$

With v_b we denote the velocity of fluid particles in contact with the solid surface. Here, the linearization is applied the second time.

As usual, we require that the perturbation velocity \mathbf{v} vanishes at infinity, except in the neighbourhood of the wake.

2.3.3 The Kutta-Joukowski Condition

Consider the plate at $-b \leq x \leq b$, $y=0$, on the z -plane. A uniform flow with complex potential $U_0 z e^{-i\alpha}$ at infinity streams past it. Here, α is the angle that the uniform flow makes with the x -axis. In the far field, this is equivalent to a uniform flow with potential $U_0 \zeta e^{-i\alpha}$ at infinity past a circle of radius $b/2$ at the origin of the ζ -plane, since from equation (2.11) it is clear that $\zeta=z$ at infinity. The solution of this problem in the ζ -plane is (Steketee [30])

$$w(\zeta) = U_0 \left(\zeta e^{-i\alpha} + \frac{a^2}{\zeta} e^{i\alpha} \right) + \frac{i\Gamma}{2\pi} \ln \zeta + \frac{\Gamma\alpha}{2\pi}, \quad (2.17)$$

i.e. a superposition of the uniform flow, a doublet of strength $2\pi U_0 a^2$ at the origin[†], and a circulation of strength Γ around the circle (the bound circulation). The term $\Gamma\alpha/2\pi$, being a constant is of no importance here. The velocity field can be calculated with equation (2.10)

$$\begin{aligned} u - iv &= \frac{dw}{d\zeta} \frac{d\zeta}{dz} \\ &= \left(U_0 e^{-i\alpha} + \frac{i\Gamma}{2\pi \zeta} - U_0 e^{i\alpha} \frac{b^2}{4\zeta^2} \right) \left(1 - \frac{b^2}{4\zeta^2} \right). \end{aligned} \quad (2.18)$$

We notice here that the value of the circulation is not unique. In fact, the circulatory flow has the circle as one of its streamlines. No matter what value it attains, it has no effect on the flow tangency condition on the circle, i.e. the normal component of velocity is not affected. Also, from equation (2.18) it appears that the flow velocity is singular at the leading and trailing edge. This is physically quite difficult. In reality, the rounded nose of an airfoil resolves the difficulty at the leading edge. For the infinite velocity at the trailing edge, we introduce the *Kutta-Joukowski condition* which requires that the flow leaves the trailing edge smoothly. Implementation of the Kutta-Joukowski condition implies that the circulation has to be chosen such that the numerator in

[†] The axis of the doublet is in the opposite direction with respect to the uniform flow.

equation (2.18) becomes zero at the trailing edge $\zeta=b/2$, hence $\Gamma=2\pi bU_0\sin\alpha$. The steady lift force is determined with the Kutta-Joukowski theorem

$$L=\rho U_0\Gamma=2\rho\pi bU_0^2\sin\alpha. \tag{2.19}$$

Some discussion about the nature of the Kutta-Joukowski condition will be given in section 2.6. Nevertheless, it seems to be pertinent to make the observation here that this condition is in fact a representation of the viscous nature of a real flow.

2.3.4 The Conservation of Circulation

In the unsteady motion of an airfoil, the Kutta-Joukowski condition has to be satisfied at every moment. Accordingly, the bound circulation varies with time. In view of the inviscid and incompressible nature of the fluid in question, the law of conservation of circulation is valid, i.e. the total circulation in the whole flow field has to be constant. As the bound circulation changes, there must be vorticity shed from the airfoil. The circulation of the shed vorticity is equal to the change of bound circulation in magnitude, but opposite in sign, such that the total circulation in the flow field is unaltered

$$\delta\Gamma_{shed}=-\frac{d\Gamma_{bound}}{dt}\delta t, \tag{2.20}$$

where δt is the time interval in which the shedding process is considered.

For the convenience of discussion, we call the streamline that emanates from the trailing edge a wake, though this is a term usually associated with the viscous flow. In the present context, the wake is seen as a sheet with infinitesimal thickness. We assume that the shed vortices are distributed on this sheet. The circulation of the distributed vortices per unit length along the wake is denoted with γ . Its dimension is $[L][T]^{-1}$. We notice that γ is different from ω in that the dimension of ω is $[T]^{-1}$.

Consider a point P which is a distance r away from a straight line vortex whose strength is Γ . From elementary fluid mechanics we know a velocity with magnitude $\Gamma/2\pi r$ will be induced at P. In the present case, we see the distributed vorticity in the wake $b \leq x < +\infty$ as an assembly of vortex elements $\gamma(x,t)dx^\dagger$. Collectively they induce on the airfoil a velocity

$$v(x,0,t) = \frac{1}{2\pi} \int_b^\infty \frac{\gamma(\xi,t)}{x-\xi} d\xi, \quad -b \leq x \leq b, \quad (2.21)$$

in the y -direction. The flow field in the neighbourhood of the airfoil is thus affected by the vortices in the wake. In fact, it is for this reason that in the unsteady airfoil problem the influence of the shed vorticity must be taken into consideration. The exception is the limiting case where the unsteadiness is very weak, the so called quasi-steady case where the wake influence can be neglected.

To evaluate the induced velocity written in equation (2.21), the distribution of the shed vortices has to be determined. In a two-dimensional inviscid flow, the vortex strength, γ (in the case of wake vortices $\gamma(x,t) = u(x,0^+,t) - u(x,0^-,t)$), is conserved by fluid elements, so that shed vorticity must move with fluid particles to which it is attached. In the classical theory, assuming small perturbations, the shed vorticity is assumed to be convected away from the airfoil with the constant main stream velocity U_0 . Observing at a point fixed in space one has then

$$\frac{\partial \gamma}{\partial t} + U_0 \frac{\partial \gamma}{\partial x} = 0, \quad (2.22)$$

or in integral form

[†] The length of the element depends on the velocity with which the shed vorticity is convected, $dx = U dt$. Considering the conservation of circulation it can be written for the shed vorticity at the trailing edge $U\gamma(b,t) = -d\Gamma_b/dt$, where the subscript b stands for *bound*.

$$\gamma = \gamma(x - U_0 t). \quad (2.23)$$

If, however, the convection velocity of the shed vorticity is, instead of constant, a function of the distance from the airfoil, $U = U(x)$, then the conservation assumes the following form

$$\frac{\partial \gamma}{\partial t} + \frac{\partial(U\gamma)}{\partial x} = 0. \quad (2.24)$$

Obviously, it reduces to equation (2.22) if $U(x) = U_0 = \text{const}$. In the classical theory equation (2.22) is used. In the present thesis equation (2.24) will be used to account for the variable convection speed $U(x)$ in the wake.

2.4 Thin Airfoil Oscillating in a Uniform Flow

In this section we are to treat the problem as posed in section 2.2, subjected to the conditions discussed in the last section. The thin airfoil is replaced with a flat plate described by $Y=Y(x,t)$, $-b \leq x \leq b$.

To elaborate the mechanism of the problem, we shall follow the conformal mapping method, constructing the solution with source and vorticity distributions. The source distribution will be used to meet the flow tangency condition on the surface, while the vorticity distribution is to satisfy the Kutta-Joukowski condition at the trailing edge. The far field condition that the perturbation velocity vanishes at infinity is automatically satisfied, since we know the perturbation velocity due to a source and/or vortex decays towards zero as the distance increases.

2.4.1 The Non-circulatory Solution.

In view of the anti-symmetric property (with respect to $y=0$) of the lift problem, a source and a sink distribution can be put on the two sides of the plate, or the two halves (upper and lower) of the circle in the ζ -plane. The distribution is anti-symmetric, i.e. $q(x,0^+,t)=-q(x,0^-,t)$. The dimension of q is $[L]^2[T]^{-1}$. It is shown in Milne-Thompson [24] that such a combination of source and sink implies that the circle itself is a streamline in the ζ -plane, i.e. for such a distribution, the normal velocity component at a boundary point depends only on the local singularity.

The singularity distribution can be determined by requiring that the normal velocity it induces on the boundary be equal to v_b calculated with equation (2.16). Consider a distribution of source on the upper surface of the plate, $q(x,0^+,t)$, $-b \leq x \leq b$. This distribution has a perturbation potential

$$\phi_s(x,y,t) = \frac{1}{2\pi} \int_{-b}^b q(\xi, 0^+, t) \ln \sqrt{(x-\xi)^2 + y^2} d\xi \quad (2.25)$$

in the flow field. Here, (ξ, η) are the coordinates of the source point, and (x, y) are the coordinates of a field point at which the perturbation potential is to be calculated.

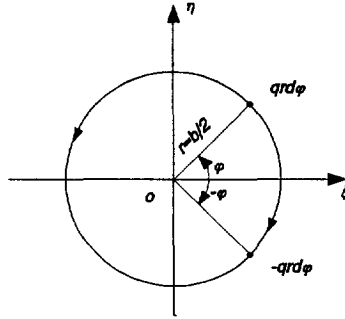


Figure 2.3 Equal strength source and sink at two mutually conjugate points have a circle as a streamline with the center at the origin.

The normal velocity component it induces near the upper surface can be calculated as follows.

$$\begin{aligned} v(x, 0^+, t) &= \lim_{y \rightarrow 0^+} \frac{\partial \phi_s}{\partial y} \\ &= \frac{1}{2\pi} \lim_{y \rightarrow 0^+} \frac{\partial}{\partial y} \int_{-b}^b q(\xi, 0^+, t) \ln \sqrt{(x-\xi)^2 + y^2} d\xi \\ &= \frac{1}{2\pi} \lim_{y \rightarrow 0^+} y \int_{-b}^b \frac{q(\xi, 0^+, t)}{(x-\xi)^2 + y^2} d\xi. \end{aligned} \quad (2.26)$$

In the limit $y \rightarrow 0^+$, the contribution of the integral is caused to vanish due to the multiplying factor, except at $\xi = x$ where the integrand is singular. By isolating this singular point with a short segment of length 2ϵ , centered at it, we have

$$v(x,0^+,t) = \frac{1}{2\pi} \lim_{y \rightarrow 0^+} y \int_{x-\varepsilon}^{x+\varepsilon} \frac{q(\xi,0^+,t)}{(x-\xi)^2 + y^2} d\xi. \quad (2.27)$$

Suppose the distribution is continuous, $|q(\xi,0^+,t) - q(x,0^+,t)|$ is $O(\varepsilon)$. Replacing $q(\xi,0^+,t)$ with $q(x,0^+,t)$, and using variable substitution $\xi' = x - \xi$, we have

$$\begin{aligned} v(x,0^+,t) &= \frac{q(x,0^+,t)}{2\pi} \lim_{y \rightarrow 0^+} y \int_{-\varepsilon}^{\varepsilon} \frac{d\xi'}{\xi'^2 + y^2} \\ &= \frac{q(x,0^+,t)}{2\pi} \lim_{y \rightarrow 0^+} [\tan^{-1}(\frac{\varepsilon}{y}) - \tan^{-1}(-\frac{\varepsilon}{y})] \\ &= \frac{1}{2} q(x,0^+,t), \end{aligned} \quad (2.28)$$

if the small quantity ε is fixed and y made approaching zero. Satisfying the boundary condition, we find the source distribution on the upper surface to be

$$q(x,0^+,t) = 2v_b(x,t). \quad (2.29)$$

In fact, this result is in agreement with what would be expected physically. The out-flux of the source distribution can only leave the sheet on its two sides. In the ζ -plane, half of the emission goes outside and the other half goes inside the circle. While in the z -plane, the exterior of the circle is mapped to fill the whole surface, and the interior is mapped into the second Riemannian surface. The slit $b \leq x \leq b, y=0$ is a cut in mathematical terms. So half of the source flux goes outward, the other half goes to the second of the two sheeted Riemannian surface. If the source distribution has a strength of q , then the normal velocity it induces at the boundary is $q/2$.

Similarly, for the sink distribution on the other surface of the plate we have $q(x,0^-,t) = -2v_b(x,t)$. In the ζ -plane, the source and sink distribution is

$$q(\frac{b}{2}, \varphi, t) = -q(\frac{b}{2}, -\varphi, t) = 4v_b \sin \varphi, \quad (2.30)$$

where $(b/2, \varphi)$ are the coordinates of the source point on the circle. The factor, 4, on

the right hand side of the equation is due to the stretching in the Joukowsky transformation (Appendix A.1).

With some trigonometrical operation (Appendix A.2), the tangential velocity at a point $(b/2, \theta)$ on the circle due to this distribution can easily be calculated

$$v_{\theta}\left(\frac{b}{2}, \theta\right) = \frac{2}{\pi} \int_0^{\pi} \frac{v_b \sin^2 \varphi d\varphi}{\cos \varphi - \cos \theta}. \quad (2.31)$$

The perturbation potential follows from

$$\phi - \phi_0 = \int_{x_0}^x \mathbf{v} \cdot d\mathbf{l}, \quad (2.32)$$

where ϕ_0 is a reference value. The path of integration does not have to be specified as long as it does not go through the circle, or the cut in the z -plane, since in a simply connected region, for an analytical function, it is not the route but the two ends that are relevant. Substituting equation (2.31) into equation (2.32), the perturbation potential on the circle surface can be determined. The pressure, p , on the surface can be calculated with the help of the linearized Bernoulli equation for unsteady flow (Steketee [30])

$$p - p_{\infty} = -\rho \left(U_0 \frac{\partial \phi}{\partial x} + \frac{\partial \phi}{\partial t} \right), \quad (2.33)$$

where p_{∞} is a constant ambient value. Integration of the pressure difference on the two sides of the plate yields the lift force

$$\begin{aligned} L_{nc} &= \int_{-b}^b (p_l - p_u) dx \\ &= 2\rho \frac{\partial}{\partial t} \int_{-b}^b \phi_u dx, \end{aligned} \quad (2.34)$$

where the subscript nc denotes the non-circulatory part of the lift, while l and u stand for lower and upper surface respectively. It is interesting to note that this part of the

lift depends solely on the unsteadiness of the motion of the plate which is assumed to be rigid. In fact this force arises from the acceleration of the fluid due to the time dependent motion of the plate. It is referred to as the *apparent mass* force. From the origin of this force, it is clear that it is proportional to the square of the frequency for an oscillatory motion. Similar conclusions also apply to the moment of the forces.

2.4.2 The Circulatory Solution

The non-circulatory solution derived in the last paragraph is generally incapable of satisfying the Kutta-Joukowski condition. To show this, we examine the tangential velocity, u , in the z -plane. From equation (A.3) it follows that

$$|u| = \frac{|v_\theta|}{|2\sin\theta|}, \quad (2.35)$$

on the plate. The denominator becomes zero at the trailing edge, which corresponds to $\theta=0, 2\pi$ in the ζ -plane. Hence, the velocity on the z -plane will generally have an infinite value at this point.

As we did in paragraph 2.3.3, a bound circulation with proper strength Γ_0^\dagger will be superimposed on the non-circulatory solution, equation (2.31), to make the numerator in equation (2.35) zero at $\theta=0, 2\pi$ in the final solution. Corresponding to the bound circulation Γ_0 , there must be a counter vortex of strength $-\Gamma_0$ in the wake so that the total circulation in the whole flow field is unchanged. The wake vortex is assumed to move with the uniform flow velocity U_0 along the x -axis in the z -plane. The positions of the bound and the wake vortex are resolved on the consideration that the flow-tangency condition satisfied with the source-sink distribution must not be violated by the superposition of the vortex pair, i.e. the plate (in the z -plane) and the circle (in the

[†] To facilitate the discussion, we consider in the first instance a discrete vortex, $-\Gamma_0$ in the wake. For continuous vortex shedding, this can be understood as a vortex element, with $\Gamma_0 = \gamma d\xi$.

ζ -plane) must be streamlines of the vortex flow. This requirement implies that corresponding to the wake vortex, the bound vortex is at the image position inside the circle (figure 2.4). For a circle with radius $b/2$, the distances of the two vortices from the center of the circle has the relation $\xi_b = b^2/4\xi_w$.

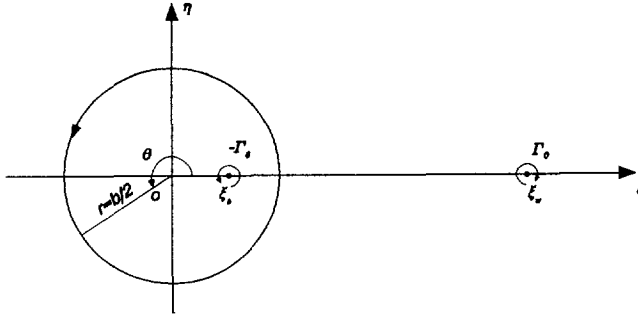


Figure 2.4 The relation of $\xi_b = b^2/4\xi_w$ implies the wake and the bound vortex have the circle of radius $b/2$ as one of their streamlines.

Differentiating this relation with respect to time, it emerges that as the wake vortex moves with velocity u_w away from the circle, the bound vorticity moves with velocity

$$u_b = -\frac{b^2}{4} \frac{1}{\zeta_w^2} u_w \quad (2.36)$$

towards the center.

Consider first the discrete vortex configuration as shown in figure 2.4. With some manipulation (Appendix A.3), the tangential velocity component on the circle due to the vortex pair can be written

$$v_\theta\left(\frac{b}{2}, \theta\right) = -\frac{\Gamma_0}{\pi b} \frac{\xi_w^2 - (b/2)^2}{\xi_w^2 + (b/2)^2 - \xi_w b \cos\theta}. \quad (2.37)$$

At $\theta=0$, i.e. the trailing edge in the z -plane, this is

$$v_{\theta}\left(\frac{b}{2}, 0\right) = -\frac{\Gamma_0}{\pi b} \frac{\xi_w + b/2}{\xi_w - b/2}. \quad (2.38)$$

The location of the wake vortex, ξ_w , is not arbitrary. It is related with the corresponding position on the x-axis in the z-plane through equation (2.11). Since the wake vortex is moving along the real axis, letting $\eta=0$ and $y=0$ in the Joukowski transformation, we have

$$x = \xi + \frac{b^2}{4\xi}, \quad y = 0. \quad (2.39)$$

This has an equivalent form

$$\sqrt{\frac{x+b}{x-b}} = \frac{\xi + b/2}{\xi - b/2}. \quad (2.40)$$

The perturbation potential on the surface can be calculated in the following way

$$\begin{aligned} \phi(\theta, t) &= -\int_{\theta}^{\pi} v_{\theta} \frac{b}{2} d\theta \\ &= \frac{\Gamma_0}{2\pi} \frac{(\xi^2 - (b/2)^2)^{\pi}}{\int_{\theta}^{\pi} \xi^2 + (b/2)^2 - \xi b \cos\theta} d\theta \\ &= \frac{\Gamma_0}{\pi} \arctan \left[\frac{\xi - b/2}{\xi + b/2} \sqrt{\frac{1 + \cos\theta}{1 - \cos\theta}} \right], \end{aligned} \quad (2.41)$$

in which it is assumed that the potential vanishes at the leading edge where $\theta = \pi$. In view of equation (2.40) this can be written

$$\phi = \frac{\Gamma_0}{\pi} \arctan \sqrt{\left[\frac{x-b}{x+b} \right] \left[\frac{1 + \cos\theta}{1 - \cos\theta} \right]}. \quad (2.42)$$

The pressure difference across the plate is

$$\begin{aligned}
p_u - p_l &= -2\rho \left[\frac{\partial\phi}{\partial t} - \frac{U_0}{b\sin\theta} \frac{\partial\phi}{\partial\theta} \right] \\
&= -2\rho \left[\frac{\partial\phi}{\partial x} \frac{dx}{dt} - \frac{U_0}{b\sin\theta} \frac{\partial\phi}{\partial\theta} \right] \\
&= -\frac{\rho U_0 \Gamma_0 (x + b\cos\theta)}{\pi b\sin\theta \sqrt{x^2 - b^2}}.
\end{aligned} \tag{2.43}$$

Concerning the continuous shedding of vortices, we replace Γ_0 in the above equations with $-\gamma dx$, and accounting for the accumulated effect of the shed vortices distributed along the whole wake. Therefore

$$\begin{aligned}
p_u - p_l &= \frac{\rho U_0}{\pi b\sin\theta} \int_b^\infty \frac{x + b\cos\theta}{\sqrt{x^2 - b^2}} \gamma(x, t) dx \\
&= \frac{\rho U_0}{\pi b\sin\theta} \int_b^\infty \left(\frac{x}{\sqrt{x^2 - b^2}} (1 - \cos\theta) + \sqrt{\frac{x+b}{x-b}} \cos\theta \right) \gamma(x, t) dx.
\end{aligned} \tag{2.44}$$

Superposing the non-circulatory flow (equation (2.31)) and the circulatory flow (integral form of equation (2.37)), we satisfy the Kutta-Joukowsky condition at $\theta=0$ with

$$\frac{2}{\pi} \int_0^\pi \frac{v_b \sin^2 \varphi d\varphi}{\cos\varphi - 1} + \frac{1}{\pi b} \int_b^\infty \sqrt{\frac{x+b}{x-b}} \gamma(x, t) dx = 0. \tag{2.45}$$

Once v_b is specified the first integral in the above equation can be calculated. Accordingly, γ can be determined from this integral equation. For convenience in further calculation, we introduce a factor Q , and rewrite equation (2.45) as follows.

$$\begin{aligned}
Q &= \frac{1}{\pi} \int_0^\pi \frac{v_b \sin^2 \phi d\phi}{\cos \phi - 1} \\
&= -\frac{1}{2\pi b} \int_b^\infty \sqrt{\frac{x+b}{x-b}} \gamma(x,t) dx.
\end{aligned} \tag{2.46}$$

Making use of this, equation (2.44) can be written

$$\begin{aligned}
p_u - p_l &= \frac{\rho U_0}{\pi b \sin \theta} \int_b^\infty \left(\frac{x}{\sqrt{x^2 - b^2}} (1 - \cos \theta) + \sqrt{\frac{x+b}{x-b}} \cos \theta \right) \gamma(x,t) dx \\
&= -2\rho U_0 Q \left(\cot \theta + \frac{1 - \cos \theta}{\sin \theta} \frac{\int_b^\infty \frac{x}{\sqrt{x^2 - b^2}} \gamma(x,t) dx}{\int_b^\infty \sqrt{\frac{x+b}{x-b}} \gamma(x,t) dx} \right).
\end{aligned} \tag{2.47}$$

The ratio of the two integral represents the effect of the wake vortices. It also appears in the calculations of force and moment.

Now, we restrict the motion of the airfoil to be simple harmonic,

$$v_b = \hat{v}(x) e^{i\omega t}, \quad -b \leq x \leq b. \tag{2.48}$$

We assume that the oscillation has gone on for an infinitely long period, so that a stationary state has been reached. In such a way, the strength of the shed vorticity in the wake varies also harmonically. In view of equation (2.23), it shows a wave pattern

$$\gamma(x,t) = \hat{\gamma} e^{i(\omega t - kx^*)}, \tag{2.49}$$

where $k = \omega b / U_0$ is the *reduced frequency*, and $x^* = x/b$ is a dimensionless distance. Recognizing that ω / U_0 is inversely proportional to the vortex wave length, we understand that the reduced frequency in fact represents the wave structure.

Observing equation (2.49), the ratio in equation (2.47) can further be calculated

$$\begin{aligned}
 C(k) &= \frac{\int_b^\infty \frac{x}{\sqrt{x^2-b^2}} \gamma dx}{\int_b^\infty \sqrt{\frac{x+b}{x-b}} \gamma dx} \\
 &= \frac{\hat{\gamma} e^{i\omega t} b \int_1^\infty \frac{x^*}{\sqrt{x^{*2}-1}} e^{-ikx^*} dx^*}{\hat{\gamma} e^{i\omega t} b \int_1^\infty \sqrt{\frac{x^*+1}{x^*-1}} e^{-ikx^*} dx^*} \\
 &= \frac{\int_1^\infty \frac{x^*}{\sqrt{x^{*2}-1}} e^{-ikx^*} dx^*}{\int_1^\infty \sqrt{\frac{x^*+1}{x^*-1}} e^{-ikx^*} dx^*}, \tag{2.50}
 \end{aligned}$$

which is a complex function of the reduced frequency only. Theodorsen identified the integral in the last line of equation (2.50) as Hankel functions of the second kind, and wrote

$$C(k) = F(k) + iG(k) = \frac{H_1^{(2)}(k)}{H_1^{(2)}(k) + iH_0^{(2)}(k)}. \tag{2.51}$$

This function is called the *Theodorsen's function*. Figure 2.5 shows a plot of this function in a polar coordinate system.

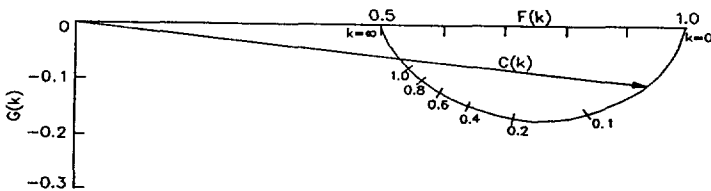


Figure 2.5 The Theodorsen's function plotted in a polar coordinate system.

The force on an oscillating airfoil therefore consists of two parts, namely, a non-circulation related force, as expressed with equation (2.34), and a circulation related force. Integration of equation (2.47) shows that the circulation related force is proportional to Theodorsen's function $C(k)$ (Bisplinghoff, Ashley & Halfman [4])

$$L_c = 2\pi\rho U_0 b Q C(k). \quad (2.52)$$

Comparing equations (2.52) with (2.19) we see that the circulation related lift force has essentially the same structure as the steady lift. In both cases, it is the upwash at the 3/4 chord point from the leading edge that determines the force (in the steady case this is $U_0 \sin\alpha$ uniformly over the chord), as we shall see below.

Consider a composite motion of heaving and pitching about the mid-chord point of the airfoil. The velocity on the plate can be written

$$\begin{aligned} v_b &= \dot{h} + U_0 \alpha + \dot{\alpha} x \\ &= \dot{h} + U_0 \alpha + \dot{\alpha} b \cos\phi, \end{aligned} \quad (2.53)$$

where the dots designate differentiation with respect to time.

Substitution of equation (2.53) into the first line of equation (2.46) yields

$$Q = \dot{h} + U_0 \alpha + \frac{b}{2} \dot{\alpha}, \quad (2.54)$$

which is the upwash at the 3/4 chord point from the leading edge. Referring to equation (2.52) we see that in fact it is the modified upwash that determines the circulation related force in the unsteady case—the "natural" upwash, Q , is modified by the perturbation of wake vortices in terms of $C(k)$. In some circumstances the influence of the wake vorticity is referred to as the *memory effect*.

The memory effect can be appreciated by considering two limiting cases. Referring to figure 2.5, we see that at very low reduced frequency, i.e. $k \rightarrow 0$, the value of the

Theodorsen's function approaches unity, implying that the wake vortices' modification to the upwash is negligible. Physically, this is because in the very slow oscillation of the plate, there is time ($\propto 1/\omega$) long enough for the shed vortices to be transported (with velocity U_0) far away from the plate, in comparison with its chord c . As a matter of fact, in such a circumstance the quasi-steady argument is valid, which assumes that the shed vortices are swept to infinity instantly, so that the lift on the plate is solely determined by the (equivalent) angle of incidence $\alpha + h_t/U_0 + \alpha_t b/2U_0$.

At very high reduced frequency, on the other hand, the vorticity wave length ($\propto U_0/\omega$) is very small with respect to the chord. Considering the phase shift of the vorticity element along the wake, it can be expected that the perturbation due to the wake vortices collectively would become constant. In fact, it is seen in figure 2.5 $C(k) \rightarrow 0.5$ as $k \rightarrow \infty$. From the two aspects discussed above, it can be concluded that the memory effect is $1-C(k)$.

2.5 The Kutta-Joukowski Condition

As mentioned in section 2.3, the Kutta-Joukowski condition represents the viscous nature of a real fluid in the terminology of potential flow. According to Prandtl and Tietjens [27], in experiment it can be observed that at the very initial phase when the airfoil is set into motion with small angle of incidence, the flow pattern is indeed as the one calculated without imposing the Kutta-Joukowski condition (e.g. $\Gamma=0$, in equation (2.18)). However, this state cannot last long. After some moments, a starting vortex is found to be shed, and the flow from the two sides of the airfoil joins smoothly at the trailing edge, indicating that the Kutta-Joukowski condition is satisfied. This state is stable until the motion is otherwise altered.

The condition results from the interaction between the outer potential flow and a thin layer of viscous flow (the boundary layer) around the airfoil in which the vorticity congregates. The interaction determines that, within restricted parameter ranges, only

those outer potential flows that satisfy a Kutta-Joukowski condition are compatible with an acceptable inner viscous structure (Crighton [11]). It seems appropriate to point out though in the stable motion, i.e. the Kutta-Joukowski condition is met, the viscous-inviscid interaction is mild (in the sense that the viscous region has only minor influence on the remainder of the flow through its thickness), the viscous flow at the trailing edge has nonetheless the strongest effect, since its existence changes the flow field completely. For motions of practical interest the thickness of the viscous layer is of higher order small with respect to the characteristic length in the potential flow, say, the chord length. So we shall leave the study of the viscous flow structure for the next chapter, since we can not see it presently with the potential flow scale.

For steady flow, satisfaction of the Kutta-Joukowski condition implies the establishment of a number of other facts.

- 1). The vorticity shedding vanishes. This statement is based on the consideration of conservation of circulation. When the steady state is reached, the bound circulation remains constant, so that there is no vorticity shedding. If we look microscopically, it appears that the circulation of the vortices carried from the boundary layers on the two sides of the plate is equal in magnitude but of opposite direction. Merging at the trailing edge they cancel each other.

This observation is equivalent to saying that the flow velocities on the two sides of the trailing edge are equal, which implies

- 2). The loading at the trailing edge is zero.

For steady potential flow Bernoulli's equation

$$p = p_{\infty} - \frac{1}{2} \rho V^2, \quad (2.55)$$

holds in the whole flow field. Designating with subscript u and l for

upper and lower surface respectively, the loading at a cusped trailing edge is

$$\begin{aligned} p_l - p_u &= \frac{1}{2} \rho (V_u^2 - V_l^2) \\ &= \rho U_0 (u_u - u_l) + O(u_u^2, u_l^2). \end{aligned} \quad (2.56)$$

If the vorticity shedding vanishes, then $u_u - u_l = \gamma = 0$ at the trailing edge. Therefore, the pressure difference at the trailing edge is zero. This is correct to at least $O(u_u^2, u_l^2)$.

3). For an airfoil with non-zero wedge angle, the stagnation streamline emanating from the trailing edge bisects the wedge angle.

There have been ambiguities about this condition, when for instance the trailing edge is not strictly *sharp*, or if the viscous layer is considered with finite thickness. In fact Küssner [17] argued explicitly that instead of coinciding with the sharp trailing edge, the rear stagnation point should be allowed a small distance away from it. As to how large this distance should be, he maintained that experimental investigation must decide. Lately, with the development of local interaction theory, it is confirmed that this conjecture is indeed the case (Brown & Stewartson [8]). The same is true for the unsteady motion of an airfoil. Corrections to the bound circulation determined with the formal Kutta-Joukowski condition were made in line with this (Brown & Cheng [6], Brown & Daniels [7], Brown & Stewartson [8]).

2.6 Discussion

The classical theory of unsteady motion of an airfoil in a uniform flow has been discussed. The boundary condition specified according to the airfoil motion was satisfied with certain singularity distributions. The functional form of the vorticity distribution in the wake was determined with Kelvin's theorem along with the

assumption that the transportation of the shed vorticity was with the uniform flow velocity U_0 , for the lifting problem. The parameters of the vorticity wave in the wake were resolved by enforcing the Kutta-Joukowski condition at the sharp trailing edge.

Subject to Kelvin's theorem, the assumption of uniform convection of the shed vorticity is specific for the isolated lift problem, under the restriction of small perturbation and potential flow. In fact, we have observed in section 2.4 that the shed vortices were transported with a non-uniform velocity away from the circle in the ζ -plane, because of the potential wake behind the circle.

Küssner [17] solved a similar problem with consideration of the finite thickness of an airfoil. He was able to show that due to the thickness of the airfoil the memory effect (wake function, in his terminology) is not $1-C(k)$, as we have seen in section 2.4 for only the lift problem. It only approaches this value in the limit where the thickness ratio tends to zero. This is because the thickness of the airfoil gives rise to a non-uniformity ('potential wake'). Instead of being uniformly the main stream speed, the convection of free vorticity must now follow the velocity development on the streamline emanating from the trailing edge. In such a way the memory pattern is changed. It should be pointed out that the non-uniformity due to the thickness effect subsides very quickly, since in the far field the thickness of the airfoil has an effect as a dipole.

In conclusion, we notice that the transportation of the free vorticity is of essential importance for the unsteady airfoil problem. In addition to the potential wake, for a real fluid there is also a viscous wake behind the body it passed. Curiosity therefore arises: will there be any modification to the memory pattern in this connection? If so, what the consequence will be?

Chapter 3

The Unsteady Flow Around an Airfoil in a Real Fluid

3.1 Introduction

In chapter 2, the potential flow due to the unsteady motion of an airfoil is discussed. There, it was assumed that the fluid is inviscid and incompressible for convenience of the study. Since the assumptions are approximations to the properties of a real fluid, they are valid only under certain restrictions.

The assumption of incompressibility is true only if the magnitude of the flow velocity is small with respect to the speed of sound. For the problem in the present study this condition is generally met. Therefore, the incompressibility assumption is considered to be valid in the present circumstances.

Fluids in reality are viscous. They react on the rate of shear strain with a shear stress. For a *Newtonian* viscous fluid which streams parallelly with $\mathbf{v}=\{u(y),0,0\}$, this is

$$\tau = \mu \frac{du}{dy}, \quad (3.1)$$

where μ is the coefficient of viscosity of the fluid. The magnitude of μ varies from fluid to fluid. For air at normal conditions (20 °C, one atmosphere pressure) it attains a small value of $1.81 \cdot 10^{-6}$ kg/(m sec). Clearly, in view of equation (3.1), the inviscid assumption is valid only when du/dy is not too large. While this is the case for the major part of the flow, it is not true in the regions close to the body surface (the boundary layer) and its down stream extension (the wake). Flows in these regions are viscous. These regions are of special interest for our problem, since we recognize that vorticity (du/dy in this case) is exclusively located there. In this chapter, we are to study the flow behaviour in these viscous regions.

In the present context, mass conservation is described by equation (2.2). However, the equation that prescribes the momentum conservation is different from the one for inviscid flow (equation (2.3)), because in addition to the inertia and pressure force, there is now also a viscous force. Considering the balance of all these, the equation for the momentum is written in the form of the Navier-Stokes equations

$$\frac{\partial \mathbf{v}}{\partial t} + (\mathbf{v} \cdot \nabla) \mathbf{v} = -\frac{1}{\rho} \nabla p + \nu \nabla^2 \mathbf{v}, \quad (3.2)$$

where $\nu = \mu/\rho$ is the kinematic viscosity of the fluid.

The distribution of vorticity is of major interest in our study, as elaborated in chapter 2. For this, we take the curl of the Navier-Stokes equation. With some vector manipulation (Appendix B), we obtain the *vorticity transport equation* for viscous flow

$$\frac{\partial \boldsymbol{\omega}}{\partial t} + (\mathbf{v} \cdot \nabla) \boldsymbol{\omega} = (\boldsymbol{\omega} \cdot \nabla) \mathbf{v} + \nu \nabla^2 \boldsymbol{\omega}. \quad (3.3)$$

The first term on the right hand side of equation (3.3) represents the stretching of a vortex line with a consequent increase in vorticity, while the second term shows the rate of change of vorticity due to viscous diffusion. In the case of two-dimensional flow, where $\mathbf{v} = \{u(x,y,t), v(x,y,t), 0\}$ and $\boldsymbol{\omega} = \{0, 0, \omega_3\}$, the stretching term drops out. The vorticity transport equation becomes

$$\frac{D\boldsymbol{\omega}}{Dt} = \nu \nabla^2 \boldsymbol{\omega}, \quad (3.4)$$

where $D/Dt = \partial/\partial t + \mathbf{v} \cdot \nabla$, is a time derivative following the motion of the fluid. From this, it is clear that for two-dimensional viscous flow the change of vorticity following a fluid particle is due to viscous diffusion.

The boundary condition on the surface of a rigid body requires that both the normal and tangential velocity component of the flow must be equal to those of the boundary itself, i.e. the flow may neither penetrate through (or separate from), nor slip over the surface of the body past which the flow takes place.

The relative magnitude of the inertia and the viscous force determines the nature of fluid motion. Based on dimensional analysis, it can be argued[†] that for steady flow the inertia force is of order $\rho U_0^2/L$ (L is a characteristic length in the flow, past which the flow velocity has a change of order U_0), while the viscous force is $O(\mu U_0/L^2)$. The Reynolds number, defined as

$$Re = \frac{U_0 L}{\nu}, \quad (3.5)$$

represents the ratio of these two forces in a global sense.

For large Reynolds number flow, as is the case in airfoil theory, the flow is essentially dominated by the inertia force, and viscous terms in the governing equations can therefore be neglected. One is left with Euler's equations for inviscid flow (equation (2.3)). Study of this leads to a so called outer solution to the flow problem. The simplification of neglecting the viscosity cannot be carried out uniformly in the whole flow field, however. In the boundary layer and wake region the viscosity may no longer be neglected. Study of the flow behaviour in these regions gives an inner solution. The two solutions have to match at the edge of the boundary layer. In this chapter we are to discuss the flow behaviour in the inner region.

[†] This is obtained by inspecting the convection term, $(\mathbf{v} \cdot \nabla)\mathbf{v}$, and the viscous term, $\nu \nabla^2 \mathbf{v}$, in the momentum equation. Assumption is made that U_0 is a typical value for flow velocity, and L is a characteristic length scale for the flow.

3.2 The Scales

Airfoil problems are usually characterized by large Reynolds number flow. Globally this indicates that the flow is essentially of inviscid nature, as assayed in the last section. In fact, this is true only for the flow at some distance away from the body. For this part of the flow it is indeed so that the velocity can have an appreciable change over a distance of the order L (in airfoil problems, L is taken to be the chord length c). Very close to the surface of the body, however, the situation is different. We consider the velocity change in the normal direction of the body surface. As the boundary condition requires, the tangential velocity of the flow is zero on the surface. Away from the surface, it increases and assumes the value of the outer inviscid flow which is $O(U_0)$. This transition happens in a region adjacent to the solid surface, which is referred to as a boundary layer. Since the flow velocity changes from zero at the solid surface to $O(U_0)$ at the outer edge of the boundary layer, the thickness of the boundary layer is the relevant characteristic length in this case. It determines the magnitude of the velocity gradient du/dy , and hence, the magnitude of the viscous force in this region, as observed in the last section. Assuming that the viscous force be of the same order of magnitude as the inertia force in the boundary layer, we can estimate its thickness δ

$$\frac{\nu U_0}{\delta^2} \sim \frac{U_0^2}{L} \Rightarrow \delta = O\left(\frac{L}{Re^{1/2}}\right). \quad (3.6)$$

Clearly, for large Reynolds number flow as we have in our problem the boundary layer thickness is small with respect to the characteristic length L .

The flow problem studied with a length scale L leads to an outer solution, in which the boundary layer cannot be perceived, since as shown in equation (3.6) its thickness is of higher order small with respect to L . In the outer solution the flow can be considered to be inviscid in view of the large Reynolds number. Close to the boundary, however, the situation is different. In the streamwise direction the characteristic length is still L .

In the normal direction the characteristic length is the boundary layer thickness δ , since flow velocity changes from 0 to U_0 within this distance. Study with these scales leads to an inner solution which satisfies both the no-slip and no-penetration condition on the wall, if the wall is impermeable. The correctness of the solution is deduced from the requirement of consistency, i.e. the inner and the outer solutions must match each other at the outer edge of the boundary layer.

The boundary condition for flow past a rigid body is quite different for inviscid and viscous flow. For inviscid flow ($\nu=0$) there is only the no-penetration condition. The fluid is allowed to slip over the body surface. While for a real flow ($\nu \neq 0$, however small it may be), in addition to the no-penetration condition, the no-slip condition has also to be satisfied. Mathematically, this can be understood by noting that from viscous to inviscid flow the momentum equation is reduced by one order, correspondingly the number of boundary conditions is also reduced by one. The reason why the no-slip condition is removed for the outer flow can be understood with some physical consideration. Since the thickness of a boundary layer is small with respect to the outer flow scale L , in the study of the outer solution it then appears that the fluid slips over the body surface.

Boundary layers interact with the outer flow generally in two ways, namely, the *weak interaction* in which the boundary layer remains attached and the outer flow is not much affected; and the *strong interaction* in which the flow separates from the body, leading to a (outer) flow pattern which differs in large degree from that predicted by the inviscid theory. In a weak interaction the boundary layer flow can be determined with the outer flow solution. It affects the outer flow with its *displacement thickness* which arises from the velocity defect, $U-u$, (U is the flow velocity outside the boundary layer) in the boundary layer. This thickness is defined as

$$\delta = \frac{1}{U} \int_0^{\infty} (U-u) dy. \quad (3.7)$$

The displacement thickness introduces a linearized pressure perturbation to the outer flow in terms of the Hilbert integral

$$p(x) = \frac{U^2}{\pi} \rho \int_{-\infty}^{\infty} \frac{\delta'(x_1)}{x-x_1} dx_1, \quad (3.8)$$

where the prime denotes the differentiation in the streamwise direction.

In boundary layer theory, streamwise gradients are assumed to be small with respect to those in the normal direction. However, there are certain regions in the flow, such as the neighbourhood of the trailing edge of a plate, or the front end of a separation bubble, where the streamwise gradient does not satisfy this assumption. Conventional boundary layer scales are not sufficient in resolving what happens locally in these regions. Instead, a large streamwise gradient appears in the usual boundary layer theory as a singularity (Meyer [22]). An appropriate stretch transformation of the coordinate in the flow direction is therefore necessary for studying the local flow structures. Efforts to this end lead to the establishment of the so called *local interaction theory*. This theory is essentially based on the following four features which are derived from physical considerations (Meyer [22]).

- 1). The displacement thickness remains of order $Re^{-1/2}$ throughout;
- 2). Changes of velocity or pressure in this region might penetrate farther into the flow than does a weak interaction, but not to distances independent of the Reynolds number;
- 3). The region is quite short in the flow direction depending on the Reynolds number (in usual boundary layer theory the length scale in this direction is L —independent of the Reynolds number.);
- 4). The flow structure in this region has to match the upstream boundary layer flow.

As we shall see in section 3.4, this theory predicts a rather complicated multi-layered structure in the neighbourhood where local interaction occurs.

3.3 The Boundary Layer and the Wake

We consider cases with two-dimensional flow past an impermeable body fixed in space. Let a coordinate system be chosen such that x measures along the tangential, y along the normal direction on the surface. We denote with u the velocity component in the tangential direction and v the component in the normal direction. For the convenience of discussion, we write the Navier-Stokes equation in component form for the two-dimensional flow

$$\begin{aligned} \frac{\partial u}{\partial t} + u \frac{\partial u}{\partial x} + v \frac{\partial u}{\partial y} &= -\frac{1}{\rho} \frac{\partial p}{\partial x} + \nu \left(\frac{\partial^2 u}{\partial x^2} + \frac{\partial^2 u}{\partial y^2} \right), \\ \frac{\partial v}{\partial t} + u \frac{\partial v}{\partial x} + v \frac{\partial v}{\partial y} &= -\frac{1}{\rho} \frac{\partial p}{\partial y} + \nu \left(\frac{\partial^2 v}{\partial x^2} + \frac{\partial^2 v}{\partial y^2} \right). \end{aligned} \quad (3.9)$$

The equation of continuity is

$$\frac{\partial u}{\partial x} + \frac{\partial v}{\partial y} = 0. \quad (3.10)$$

We refer all the linear dimensions to the characteristic length L . The thickness of the boundary layer, δ , is a small quantity with respect to L for large Reynolds number flow (equation (3.6)). Let U_0 be some typical value for u . Then, we have for the boundary layer flow $\partial u/\partial x \sim O(U_0/L)$ and $\partial v/\partial y \sim O(v/\delta)$. In view of equation (3.10) terms $\partial u/\partial x$ and $\partial v/\partial y$ must be of the same order of magnitude. Recognizing that $v=0$ at the wall, it can be concluded that v is $O(U_0\delta/L)$, i.e. a small quantity with respect to U_0 . Based on these, the following properties can be inferred

$$\begin{aligned} u \frac{\partial u}{\partial x} &= O\left(\frac{U_0^2}{L}\right), & v \frac{\partial u}{\partial y} &= O\left(\frac{U_0^2}{L}\right), & \frac{\partial^2 u}{\partial x^2} &= O\left(\frac{U_0}{L^2}\right), & \frac{\partial^2 u}{\partial y^2} &= O\left(\frac{U_0}{\delta^2}\right); \\ u \frac{\partial v}{\partial x} &= O\left(\frac{U_0^2 \delta}{L^2}\right), & v \frac{\partial v}{\partial y} &= O\left(\frac{U_0^2 \delta}{L^2}\right), & \frac{\partial^2 v}{\partial x^2} &= O\left(\frac{U_0 \delta}{L^3}\right), & \frac{\partial^2 v}{\partial y^2} &= O\left(\frac{U_0}{L\delta}\right). \end{aligned} \quad (3.11)$$

The magnitude of the kinematic viscosity ν can be written $O(U_0\delta^2/L)$ by virtue of equations (3.5) and (3.6). Substituting these into equations (3.9) and viewing them as

expressions for $\partial p/\partial x$ and $\partial p/\partial y$ respectively, it follows that $|\partial p/\partial y| \ll |\partial p/\partial x|$. Considering the estimation of order of magnitude made above, the Navier-Stokes equations can be simplified as

$$\frac{\partial u}{\partial t} + u \frac{\partial u}{\partial x} + v \frac{\partial u}{\partial y} = -\frac{1}{\rho} \frac{dp}{dx} + \nu \frac{\partial^2 u}{\partial y^2}, \quad (3.12)$$

if terms involving small quantity δ are neglected. The boundary conditions are $u(x,0)=v(x,0)=0$, and at the outer edge of the boundary layer where $y/\delta \rightarrow \infty$ (y is with the length scale of outer flow, $O(L)$), the tangential velocity should approach the value in the outer flow, i.e. $u \rightarrow U$.

The magnitude of the time derivative term, $\partial u/\partial t$, deserves some consideration. If $\partial u/\partial t$ is $O(U_0^2/L)$, then the time derivative term is of the same order of magnitude as the other terms. The equation describes the flow motion in an unsteady boundary layer. In this case the time scale must be $O(L/U_0)$. If the time scale in an actual problem is larger than this (the variation in time happens more slowly), the time derivative term drops out and the problem reduces to a steady one. If, on the other hand, the time scale is smaller than $O(L/U_0)$ the variation is too rapid so that the viscous flow exhibits other features, as we shall see below.

Vorticity is generated at a solid boundary when flow passes a body. Considering equation (3.4) we see that the viscosity of the fluid has the effect of diffusing the vorticity, while the convection of the flow (represented by the nonlinear terms on the left hand side of the equation) carries the vorticity down stream. In fact, it is the interplay of these two effects that suggests the thickness of the boundary layer. Given the coefficient of kinematic viscosity ν , the time taken for vorticity to diffuse a distance of order δ (the thickness of boundary layer) is $O(\delta^2/\nu)$ —a typical time scale for diffusion problems. In the mean while the vorticity is convected a distance $x=O(U\delta^2/\nu)$, so that

$$\delta(x) \propto \left(\frac{\nu x}{U_0} \right)^{\frac{1}{2}} = \frac{x}{\sqrt{Re(x)}}. \quad (3.13)$$

The time scale in the above discussion is $O(L/U_0)$. We now consider a case, where the time is not limited to this, through the second problem of Stokes. This problem concerns an infinite flat plate oscillating parallel to itself (in the x -direction) with an angular frequency ω in a stagnant viscous fluid (Schlichting [29]). In such a case the Navier-Stokes equation is simplified to a diffusion equation

$$\frac{\partial u}{\partial t} = \nu \frac{\partial^2 u}{\partial y^2}, \quad (3.14)$$

with boundary condition $u(0, t) = \hat{a} \cos \omega t$ on $y=0$. The solution of this is

$$u(y, t) = \hat{a} e^{-\sqrt{\omega/2\nu}y} \cos(\omega t - \sqrt{\omega/2\nu}y). \quad (3.15)$$

It is clear that u decreases exponentially with the distance from the wall. Over a distance

$$\delta_s \sim O(\sqrt{\nu/\omega}), \quad (3.16)$$

the amplitude of the velocity reduces to $U_0 e^{-1}$. This defines the thickness of a *Stokes layer*. It is sometimes referred to as the *penetration depth*. Vorticity generated by the unsteady motion of the body is largely confined to this layer. Clearly, the thickness of the Stokes layer decreases with increasing frequency. We notice that the Stokes layer has the feature that the viscous term in the equation of motion is balanced by the term involving the time derivative.

We now return to the usual boundary layer problem, and let a plate of finite length L oscillate in a uniform flow (the flow is parallel to the plate) U_0 . If ω is $O(L/U_0)$, then the penetration depth is of the same order of magnitude as the boundary layer thickness. This is very easily checked with the relation (3.16). If ω is large with respect to U_0/L , the Stokes layer is embedded in the boundary layer.

Friction of the viscous flow in the boundary layer consumes energy. In the case where the flow has to go against a substantial pressure rise, i.e. $dp/dx > 0$, the kinetic energy having been consumed so, the fluid particles in the boundary layer cannot accommodate

the pressure rise (their kinetic energy is less than the pressure energy implied by the outer flow). Boundary layer separation will then occur (Schlichting [29]).

When flow separates from a body and does not reattach, it leaves a wake behind it. The wake distinguishes itself from the outer flow by a velocity defect and the presence of vorticity in it, as in the boundary layer flow. We shall confine ourselves to a thin wake, such as the one behind an airfoil at small angle of incidence. In such a case, the transverse length scale is small with respect to that in the main direction of the flow, so that the velocity gradient is large across the wake. Flow in this region is still of a boundary layer nature. A fundamental difference between boundary layer and wake flow is that in boundary layer flow the velocity defect is not filled up—the diffusion of momentum from the outer flow counteracts the friction at the wall; while in a wake flow there is no wall friction so that the diffusion effect gradually fills up the velocity defect as the distance from the body is increased. The development of the wake thickness is also due to the interplay of the diffusion and convection effect as in the boundary layer. Following similar arguments, the thickening of the wake is found to have the behaviour as that for a two-dimensional boundary layer $\delta = O((\nu x/U_0)^{1/2})$.

3.4 The Triple-deck Structure

We consider here two-dimensional parallel flow past a flat plate of finite length L . When the flow leaves the trailing edge, the boundary condition is suddenly changed: the no-slip condition on the plate surface is replaced by the condition of zero stress ($\partial u/\partial y = 0$) at the wake centerline. This abrupt change of boundary condition gives rise to a large acceleration to the flow, since the wall constraint is suddenly removed.

Assuming the initial velocity profile at the trailing edge as the one in Blasius' solution for boundary layer on an infinite plate, Goldstein [15] derived a solution for the flow development in the near wake with a conventional boundary layer method. The flow in

this region was identified to have a two layered structure. In the inner wake the flow is accelerating because of the removal of the wall constraint, while the outer wake would have to accommodate this acceleration. In this work, an infinite acceleration of the centerline velocity is found just at the trailing edge, as can be seen in figure 3.1.

In fact, Messiter [20] has shown that Goldstein's solution is no longer valid within a distance that is $O(LRe^{-3/8})$ from the edge in the flow direction. Because of the localized behaviour, a new stretching transformation of the coordinates is necessary. Distinct from the usual boundary layer calculation, in this case the local pressure distribution is not specified in advance, since the local interaction is found to induce in the external flow a pressure gradient exceeding the first term in the range $x=O(LRe^{-3/8})$. It has to be determined by the coupling of a boundary layer solution for the sub-layer with a small disturbance description of the external flow. Efforts in this direction (Messiter [20], Stewartson [31], [32]), lead to the recognition of a triple-deck structure in the neighbourhood of the local interaction point. In this section we shall briefly outline the studies in this respect.

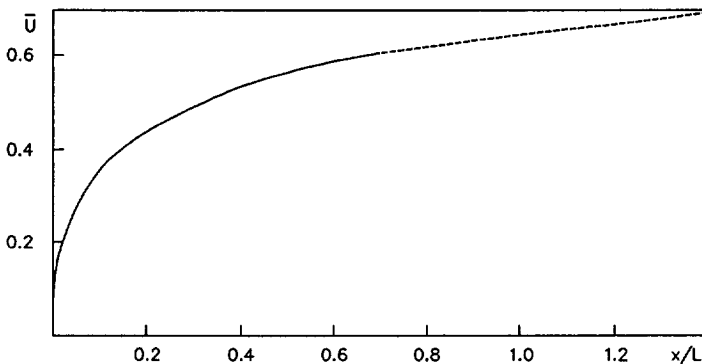


Figure 3.1 Goldstein's solution of the centerline velocity in the near wake (adapted from Goldstein [15]).

Let ψ be the stream function measured from the body surface in units of U_0L . The velocity components are related to the stream function in the following way

$$\mathbf{u} = \frac{\partial \psi}{\partial y}, \quad \mathbf{v} = -\frac{\partial \psi}{\partial x}. \quad (3.17)$$

In such a way the equation of mass conservation is automatically satisfied, and the Navier-Stokes equation for the steady case can be written in the following (dimensionless) form

$$\begin{aligned} \psi_y \psi_{xy} - \psi_x \psi_{yy} &= -p_x + Re^{-1}(\psi_{yxx} + \psi_{yyy}), \\ \psi_x \psi_{xy} - \psi_y \psi_{xx} &= -p_y - Re^{-1}(\psi_{xxx} + \psi_{xyy}), \end{aligned} \quad (3.18)$$

where p is the pressure, measured in units of ρU_0^2 . The subscripts denote partial differentiation.

According to the features observed in section 3.2 we shall proceed with the discussion of the flow structure in the neighbourhood of the trailing edge. In view of features 3), which states that the region of local interaction is quite short and dependent on the Reynolds' Number, a coordinate stretching in the flow direction will be applied. Feature 4), which points out that the flow structure in the local interaction region has to match the upstream boundary layer flow, suggests a scale of the boundary layer thickness in the normal direction. So that we write

$$\tilde{x} = x Re^\alpha, \quad \tilde{y} = y Re^{1/2} \quad (3.19)$$

where x and y are measured in units of L . The pressure perturbation with respect to the value determined by the external flow is a small quantity, which has to be seen with a magnification factor $\tilde{\pi}(Re)$ such that

$$\tilde{p}(\tilde{x}, \tilde{y}) = \frac{1}{\tilde{\pi}(Re)} [p(x, y) - p_e(x, y)], \quad (3.20)$$

where p and p_e are measured in units of ρU_0^2 , the subscript e stands for *external*. According to feature 4), and conforming with boundary layer solution, the stretching transformation for the stream function can be written

$$\hat{\psi}(\hat{x}, \hat{y}) = Re^{-1/2} \psi(x, y). \quad (3.21)$$

Since $x \rightarrow 0$ as $Re \rightarrow \infty$ at all \bar{x} , only the values $p_e(0)$ and $u_e(0)$ enter the argument. The above transformations cannot account for feature 2), which requires a farther penetration of the pressure perturbation. Another set of stretching needs to be introduced in order to bring greater distance from the body surface into view[†]

$$\hat{x} = x Re^\alpha, \quad \hat{y} = y Re^\alpha, \quad (3.22)$$

$$\hat{p}(\hat{x}, \hat{y}) = \frac{1}{\hat{\pi}(Re)} [p(x, y) - p_e(x, y)], \quad (3.23)$$

$$\hat{\psi}(\hat{x}, \hat{y}) = \frac{1}{\hat{\sigma}(Re)} [\psi(x, y) - u_e y]. \quad (3.24)$$

In order that the penetration be significantly beyond the boundary layer, α must satisfy $0 < \alpha < 1/2$. Feature 1), which requires that the mass-flow deficiency $u_e y - \psi$ be of the same order as that of a boundary flow implies

$$\hat{\sigma} = \tilde{\sigma} = Re^{-1/2}. \quad (3.25)$$

As can be seen from the coordinate stretching, the transformation denoted with a tilde $\tilde{\sim}$ reveals a flow structure correspondent to the boundary layer in the normal direction, while the transformation denoted with a hat $\hat{\sim}$ reveals a structure beyond the boundary layer. For this reason, the region corresponding to transformation $\tilde{\sim}$ is called the *main*

[†] At this larger distance, streamlines come from the external flow as implied by feature 4). Streamlines in the boundary layer would not enter this region. This is implied by feature 1), which states that the displacement thickness remains $O(Re^{-1/2})$. By Kelvin's theorem, the flow in this region remains an irrotational one, which has no distinguished direction of influence (Meyer [22]). Therefore, the stretching transformation in this region is the same in x and y direction.

deck, the other, corresponding to transformation $\hat{\cdot}$, is called the *upper deck*.

Substitution of the stretching transformations into the equations (3.18), and taking the limit $Re \rightarrow \infty$, yield the following limit equations

$$\begin{aligned} \tilde{D} \frac{\partial \tilde{\Psi}}{\partial \tilde{y}} + \tilde{\pi} \frac{\partial \tilde{p}}{\partial \tilde{x}} &\rightarrow 0, \\ -\tilde{D} \frac{\partial \tilde{\Psi}}{\partial \tilde{x}} + \tilde{\pi} Re^{1-2\alpha} \frac{\partial \tilde{p}}{\partial \tilde{y}} &\rightarrow 0, \end{aligned} \quad (3.26)$$

for the main deck, and

$$\begin{aligned} \hat{D} \frac{\partial \hat{\Psi}}{\partial \hat{y}} + \hat{\pi} Re^{1-2\alpha} \frac{\partial \hat{p}}{\partial \hat{x}} &\rightarrow 0, \\ -\hat{D} \frac{\partial \hat{\Psi}}{\partial \hat{x}} + \hat{\pi} Re^{1-2\alpha} \frac{\partial \hat{p}}{\partial \hat{y}} &\rightarrow 0, \end{aligned} \quad (3.27)$$

for the upper deck. In equations (3.26) and (3.27)

$$D = \frac{\partial \Psi}{\partial y} \frac{\partial}{\partial x} - \frac{\partial \Psi}{\partial x} \frac{\partial}{\partial y}, \quad (3.28)$$

for corresponding stretched variables. It is remarkable to see that the enhanced streamwise changes in the local interaction overshadow the viscous shear even in the main deck such that the governing equations are inviscid in the limit. This is because due to the shortening of the x scale (from $O(L)$ to $O(LRe^{-3/8})$), the acceleration and pressure force are increased, while the viscous force remains of the same order since the thickness of the main deck remains of the same order as the boundary layer thickness. Eventually in this region it is the balance between the inertia and pressure force that constitutes the fluid motion. In view of the properties of the two decks discussed above, we understand that the flow in the upper deck is rotation free. In the main deck, however, the flow is rotational, the vorticity being carried from the upstream boundary layers along the streamlines.

By considering the nature of velocity and pressure perturbation in view of equations (3.26) and (3.27), and the matching of the two decks the proper choice of the pressure

scaling factor $\bar{\pi}$ and $\hat{\pi}$ is found to be (Meyer [22])

$$\bar{\pi} = \hat{\pi} = Re^{2\alpha-1}. \quad (3.29)$$

In the main deck, the pressure and the streamline slope, defined as $\theta = -(\partial\bar{\psi}/\partial\bar{x})/(\partial\bar{\psi}/\partial\bar{y})$, are shown to be independent of \bar{y} (Meyer [22]). It is thus concluded that the main deck merely transmits the perturbation of pressure and the streamline slope from the upper deck towards the body surface.

It is clear that the main deck cannot satisfy the boundary condition for viscous flow. Another deck, analogous to the Prandtl boundary layer, has to be introduced. In view of the boundary condition at the body surface, the momentum near it must be arbitrarily small, and non-trivial pressure changes in the local interaction can be balanced near the body surface only by the enhanced shear stress in this *lower deck*. To solve for the flow in this region, the following transformations are written

$$\bar{x} = xRe^\alpha, \quad \bar{y} = yRe^\beta, \quad \beta > 1/2, \quad (3.30)$$

$$\bar{p}(\bar{x}, \bar{y}) = \frac{1}{\pi} [p(x, y) - p_e(x, y)], \quad (3.31)$$

$$\bar{\Psi}(\bar{x}, \bar{y}) = \frac{1}{\bar{\sigma}(Re)} \Psi(x, y), \quad (3.32)$$

with again $\bar{\pi} = Re^{2\alpha-1}$ for consistency with the transmitted pressure. Considering the mass flow in this lower deck and matching the velocity in the lower and the main deck as $\bar{y} \rightarrow \infty$, it is found (Meyer [22]) that $\bar{\sigma} = Re^{-2\beta+1/2}$. Substitution of equations (3.31) through (3.32) into the Navier-Stokes equation (equation (3.18)) and taking the limit $Re \rightarrow \infty$, yield

$$\begin{aligned} \bar{D} \frac{\partial \bar{\Psi}}{\partial \bar{y}} + Re^{2(\alpha+\beta-1)} \frac{\partial \bar{p}}{\partial \bar{x}} - Re^{3\beta-\alpha-3/2} \frac{\partial^3 \bar{\Psi}}{\partial \bar{y}^3} = 0, \\ \frac{\partial \bar{p}}{\partial \bar{y}} = 0. \end{aligned} \quad (3.33)$$

In equation (3.33) positive and negative values of $\alpha+\beta-1$ or $3\beta-\alpha-3/2$ imply truncation of the equation that are either degenerations inconsistent with a mild interaction or are reduced forms describing only sub-layers $\bar{y} \rightarrow 0$ or $\bar{y} \rightarrow \infty$ of the stretching (Meyer [22]). Therefore they have to be zero. This leads to

$$\alpha = 3/8, \quad \beta = 5/8, \quad \bar{\sigma} = Re^{-3/4}, \quad \bar{\pi} = \bar{\pi} = \hat{\pi} = Re^{-1/4}. \quad (3.34)$$

Substituting the transformation back to the Navier-Stokes equations, and taking the limit $Re \rightarrow \infty$, the lower deck is found to be governed by the following equations

$$\bar{u} \frac{\partial \bar{u}}{\partial \bar{x}} + \bar{v} \frac{\partial \bar{u}}{\partial \bar{y}} = - \frac{\partial \bar{p}}{\partial \bar{x}} + \frac{\partial^2 \bar{u}}{\partial \bar{y}^2}, \quad (3.35)$$

$$\frac{\partial \bar{p}}{\partial \bar{y}} = 0. \quad (3.36)$$

This set of equations has the same form as the Prandtl boundary layer equations. Their boundary condition at $y=0$ is as usual. Apparently, the flow in the lower deck is driven by the pressure gradient of the upper deck, since we have seen that the main deck merely transmits the pressure perturbation (\bar{p} independent of \bar{y}). On the other hand, the flow in the lower deck induces a pressure perturbation in the main deck, because of its displacement thickness. The pressure perturbation is related with the lower deck flow with the Hilbert integral equation (equation (3.8)).

3.5 The Kutta-Joukowski Condition

In chapter 2, the importance of the Kutta-Joukowski condition in the classical airfoil theory has been discussed. However, the physical arguments at the root of it cannot be explained if the viscous nature of the flow is not accounted for, and one could only accept it with an intuitive approval. In fact, the Kutta-Joukowski condition is a statement of the effect of the boundary layer flow in terms consistent with potential theory. Satisfying this condition implies that an outer solution is properly chosen, such that it matches the inner viscous flow structure in the limit $Re \rightarrow \infty$ (Crighton [11]).

When a flat plate is mounted in a parallel flow with a certain angle of incidence α , potential theory (without applying the Kutta-Joukowski condition) predicts a pressure rise at the (rear) stagnation point, and an infinite under-pressure at the trailing edge, as sketched in figure 3.2. This is consistent for the outer potential flow itself. But for the boundary layer flows approaching the stagnation point, this pressure distribution is unfavourable—since the flow would have to go against a pressure gradient. Separation of the boundary layer would generally result. In such a way, the outer and the inner flow adapt to each other until a stable state is reached. This stable state is prescribed by the Kutta-Joukowski condition.

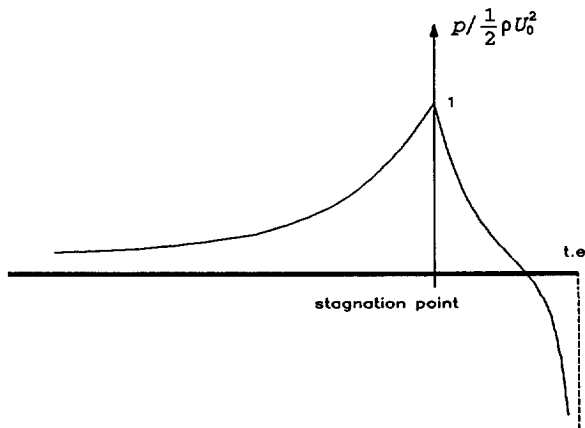


Figure 3.2 Schematic drawing of the pressure distribution in the neighbourhood of the rear stagnation point.

It is generally true that potential theory in conjunction with the Kutta-Joukowski condition provides correct solutions for usual airfoil problems. In some cases, however, this is limited, for instance, at certain larger angles of incidence when *trailing edge stall* (catastrophic separation of flow at the trailing edge) sets in. The Kutta-Joukowski condition does not apply in this circumstance, neither does it explain why the stall happens. In order to clarify this, we would have to consider the local interaction at the trailing edge, where flow from the two sides of the plate join the wake.

Consider a case in which a plate is inclined with a certain angle α to a uniform stream. Classical airfoil theory (Kutta-Joukowski condition satisfied, thus) predicts for this case a flow with pressure distribution $O(-\alpha r^{1/2})$ on the suction side near the trailing edge, where r is the distance measured from the edge (over-pressure side is not considered, because flow is accelerating there). This distribution is evidently unfavourable for the oncoming boundary layer flow.

On the other hand, considering the local interaction at the trailing edge, it appears that the acceleration of the viscous flow in the wake induces a favourable pressure distribution which can be felt in a range $O(\text{Re}^{-3/8}L)$ from the edge. The magnitude of this perturbation is Reynolds number dependent. In fact it is a fraction $O(\text{Re}^{-1/4})$ of the dynamic head ρU_0^2 , as can be seen from the scaling factor $\pi(\text{Re})$ (equation (3.34)). So that the pressure gradient in this neighbourhood is a fraction of $O(\text{Re}^{1/8})$ of $\rho U_0^2/L$. It is argued in Brown and Stewartson [8] that the unfavourable pressure gradient discussed in the last paragraph is counter-acted by this agent so that, with the angle of incidence bounded up to a certain critical order, the boundary layer nevertheless keeps attached until it reaches the trailing edge. The critical order of α can be determined by arguing that the potential pressure gradient in the triple deck region be of the same order. Consequently, this is found to be $O(\text{Re}^{-1/16})$. If the order of magnitude of the angles of incidence is smaller than this, the triple deck perturbation is dominant. Flow keeps attached up till the trailing edge. It is in effect a small perturbation to the unseparated zero-incidence case, as studied by Stewartson [32] and Messiter [20]. When the angle is larger, separation occurs at a distance, which is noticeable in the outer flow scale,

upstream of the trailing edge. In the critical range, the two pressure gradients are comparable, the flow will separate in the immediate neighbourhood of the trailing edge. In line with this Brown and Stewartson [8] were able to identify that for large but finite Reynolds number the interaction results in a stagnation point in the outer flow at a distance $x/L = O(Re^{-7/8})$ ahead of the trailing edge. Corresponding to this the lift coefficient is modified by a fraction $O(Re^{-3/8})$.

Brown and Daniels [7] studied the problem of an airfoil undergoing pitching motion about its mid chord point with angular frequency ω and amplitude α . The relevant parameters here are the amplitude α , the reduced frequency $k (= \omega L / 2U_0)$, and the Reynolds number Re . The orders of magnitude of amplitude and the reduced frequency will be determined in terms of the Reynolds number as follows. Upon reaching the trailing edge, the upstream perturbed Blasius flow is to enter the triple deck. As discussed in the last section, the main deck of the triple deck is of thickness $O(LRe^{-1/2})$, i.e. the boundary layer thickness. The thickness of the lower deck is $O(LRe^{-5/8})$. Due to the oscillation, there is a Stokes layer in the neighbourhood of the wall whose thickness is $O((\nu/\omega)^{1/2})$, (equation (3.16)). In order that the solution in the Stokes layer will match that in the lower deck, Brown and Daniels [7] choose the order of the reduced frequency so that the two layers have the same thickness. It then follows $k = O(Re^{1/4})$. It is argued that if the order of magnitude of k is smaller than this the flow will be merely a perturbation of that for a steady airfoil at incidence; if it is larger it is probable that the triple deck flow structure will be destroyed by the rapid oscillation.

For oscillation of the airfoil, the potential pressure (Kutta-Joukowski condition satisfied) near the trailing edge is $O(\alpha k^2 r^{1/2})$. Like that in the steady case, this pressure distribution is unfavourable for the boundary layer flow approaching the trailing edge. It has to be counter-acted by the favourable pressure gradient induced by the triple deck such that the flow could reach the trailing edge without separation. In line with this, the order of magnitude of the oscillation is found to be $O(Re^{9/16})$ (Brown & Daniels [7]). Figure 3.3 shows the flow structure they identified in the study.

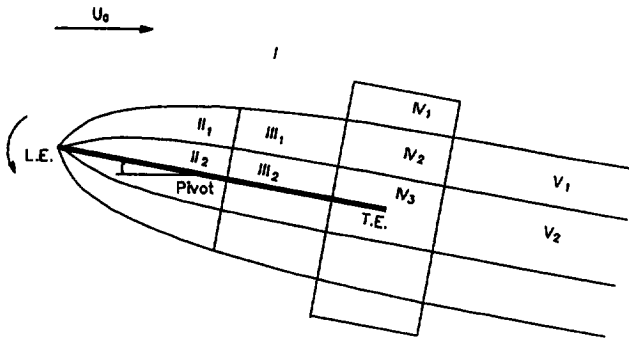


Figure 3.3 Structure of uniform flow U_0 past a flat plate, oscillating about a pivot with angular frequency ω and incidence amplitude α . I, potential flow; II, perturbed Blasius boundary layer and Stokes layer; III, foredeck; IV, triple deck; V, modified Goldstein wake. (adapted from Brown and Daniels [7])

3.6 Turbulent Boundary Layer and the Near Wake

Up to this point the discussion has been restricted to laminar flows. However, most flows of practical interest are turbulent. Understanding of turbulent flows has been limited, even a precise definition is very difficult to give. All one can do is list some of the characteristics of turbulent flows (Tennekes & Lumley [33]).

One characteristic of all turbulent flow is the randomness. In addition to the mean motion, the physical quantities (e.g. velocity, pressure) exhibit a random fluctuation. The random fluctuation of a turbulent flow has an effect which is in a way similar to the molecular diffusivity[†]. It increases the rate of momentum exchange which, in laminar flow, is accomplished by only viscous (molecular) diffusion. Three-dimensionality is another characteristic of turbulent flows. Two-dimensional flows can

[†] The difference can be stated that the molecular diffusivity is a property of the fluid (the mean free path of molecular is small with respect to the flow scale), while the turbulent diffusivity depends on the flow condition.

be studied in the sense of mean motion.

In view of the enhanced viscosity of the mean flow, we expect that a turbulent boundary layer would be thicker or, more precisely, grows faster than a laminar one. In fact the level of turbulent velocity fluctuation can be written in terms of a friction velocity which is defined as $u_* = (\tau_t/\rho)^{1/2}$, where τ_t is the turbulence shear stress at the wall. In turbulent boundary layer flow the velocity in the normal direction results from the turbulent fluctuation so that it must be $O(u_*)$. Consider the boundary layer is defined by a certain streamline with distance $\delta(x)$ from the surface we can write $d\delta/dx \sim u_*/U$, so that $\delta \sim xu_*/U$. Here u_* varies slowly in the streamwise direction depending on the flow situation. For a flat plate with zero pressure gradient it is found to be $\delta \sim x^{4/5}$ (Schlichting [29]).

Similar to that in a laminar boundary layer, in a thin region close to the wall the flow velocity must reduce to zero in order to satisfy the boundary condition. Microscopically the Reynolds number is small there, because both the velocity and the dimensions are small in this region. Therefore in this thin, near wall region the viscous force is dominant. The turbulent fluctuation, which is basically of inertia nature, is prohibited. Hence, a turbulent boundary layer can be distinguished into two parts. Near the wall, there is an inner viscous *sub-layer*[†], where viscosity of the fluid is dominant. The large viscous shear force in the sub-layer implies a large velocity gradient, or vorticity concentration. Outside of this is the main part of the turbulent boundary layer in which the enhanced mixing due to the turbulent fluctuation makes the diffusion of momentum or vorticity more effective. Therefore, a turbulent boundary layer is seen to be thicker than a laminar one.

Local interaction occurs in the turbulent case as well. In Melnik and Chow [19] it is found that a multi-layered flow structure exists in the neighbourhood of the trailing

[†] Not to be confused with the Stokes layer which is due to stronger unsteadiness of the motion.

edge. It is established that in the outer layer the flow is basically inviscid and rotational. The region of local interaction includes most of the boundary layer and part of the irrotational flow outside of the boundary layer. This property is similar to the upper and main deck in the laminar case. Vorticity from the upstream boundary layer is transmitted through it in to the outer near wake. Immediately next to the wall there is an inner wall layer which is similar to the lower deck. It matches the wall layer up stream of it. Between these two layers there is a 'blending' layer which resolves the discontinuity in Reynolds stress in the outer and inner layer. The displacement effect mainly affects the two inner layers.

In Bogucz and Walker [5], it is demonstrated that the turbulent near wake also shows a two-layered structure. The flow in the outer layer passes into the outer near wake relatively undisturbed. The primary effect of the change in boundary condition at the trailing edge is confined in the thin inner near wake. The outer wake would have a transverse velocity in order to accommodate the acceleration in the inner wake.

3.7 Discussion

Kinematically, boundary layer and wake flow distinguish themselves from the outer flow by velocity defect and vorticity concentration. The vorticity is generated on the solid surface by the friction force. The flow in these regions is also characterized by the viscosity. Due to the viscosity the vorticity is diffused outwards into the flow, as it is convected along a certain streamline in the viscous region. For large Reynolds number flow the diffusion effect is relatively weak with respect to the convection. In view of the velocity defect in these regions, we expect a retardation in the vorticity convection, i.e. the vorticity is convected with a speed which is lower than that of the outer flow.

Study of local interaction in the neighbourhood of the trailing edge and the near wake reveals that a multi-layered flow structure exists there. Corresponding to this, we postulate that vorticity convection should also have different behaviour in the different

regions. In the outer wake where the velocity defect is small, vorticity would be convected with a speed not much different from the outer flow velocity. While in the inner wake the velocity varies largely with the distance from the body. The velocity defect, being large in the inner (near) wake, is gradually filled up by the diffusion mechanism (viscous, turbulence). We expect that the convection of vorticity in this region would be rather slow initially. It accelerates due to the growth of flow velocity in this region. On account of these effects, it seems reasonable to expect that the convection of the shed vorticity in the near wake is conceived in a layered structure.

Of course, the postulation of the layered vorticity convection structure is only qualitative, since diffusion would soon smear it out. But in the near wake region it should be more pronounced.

Chapter 4

The Experimental Studies

4.1 Introduction

In chapter 2 we studied the unsteady airfoil problem within the framework of potential theory. It was noticed that the effect of the shed vortices accompanying the unsteady motion of the airfoil is one of the major aspects which make the unsteady problems different from the steady ones. This influence enters from the shed vortices' perturbation into the upwash field of the airfoil. From equation (2.21) we see that the perturbation depends on both the strength of the shed vortices and their position in the wake. They can be determined with the Kutta-Joukowski condition. Obviously, the position of the shed vortices depends on the velocity with which they are transported.

For thin airfoils performing small amplitude oscillations in an inviscid flow, it is consistent to assume that the shed vorticity is convected away from the airfoil with the velocity of the uniform flow at infinity, U_0 . If the oscillation of the airfoil is harmonic, one would then observe a vortex wave extending from the trailing edge of the airfoil down stream, with the wave length $\lambda = U_0 T$, where T is the period of the oscillation. The structure of this vortex wave is determined by a dimensionless parameter, the reduced frequency, defined as $k = \omega c / 2U_0 = \omega b / U_0$. In terms of this parameter, the vortex wave in the wake perturbs the flow field so that the upwash at the rear aerodynamic centre of the airfoil is modified with a factor $C(k)$, where $C(k)$ is Theodorsen's function as defined in equation (2.51).

As a matter of fact, in potential theory for thin airfoils one has to assume that the shed vorticity is transported with velocity U_0 of the uniform flow (except for e.g. Küssner's effect, cf. section 2.7). In this context, the wake simply represents an infinitely thin vortex sheet which has no mass. If the shed vorticity is transported with a speed other than U_0 , it would be subject to a pressure jump. Consequently, an infinite acceleration

of the vortex sheet in the lateral direction would result, which is physically unacceptable.

However, when a real flow is considered, the convection of shed vorticity assumed in the potential theory raises some inconsistency. Concerning large Reynolds number flow, we saw in chapter 3 that vortices are solely confined in the thin, viscous regions, i.e. the boundary layer and the wake[†]. Kinematically, flow in these viscous regions is characterized by a velocity defect and corresponding velocity gradients. In the last chapter we have learned that, for two dimensional flow, the rate of change of vorticity observed at a point fixed in space is due to two factors, namely, convection and viscous diffusion (equation (3.3)). In airfoil theory, flow of practical interest has a large Reynolds number. In this connection, the effect of convection is overwhelming. In view of Kelvin's theorem, we argue that the convection of shed vortices (in the viscous region) will take place with a velocity which is somewhat less than that of the outer flow since the velocity defect is quite appreciable in the near wake. The convection velocity will gradually increase due to the viscous forces. In making this argument, we notice that a thin viscous wake is essentially different from a shear layer in the sense that it has a finite thickness, though it is small with respect to the chord length of the airfoil. It therefore has a non-vanishing mass per unit length—a model which is fundamentally different from the vortex sheet in the potential theory. Further discussion of this will be found in chapter 5.

In the present chapter we are to investigate whether indeed the convection of shed vorticity is retarded with respect to U_0 or is it just uniform at speed U_0 as assumed in the classical potential theory. Harmonic decomposition of the unsteady velocity perturbation ($u' = u - U$, U is the steady part of perturbation due to the airfoil) is another

[†] Far down stream in the wake, the velocity defect is filled up. The flow becomes uniform. In this case vortices appear to exist in a potential flow. But at this distance the effect of the vorticity on the flow field near the airfoil is small. So that, we are interested in the shed vortices in the wake which is not too far from the airfoil.

interest in our study. We believe that this would reveal the nature of the process of vortex shedding due to the unsteady motion of the airfoil. Also of interest is the relation between the perturbation and the related parameters, e.g. the reduced frequency, the Reynolds number, and the amplitude of the airfoil oscillation. The latter actually concerns the investigation of the linearity of the problem. They are not less important because the special case of harmonic oscillation is studied on the assumption that a more complex motion can be related to it by way of Fourier transformation, provided the process is linear and allows of superposition.

A direct calculation of the vorticity convection might be difficult, since in the neighbourhood of the trailing edge stronger interaction gets involved, as we saw in the last chapter. Moreover, closure models for the turbulent flow might be different depending on the modes of motion. In the present study we shall approach the problem with a novel method that combines experimental measurement and numerical calculation in the way described below. It might appear that the title of the present chapter is not quite consistent with the content, since numerical calculations are also involved. However the choice seems justified since the experimental effort forms the bulk of the study described in the present chapter, while the numerical calculation is an indispensable auxiliary whose outcome serves as reference in the interpretation of the experimental results.

The perturbation that the shed vortices give to the flow field is the integrated contribution of all the vortices distributed in the entire wake. In view of the global effect numerous individual vortices (if one consider the wake consists of infinitesimal vortex elements) would have to be traced—this would be too laborious to be executed. Moreover there is also a practical limitation: we are not in possession of a vorticity meter which can detect local vorticity. It is for these reasons, we devised the new approach which combines experimental and numerical studies. Experimentally, we shall measure the velocity perturbation in the space. Corresponding to the measured perturbation, we are to make numerical calculations based on the classical theory as

discussed in chapter 2[†]. The scheme of the numerical calculation is described in chapter 5. From the comparison between the measured and the calculated results we can infer the transportation of the shed vorticity. A direct analysis of the sampled signals will provide information concerning the parameter dependency and the harmonic composition of the perturbation.

The experiments were conducted in the M-Tunnel of the Low Speed Laboratory of the Department of Aerospace Engineering, TU Delft. The inner cross section of the tunnel is 40×40 cm. A standard NACA 0012 airfoil (Abbott & von Doenhoff [1]), with chord length $c=15$ cm, was used in the experiment. The airfoil spanned the whole width of the tunnel. In the whole set of measurements the airfoil was placed at the open end of the tunnel, in order to avoid the influence of the vortices image from the upper and lower wall of the tunnel, which may introduce some extra complications. As a price, the two dimensionality provided by the two side walls is lost which may reduce the intensity of the perturbation signal. But since we are measuring along the centerline the symmetry in the horizontal (spanwise) direction is preserved.

The airfoil was forced to oscillate in a uniform flow with Reynolds number to the order of 10^5 , based on the airfoil chord. It is hinged at the trailing edge, at the two ends of its span. The unsteady streamwise velocity component, as well as the mean velocity were measured both along and across the wake. The reduced frequency ranges from 0.9 to 10. A measurement of the steady near wake was also made. Some interesting features, such as the "potential wake" as discussed in chapter 2, were observed.

Transition of the boundary layer may occur at a certain Reynolds number. It is likely that the transition point will move to and fro accompanying the oscillation of the airfoil,

[†] More precisely, the mechanism of the numerical modelling is based on the classical theory. For the shed vorticity convection, however, we are not limited with the uniform velocity U_0 as assumed in the classical theory. In some cases we assume a convection velocity which is a function of the distance from the trailing edge of the airfoil.

introducing another uncertain factor in our problem. To avoid this, the airfoil was tripped with a plastic zig-zag tape at 30 mm distance from the leading edge, on both sides, to ensure a fully developed turbulent boundary layer. A check with a microphone in the boundary layer, at the usual Reynolds number we operate, confirmed this effort.

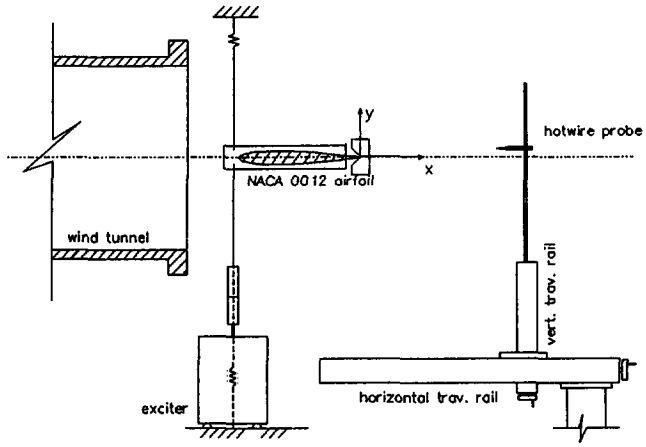
4.2 The Experiment

An overview of the experimental set-up is shown schematically in figure 4.1. The inner cross section of the wind tunnel measures 40*40 cm. A standard NACA 0012 airfoil, with chord length $c=15$ cm, was used in the experiment. The airfoil spanned the whole width of the tunnel. In the whole set of measurements the airfoil was placed at the open end of the tunnel, in order to avoid the influence of the image vortices from the upper and lower wall of the tunnel, which may introduce some extra complications. As a price, the two dimensionality provided by the two side walls is lost which may reduce the intensity of the perturbation signal. But since we are measuring along the centerline the symmetry in the horizontal direction is preserved. The experiment was conducted at the Reynolds number of order of 10^5 based on the airfoil chord, and in the reduced frequency range from 0.9 to 10.

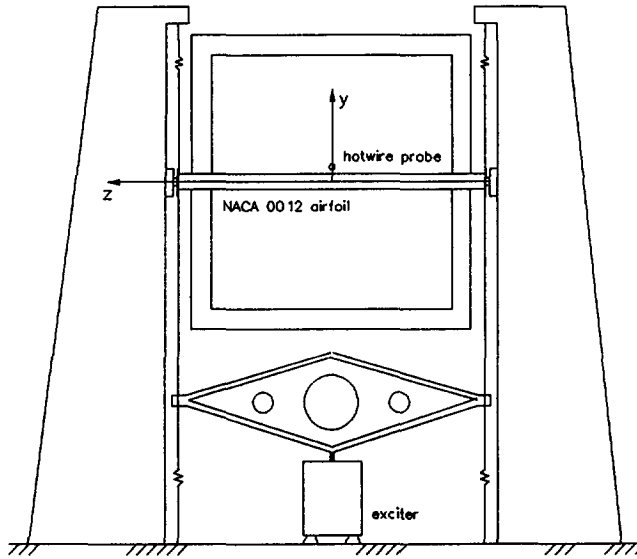
The airfoil is forced to perform a pitching oscillation about its trailing edge. The reason why we choose the pivot at the trailing edge is to minimize the undulation of the wake in the vertical direction. The driving of the oscillation is provided by a Brüel & Kjær vibration exciter, type 4809. The exciter has a frequency range from 10 Hz to 20 kHz. The maximum displacement the exciter can reach is 8 mm, peak-to-peak.

The oscillation of the exciter is controlled by a Prodera digital frequency generator (*Générateur Numérique*), GN484, which guarantees a harmonic distortion $\leq 0.7\%$ and noise-to-signal ratio ≤ 60 db. The frequency range of the generator extends from 0.100 to 1999.999 Hz.

A Brüel & Kjær power amplifier (type 2706) is used to amplify the signal produced by the frequency generator, before it is transmitted to the vibration exciter. The frequency range of the power amplifier is from 10 Hz to 20 Khz. The harmonic distortion is specified to be less than 0.2% in the frequency range 20 Hz to 10 Khz.



a). side view.



b). rear view.

Figure 4.1 An overview of the experimental set-up.

The measurement arrangement is shown in figure 4.2. Data acquisition and storage were executed with a HP-1000 laboratory computer. The oscillation of the airfoil is measured with an Endevco piezo-electric accelerometer, type 2220c mounted at one of its ends, 30 mm from the leading edge. Its frequency response is in the range from 5 Hz to 10 kHz. The amplitude range is from 0 to 5000 times the gravitational acceleration.

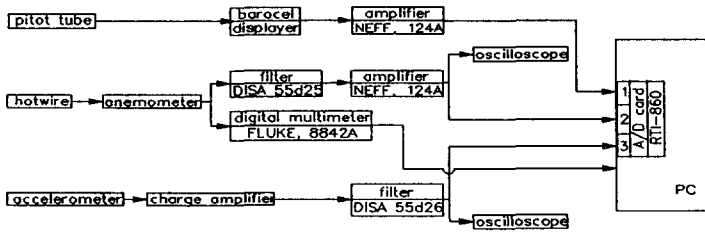


Figure 4.2 Schematic drawing of the measurement arrangement.

The electrical signal of the acceleration is amplified with an Endevco charge amplifier, model 2721A. The signal is then filtered with a Disa 55d26 signal conditioner. The frequency range of which is from 0 to 1 MHz, selectable in steps of 1/3 octave. The processed signal is simultaneously monitored with an oscilloscope, and transmitted to the third channel of the A/D card (Analog Devices, RTI-860), where it is sampled. The sampled data are stored in the extended memory of the laboratory computer.

For the measurement of the (perturbation) velocity of the flow, a single-wired hot wire was used. The hot wire was manufactured in the Low Speed Laboratory. Its sensitive part has a length of 1 mm, and a diameter of 5 μm . The hot wire probe was supported with a sting, which held it at the centerline with respect to the extension of the two vertical walls of the tunnel. The traversing mechanism made it moveable in both the x- (streamwise), and the y- (perpendicular to x and the span, pointing upwards) direction, see figure 4.1.

The hot-wire was connected to a linearized constant temperature hot-wire anemometer, as described in Miller [23]. The frequency response of the anemometer is in excess of

100 kHz for the bridge, and 7.5 kHz for the linearizer. In order to achieve a higher resolution of the unsteady part of the velocity signal the output from the anemometer was split into two parts, namely, a DC part which is measured by a digital multimeter (Fluke, 8842A), and an AC part that goes through a Disa 55d25 bandpass filter. The measurement of the DC component was directly fed to the Laboratory Computer via the IEEE-488 interface. The filtered signal of the unsteady part of the velocity was amplified with a NEFF 124A wideband differential amplifier. It was then fed to the second channel of the A/D card, and sampled in a like manner as that for the acceleration signal. The AC part of the velocity signal is also monitored with an oscilloscope as it is being sampled at the laboratory computer.

The tunnel speed was measured with a Pitot tube mounted in front of the airfoil. The Pitot tube was connected to a barocell (Datametrix, type 572), where the pressure was transformed into an electrical signal. The signal was fed to the first channel of the A/D card after it was amplified (NEFF, 124A).

Data acquisition of channels 2 and 3 was executed simultaneously with the A/D card, installed in the Laboratory Computer. The sampling rate can be as high as 62.5 kHz (8 bits), 60 KHz (12 bits). The sampling of the pressure signal was done separately.

4.3 The Study of the Near Wake for an Airfoil at Zero Angle of Incidence

The near wake distinguishes itself from the far wake in a number of aspects. First of all, in contrast to the case of the far wake, the presence of the solid body gives rise to a non-negligible perturbation to the pressure field of the uniform flow in the range of the near wake. The perturbation subsides as the distance from the body is increased. Therefore, distinct from the study of the far wake (Schlichting [29]), in the consideration of the momentum balance, pressure differences must be taken into account. This feature arises from the 'potential aspect' of the flow, since in a far field view the body can be represented with a dipole in the uniform flow. Secondly, as was noted in the last chapter, the outer and inner flow in the near wake region involves a stronger interaction compared to what happens in the far wake. So that we expect a different development of the near wake. In view of these peculiarities, the study of the steady near wake is of interest. In the present study, it moreover serves as a preparation for the unsteady near wake measurement.

In the present measurement the airfoil was mounted at zero angle of incidence near the open end of the tunnel. The distance from the tunnel end to the leading edge of the airfoil is 100 mm. The Reynolds number based on the airfoil chord length was $O(10^5)$. The wake traversing was done in the range of 1 ~ 100% chord length behind the trailing edge, in the streamwise direction. In the vertical direction the traverse ranged from -50 to 50 mm, with $y=0$ taken at the wake centerline (figure 4.1a).

In relation with the unsteady near wake measurement that is to follow, we are interested in the flow geometry. Since we are to measure the perturbation velocity in the 'potential' part of the flow, we need to know the lateral dimension of the wake. Tripping the boundary layer with a zig-zag tape appears to be not so uniform as with sand paper. So we wish to know whether this will give rise to asymmetry of the wake flow. Also, since the measurements are conducted in an open jet, we should like to

know the two-dimensionality of the wake. This information is relevant for the interpretation of the unsteady measurements.

Mean velocity profiles of the streamwise component were measured in 5 different streamwise stations. It was found that, extending from the trailing edge of the airfoil, the wake slightly curled up with a rate of about 5% with respect to the chord length of the airfoil. Since the later measurements are to be conducted in a short range (1 ~ 2 chord) from the trailing edge, this would not give much of a problem. Shifting the wake centerline back to $y=0$, we obtain the mean velocity profiles shown in figure 4.3. It is clear that good symmetry of the flow with respect to the wake centerline is attained. Hence, it can be concluded that though the teeth of the zig-zag tripping tapes on the two sides of the airfoil are somewhat arbitrarily spaced (with respect to each other), it does not actually affect the mean velocity profile in the wake. This can also be seen in the profile of velocity fluctuation later in this section.

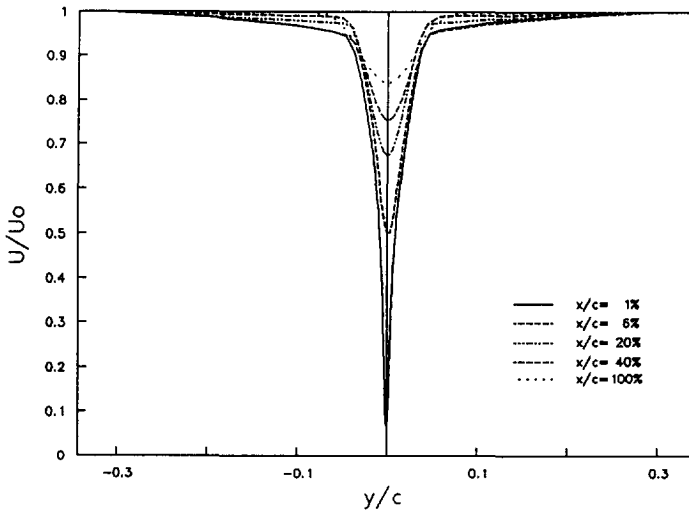


Figure 4.3 The symmetry of the velocity profiles measured at different streamwise stations.

We notice from the profiles in figure 4.3 that the near wake, at least in the range of our

measurement, can be distinguished into two parts, namely, an inner wake and an outer wake. Clearly, the velocity defect and the velocity gradient, dU/dy , in the inner region are much larger than in the outer region. The large velocity gradient in the inner wake indicates that the shear stress in this region will also be large. In view of the small velocity gradient in the outer wake we expect that the flow here is more of an inviscid nature.

In fact, the small velocity defect in the outer part can be identified to be due to a potential wake as referred to in chapter 2, the velocity and/or pressure perturbation being the result of the finite thickness of the airfoil. Writing the surface contour of the airfoil with function $y = \pm y(x)/2$ with reference to the chordline $y = 0$, in order to satisfy the no-penetration condition in a uniform flow with velocity U_0 , we then find that the airfoil can be represented with a source distribution, $q(x) = U_0 y'(x)$, along the chordline (Steketee [30]) (figure 4.4).

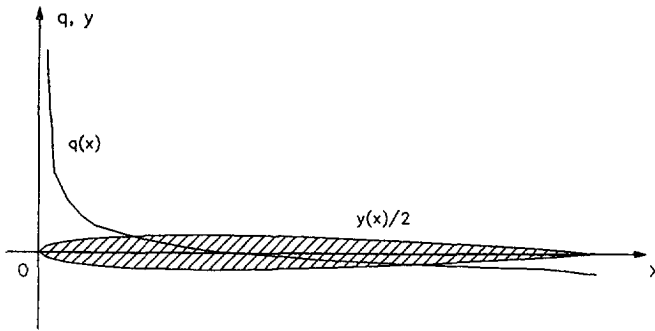


Figure 4.4 Representation of the thickness of an airfoil with a source-sink distribution.

The net flux through a circuit which encloses the distribution has to be zero, since the body is finite. This, in a far field view, is in effect a dipole located on the chord, with its axis along the chordline pointing against the uniform flow. To quantify this, a numerical calculation was made for a parallel flow past a NACA 0012 airfoil at zero angle of incidence. The calculation was based on an algorithm for inviscid flow devised

in Moran [25]. The calculated (potential) velocity profile is in fairly good agreement with the measured one in the outer region as can be seen in figure 4.5 ($x/c=6\%$). The discrepancy (the measured value is larger than the calculated one) can be attributed to the displacement effect of the viscous flow (boundary layer and the wake). The thickening of the wake is equivalent to distributing a source layer on the wake centerline. This introduces a net mass flux into the outer flow. In order to maintain mass balance the flow velocity would have to be larger outside the wake.

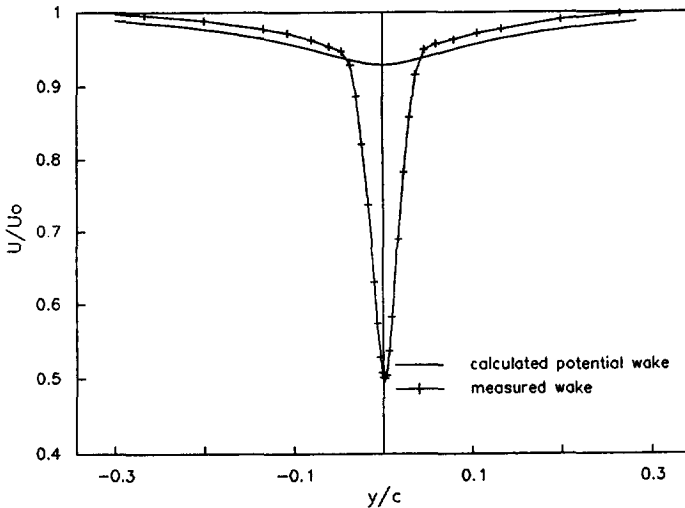


Figure 4.5 A comparison of the calculated potential wake and the measured wake ($x/c=6\%$).

We understand that in figure 4.3, the velocity measured near the wake centerline in the very close neighbourhood ($x/c=1\%$, for instance) of the trailing edge might be inaccurate. Because the mean velocity of the flow, U , is very low in this region, the velocity fluctuations, u' , can be of the same order of magnitude. The measured value of the mean velocity at this locality includes the velocity fluctuation, since the hot-wire anemometer cannot distinguish the direction of the flow. In fact the histogram of the measured velocity fluctuation is not a Gaussian distribution as normally would be observed in the region further downstream. Nevertheless, the general trend of the curve

indicates that in the very close range from the trailing edge, the velocity profile is in effect a merging of the two turbulent boundary layers from the two sides of the airfoil. Similar features last up to $x/c=5\%$, where a normal wake velocity profile starts to appear. This fact suggests that, phenomenologically, the transition from wall boundary layer structure to free shear layer takes place in the range from 0 to about 5% of the chord length.

To study the self similarity characteristics of the wake velocity profile, a length scale, *half-wake-width*, was introduced. This scale is defined as the distance between two points on a velocity profile at which the velocity defect recovers half of its (local) maximum at the centerline of the wake. The half-wake-width is not a constant along the wake. It changes as the wake develops in the streamwise direction. The growth of the half-wake-width is found to be approximately proportional to the fourth root of the distance from the trailing edge, in agreement with the result reported in Chen and Ho [9] (figure 4.6).

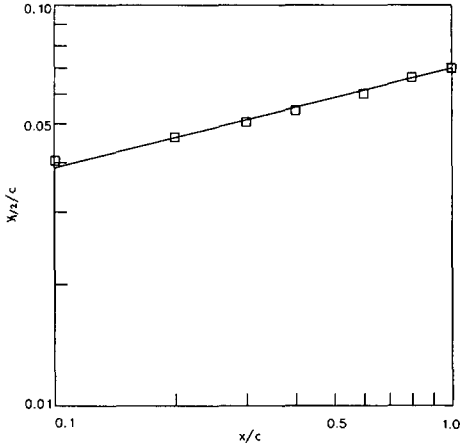


Figure 4.6 The growth of the half-wake-width.

In figure 4.7 we show a plot of velocity defect, scaled with the local maximum defect $U_0 - U_{min}$, where U_0 is the free stream velocity, versus the y -distance, scaled with half-

wake-width $y_{1/2}$. It appears that for the inner viscous wake, self-preservation of the velocity profile is reached in a distance between $x/c=10$ and 20%. For the outer potential wake no self-preservation is observed in the range of our measurement. This fact indicates that the development of the velocity profile in these two regions follows different mechanisms.

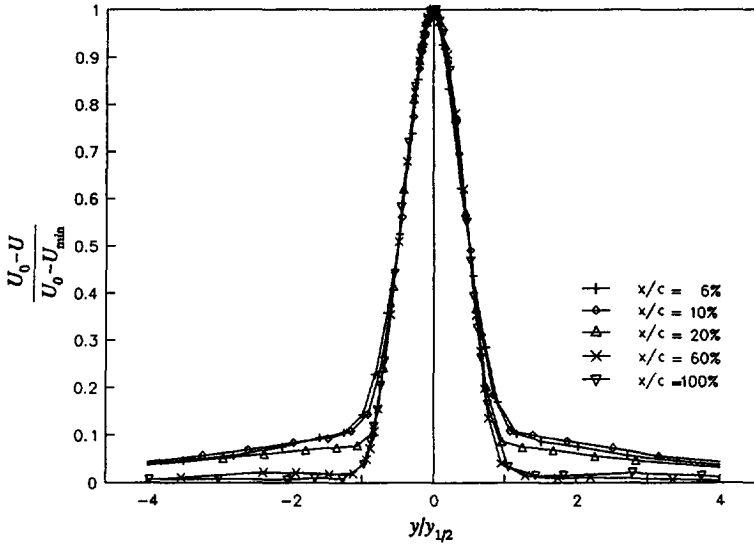


Figure 4.7 Self-similarity of the velocity profiles in the viscous wake. The deviations in the outer part of the wake are attributed to the different mechanism of wake development.

The turbulent velocity fluctuation is defined as the root-mean-square value of the fluctuating part of the velocity signal and is one of the points of interest. In the present study, with the single wire anemometer we measured only the fluctuation component in the mean flow direction. Shown in figure 4.8 is a plot of the velocity fluctuation measured at 5 different streamwise stations. The fluctuation is scaled with the local maximum velocity defect, and the distance in y -direction is scaled with the local half-wake-width. The symmetry of the profile suggests that the tripping on the two sides of the airfoil does not seem to affect the symmetry of the flow. The profiles are qualitatively in agreement with the measurement of Chen and Ho [9], obtained in a

closed wind tunnel. High intensity of fluctuation is mainly confined in a region which corresponds to the viscous inner wake. In the outer potential wake region the fluctuation is small. Self-preservation of the fluctuation profile is not observed in the range of our measurement.

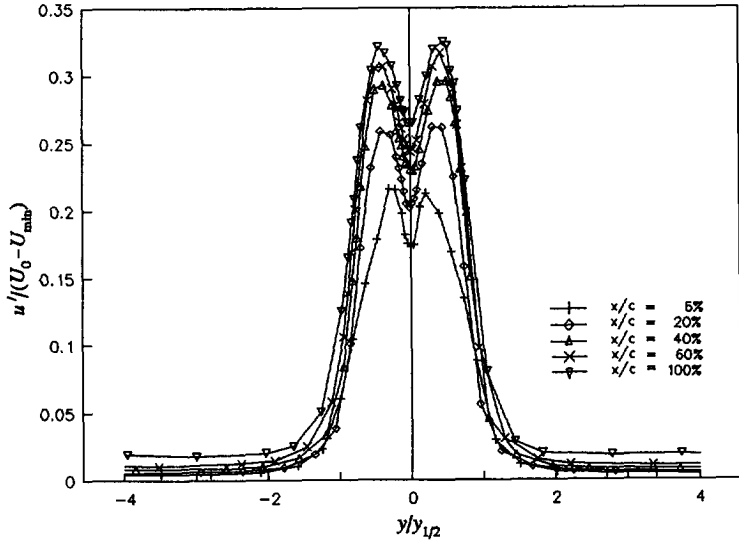


Figure 4.8 Velocity fluctuation profiles at several streamwise stations.

Since the experiment was carried out in a free jet, the two-dimensionality of the flow was uncertain. To check this, extra measurements were made. The measuring points for the checking traverse were shifted 40 mm horizontally (in z-direction) from the routine measurement points ($z=0$) in the spanwise direction. Figure 4.9 shows a comparison of the mean velocity profiles at station $x/c=100\%$ from the two sets of experiment. In this plot, the velocity was scaled with the corresponding outer flow velocity, and the y-distance was scaled with the corresponding half-wake-width. Small discrepancy in the velocity, at the highest of about 2%, is observed.

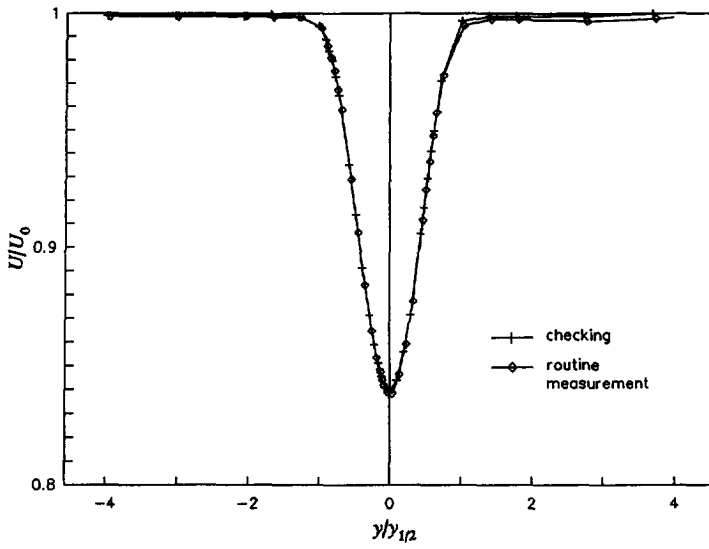


Figure 4.9 Check of two-dimensionality; mean velocity profiles at $x/c=100\%$.

Checking traverse is made at $z=40$ mm.

4.4 Experimental Study of the Periodic Flows

The experimental arrangement for the study of the unsteady motion of the airfoil is essentially the same as in the steady wake study. The mean angle of incidence of the airfoil is zero. The oscillation of the airfoil is driven with a B&K vibration exciter as described in section 4.2. The power transmission from the exciter to the airfoil is accomplished with two piano wires ($\phi 0.2$ mm), attached at the two ends of the airfoil (see figure 4.1). The amplitude of the oscillation of the airfoil was maintained to be small[†] ($\sim 0.1^\circ$). A small amplitude oscillation is also favourable in the sense that it may avoid the complication of the rolling-up of the vortex layer in the wake.

Accompanying the oscillation of the airfoil, the angle of incidence varies continuously with time. Consequently the bound circulation changes and free vorticity is being shed into the wake, as explained in chapter 2. It is the time dependent variation of bound vorticity and the accompanying vortex shedding that determine the unsteady perturbation to the flow. In the present experimental study we are to measure this unsteady perturbation of velocity and compare it with a numerical calculation based on the classical theory as described in chapter 2.

The motion of the airfoil and the velocity of the flow were measured with an accelerometer and a hot-wire anemometer respectively. The sampling frequency of these signals was kept to be 50 times the input frequency of the excitation in order to have a sufficient frequency reach (Bendat & Piersol [3]). According to the Nyquist sampling theorem, the upper limit of the signal filtering was correspondingly set. This is necessary because, if otherwise, harmonics with frequency higher than the Nyquist frequency will be mis-interpreted as low frequency harmonics (the aliasing effect).

[†] In the study of aeroelasticity problems, as Theodorsen's theory is chiefly concerned with, the amplitude of the oscillation is assumed to be infinitesimally small. But this is impractical in the experiment. Here we restrain the amplitude to be small, yet sufficient in yielding a detectable perturbation signal.

4.4.1 Calibration of the Motion of the Airfoil

The construction of the airfoil is described in full detail in appendix C. The material used is wood, in view of its favourable stiffness-to-weight ratio. The support and the loading condition of the airfoil in the oscillation is shown in figure 4.10.

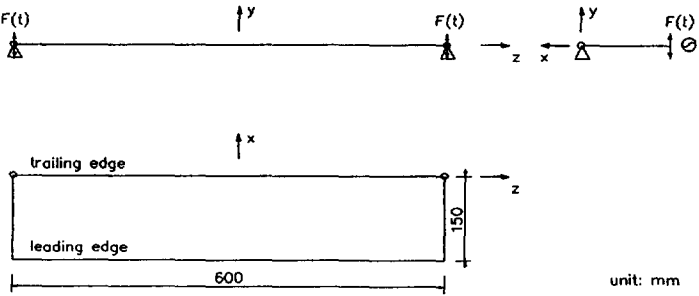


Figure 4.10 Perspective view of the support and the loading condition of the airfoil for unsteady motion. Forcing is applied at the two end points on the leading edge.

Due to the harmonic excitation $F(t) = A \sin \omega t$ the airfoil is undergoing a forced oscillation, with frequency ω . As a first estimate we may consider the airfoil as a beam which is forced to perform a harmonic oscillation $y(t) = -B \sin \omega t$ at its two ends. This motion results in inertia forces distributed on the beam. The force can in general be written as $R(z, t) = -m(z)y''$, where $m(z)$ is the mass distribution in the spanwise direction and y'' denotes the second derivative with respect to time. In view of the finite stiffness of the beam, the oscillation may be not constant in amplitude, or even in phase along the z -axis under the influence of the inertia forces. Of course, what actually happens depends on the frequency. However, we observe that if the damping of the structure is neglected, its vibration can only be in phase or in counter-phase. This is because for a linear, damping free system its eigenvalues and eigenvectors are real so that no phase shift can take place. When the two dimensionality of the airfoil cross section, and non-uniform mass distribution in the chordwise direction is taken into account, the above discussion should qualitatively be true, but more complications are involved.

In this connection the calibration of the dynamic behaviour of the airfoil appears to be necessary. For the numerical calculation the calibration provides a prescription of the actual mode of oscillation, so that appropriate comparisons can be made.

As mentioned in section 4.2, the motion of the airfoil is measured with an accelerometer fixed at one end of the airfoil, of a distance 30 mm from the leading edge. Knowing the frequency of oscillation, the displacement at the point on the airfoil can be calculated from the relation $y'' = -B\omega^2 y$. In the calibration, we use the output of this accelerometer as a reference. Another accelerometer is used to detect the motion elsewhere on the airfoil. Referring to the coordinate system ($x=0$ is at the trailing edge) indicated in figure 4.10, the calibration points are

Table 4.1 The coordinates (z,x) of the calibration points, (unit: mm).

(-300,-30)	(-150,-30)	(0,-30)
(-300,-70)	(-150,-70)	(0,-70)
(-300,-120)	(-150,-120)	(0,-120)

Measurements were made in terms of both the vibration amplitude and the phase with respect to the reference point (-300,-120). The results are presented in figure 4.11. The frequencies used in the calibration are the ones used in the subsequent experiments. With the formulation discussed above, it is not surprising to see that at low frequency of oscillation, e.g. 20 Hz, the amplitude and phase are essentially constant along the span. As the frequency is increased the inertia forces increase correspondingly, and the distortion of the displacement is also increased. This can be clearly seen in figure 4.11b, c and d. We observe that though the amplitude ceases to be constant, the vibration is in phase. At still higher frequency e.g. 120 Hz and 160 Hz, we see besides the distortion in some part of the airfoil the vibration is in counter-phase (separated with broken lines in the figures) with respect to the reference point. The fact that the vibration is either in phase or in counter-phase indicates that piecewisely (in spanwise

direction) the oscillation of the airfoil has a fixed nodal point. So that at every spanwise position a definite pitching oscillation can be determined. This will be important when two-dimensional strip model is to be applied. Also of importance, we point out that the calibration is consistent at different levels of forcing. This testifies to the linearity of the structure.

Lastly, we should like to make it clear that the kinks appearing in figures 4.11c through 4.11f are due to the limitation of the drawing programme which does not have a spline function, so that linear interpolation is applied.

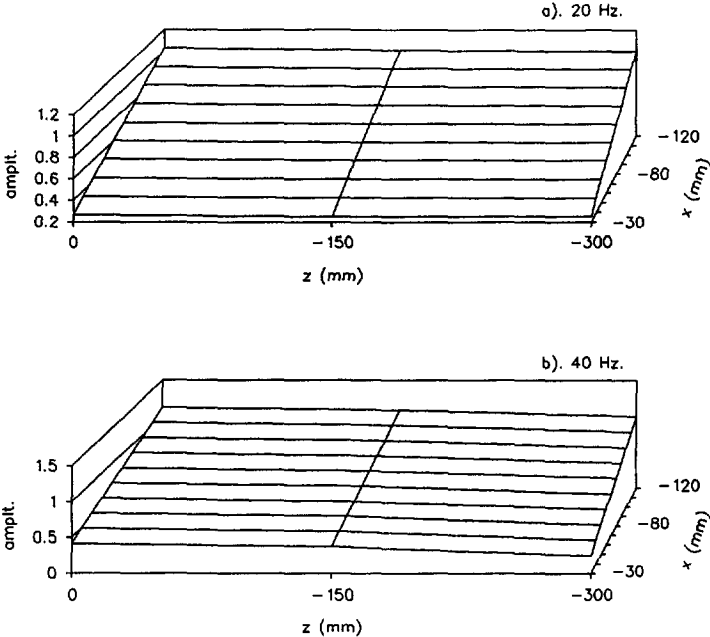


Figure 4.11(a,b) For caption see next page.

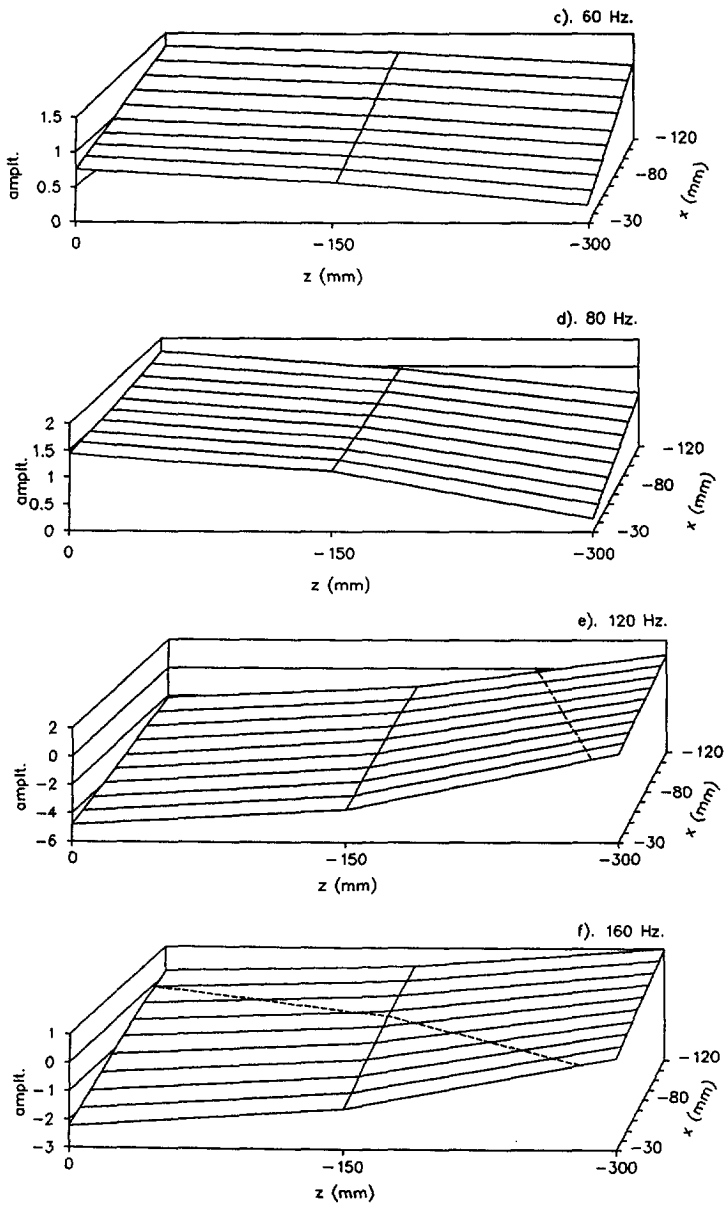


Figure 4.11 Amplitude of displacement calibrated with respect to the displacement at point (-300,-120). The sign difference on the two sides of the broken line in e). and f). shows the two parts are in counter-phase.

4.4.2 The Spectra of the Signals

The problem we are studying is unsteady. With the input of excitation (oscillation of the airfoil), there are various kinds of responses, e.g. vortex shedding, unsteady perturbation to the flow field, loadings, etc., while we are mainly interested in the velocity perturbation, i.e. the kinematics of the flow. We refer to the physics happening between the input and the output as a process. Generally, it can be stated that the process we are interested in involves the interaction of potential and viscous flow. A formal analysis of this process would be too difficult to be carried out. Therefore, in the present experimental study we approach the problem by studying the input and its response. In such a way we could infer some of the general properties of the process. Besides its intrinsic interest, this is also important for the interpretation of the results, and directing the study. A numerical frequency analysis was therefore made first to the recorded signals in order to study the harmonic composition.

The FFT algorithm used in the analysis is as described in Press *et al* [28]. The analysis was made to a registration with length of 41 periods of the first harmonic, i.e. 2050 data points. To meet the requirement of the FFT algorithm that the number of the input time series data be an integer power of 2, we took 2048 ($\approx 2^{11}$) data points. By doing so, an error is introduced. Quantitatively, the relative error amounts to 0.009% of the period of the first harmonic.

In figure 4.12 we show typical amplitude spectra of the fluctuating part (not the RMS value of it) of the velocity component in x-direction measured both outside and inside the near wake, and the corresponding amplitude spectrum of the acceleration of the airfoil. It is clear that for the velocity perturbation outside the wake, corresponding to an excitation of certain specific frequency there is a distinctive response in the first harmonic, no frequency shift is present. Higher harmonics, if any, can hardly be distinguished from the ambient turbulence. The same is true for the velocity measured inside the wake, though the signal-to-noise ratio is low due to the higher intensity of the turbulence.

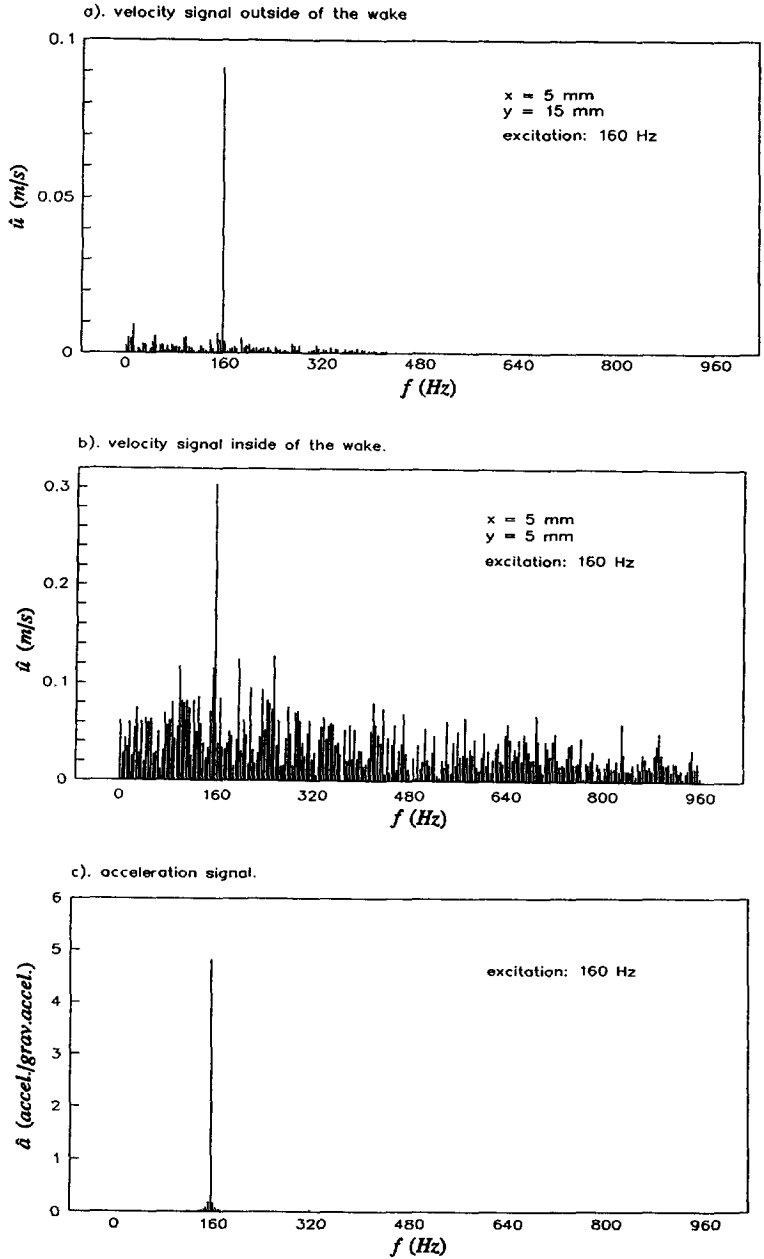


Figure 4.12 Typical amplitude spectra of velocity and acceleration signals.

This satisfies the additive property of a linear process ($f(x_1+x_2)=f(x_1)+f(x_2)$, where x_1 and x_2 are the inputs). The homogeneous property ($f(cx)=cf(x)$, where c is a constant and x is the input) will be shown in paragraph 4.4.3. In what follows we shall concentrate on the first harmonics of the velocity perturbation.

4.4.3 The First Harmonic Velocity Perturbation

The information of the first harmonic velocity perturbation was obtained by fitting the measured velocity signal with a harmonic wave of properly selected frequency. An average over 20 to 40 periods was made at each of the measuring points.

To gain some insight of the mean flow condition for the case where the airfoil is performing a small amplitude oscillation, velocity profiles of the streamwise component in the unsteady near wake was measured. The result from a measurement is shown in figure 4.13.

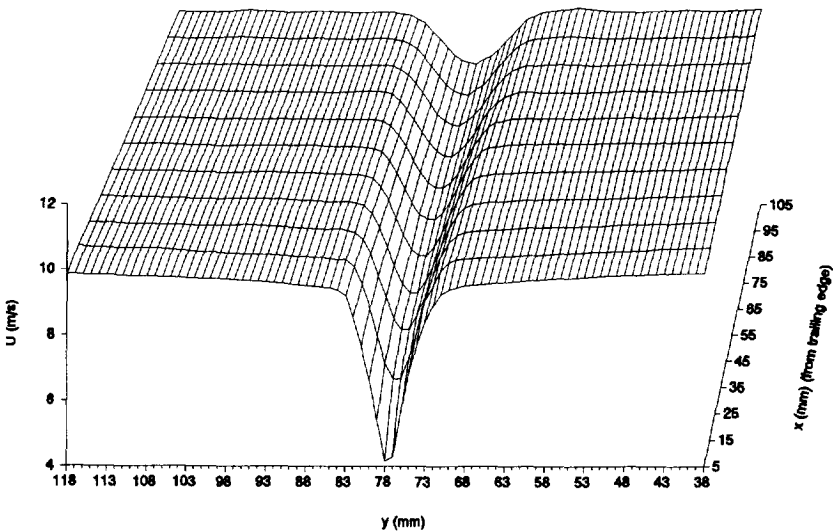


Figure 4.13 The mean velocity profile of an unsteady wake. Trailing edge is at $y=78$ mm here.

In this measurement the uniform flow velocity U_0 is 10 m/s, and the oscillation frequency of the airfoil is 160 Hz. Comparing with figure 4.3 (velocity profiles of a steady wake), qualitative resemblance is evident. In figure 4.13 the profiles appear to be nicely symmetric, suggesting that the mean angle-of-incidence of the airfoil is zero. It also appears that no large scale boundary layer separation occurs.

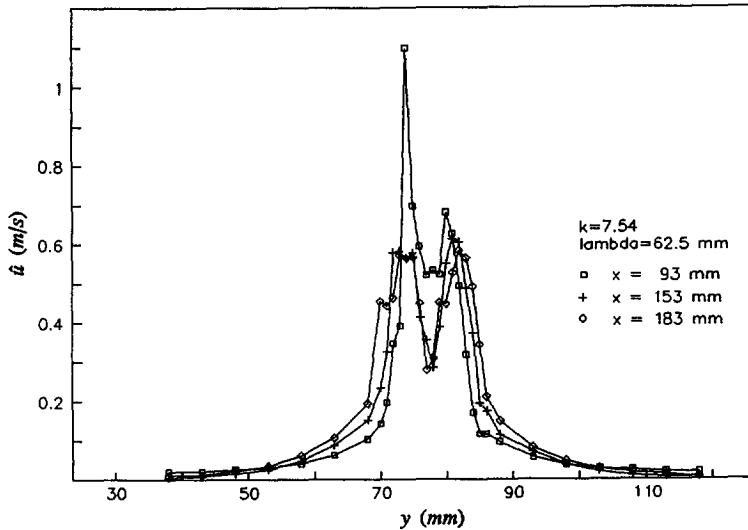


Figure 4.14 The amplitude of the harmonic velocity perturbation versus the distance from the wake centerline. Trailing edge at $x=78$ mm, $y=78$ mm in the present plot.

The viscous wake is the region where shed vorticity is contained. The shed vortices are assumed to induce a velocity perturbation in the space according to Biot-Savart's law. It is therefore expected that closer to the wake (but still in the 'potential' region) the velocity perturbation due to the vortices would be stronger. The perturbation should decrease as the distance from the wake is increased. Figure 4.14 shows the amplitude of the first harmonic of the velocity perturbation obtained from the vertical traverse. It is clear that when measuring closer to the wake the amplitude of the perturbation becomes larger, as was expected. The results measured inside the wake are not quite reliable because of the high intensity of turbulence noise which may account for the

abnormal shoot-up at the edge of the viscous wake.

The wake thickens as the distance from the body is increased, as a result of momentum diffusion. Imagine the wake as a vortex sheet, when traversing in the streamwise direction at a constant y-elevation, effectively it would appear that the hotwire probe is closer to the sheet at a larger distance downstream. Therefore the measured perturbation would be larger. This effect can be seen in figure 4.14: outside of the wake, at the same value of y the perturbation amplitude is larger for measurement further downstream.

In the frequency analysis discussed in the previous section we have shown that the frequency correspondence between the excitation and the velocity perturbation is one to one, no frequency shift is present. Upon this fact it was observed the present process satisfies the additive property. As promised, we are to show the homogeneous property of our process here. For this purpose, we refer to figure 4.15.

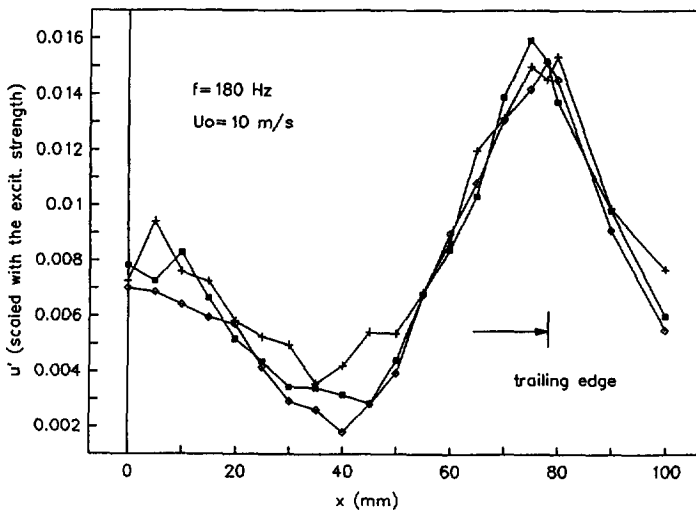


Figure 4.15 The linear dependency of the perturbation on the strength of excitation. Trailing edge is at $x=78$ mm in this plot.

The three curves in this figure represent the harmonic perturbation amplitudes from three sets of measurements. The reduced frequency and the Reynolds number were kept to be identical in all the 3 sets of measurement, except that the strength of the excitation (the oscillation of the airfoil) was adjusted to different levels with ratio of about 1:2:3. Presented in this graph, the harmonic velocity perturbation amplitudes are scaled with the corresponding strength of excitation (amplitude of the airfoil oscillation). It appears quite clearly that with such a scaling, the three curves are fairly well reduced to a single one. This furnishes the homogeneous property of the process. Therefore, we can conclude that the process we are concerned with is a linear one in the range considered. This is quite a remarkable observation, since in a fluid flow higher harmonics might be introduced through the non-linear convection terms in the equations of motion. But apparently this is not the case in our problem. This observation is also relevant to the study of aeroelasticity problem in the sense that experimental studies can be related to the theoretical ones by way of linear extrapolation.

Besides the amplitude of oscillation of the airfoil, there are two other parameters relevant to the experiment, namely, the reduced frequency, k , and the Reynolds number, Re . The reduced frequency is defined as $k = \omega c / 2U_0$ and can be interpreted as a parameter representing the ratio between the chord length of the airfoil and the linear wave length $\lambda = U_0 T$. So that, in a way, the reduced frequency gives an indication on the distribution of the shed vortices in terms of a vortex wave. In view of the mechanism following which the velocity perturbation is generated, it is to be expected that the reduced frequency is more relevant to the velocity perturbation in the space than the Reynolds number. This argument is in agreement with the experimental results as shown in figure 4.16. In this experiment, two sets of streamwise traverse were made. The oscillation frequency of the airfoil was set at 80 and 160 Hz respectively. The flow speed was adjusted accordingly, in order to keep the reduced frequency unaltered. But due to the difficulty in the setting of the tunnel speed, instead of 14 m/s we had 14.1 m/s for the 160 Hz measurement. In the graph, the amplitude of the velocity perturbation was scaled with its value at the trailing edge. The similarity of the two curves demonstrates the dependency of velocity perturbation on the wave structure of

the shed vorticity in the wake.

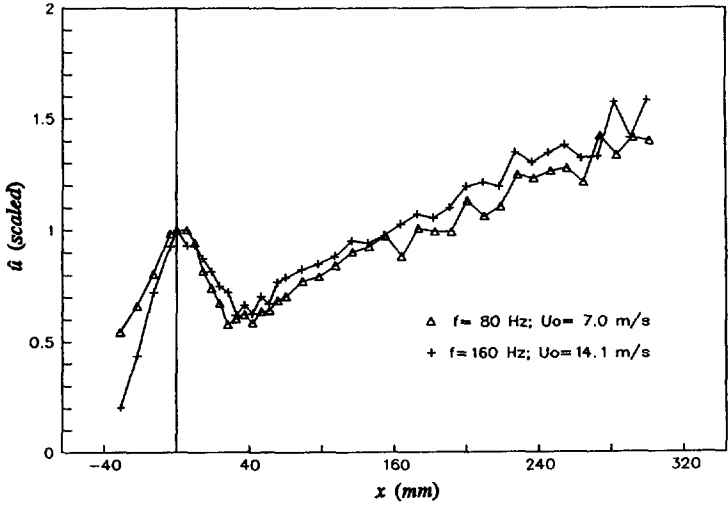


Figure 4.16 The relevance of the reduced frequency to the velocity perturbation.

4.5 The Viscous Effect on Vorticity Convection

In figure 4.16, we notice that the amplitude of the velocity perturbation shows a peculiar behaviour as one traverses in the streamwise direction. Distinctively, there is a maximum occurring in the neighbourhood of the trailing edge, and a minimum at less than a linear wave length, $U_0 T$, downstream. In fact, the same feature is found to happen in the whole parameter range we measured, though the magnitude of the amplitude defect (the depth from the maximum at the trailing edge to the minimum on the curves) is different for different reduced frequencies. The observation of the relevance of the reduced frequency to the velocity perturbation, made in the last section, is of great importance. In terms of the interpretation of the reduced frequency that $k \propto \text{chord length/wave length}$, we recognize the dependence of the perturbation on the structure of the vortex wave. Therefore, it is expected that from the measurement of the velocity perturbation in the outer flow, one may be able to infer the vortex wave in the wake.

In line with this, we base the interpretation of the experimental results on comparisons with those from numerical calculations which is modelled according to the principle of the classical theory of Theodorsen as discussed in chapter 2. The numerical calculation serves here as a reference. The calculation is realized with a panel method which is described in detail in chapter 5. However, to facilitate the discussion in the remainder of this chapter we give here a brief summary for the calculation procedure. In the numerical calculation the airfoil was replaced with a flat plate. The plate was divided into a number of panels on which vorticity distribution is to be calculated so as to satisfy the flow tangency boundary condition. The vorticity shedding due to the unsteady motion of the plate is determined by the Kutta-Joukowski condition which requires that the loading at the trailing edge be zero. The convection of the shed vorticity is assumed with the uniform velocity U_0 along the centerline. The strength of the vorticity distribution over the wake element is $\gamma = -\delta\Gamma/\delta s$, where $\delta\Gamma$ is the change of bound circulation between two successive time steps, and $\delta s = U_0 \delta t$ is the length of the wake element. The velocity perturbation in the flow is calculated by taking into

account the contributions from both the bound and the shed vorticity. The points at which the perturbation is to be calculated is coordinated in accordance with the ones in the experiment.

4.5.1 Some Consideration of the Flow Conditions

According to the calibration, the shape of oscillations of the airfoil at different frequencies was determined (cf. figure 4.11). Based on this, numerical calculations were made to compare with the experimental results. Before we go into the detailed discussion of numerical-experimental comparison, a few remarks should be made.

As mentioned in section 4.2, we notice that the experiment is conducted in a jet. The usual two-dimensionality assumed for experiments inside wind tunnels is some what affected, since the side walls which act as mirrors extending the finite span to infinity do not exist in our experiment. Therefore, in the interpretation of the experimental results the effect of three-dimensionality should be taken into account.

Three-dimensionality of the airfoil problem addresses itself to the particular feature of trailing vortices (Prandtl & Tietjens [27]). The trailing vortices have two effects, namely, the modification of the bound circulation and the induced drag. Both arise from the perturbation of the upwash field due to the trailing vortices. These effects are accounted for in the lifting line theory. In Steketee [30] it can be found that for the quasi-steady case, an airfoil with aspect ratio $A=b/c$, where b is the length of the span, the lift coefficient is modified by a factor $(1+2/A)^{-1}$ in an infinite expanse of uniform flow. As a consequence, we can expect that the results of calculations assuming two dimensionality at the mid-span would be larger than the measured ones. The three-dimensionality effect, however, would become smaller with increasing reduced frequency.

Three-dimensionality enters in another way, namely, the finite stiffness of the airfoil

in the spanwise direction. Due to the non-constant amplitude of oscillation at higher frequency (figure 4.11), we expect that the bound circulation will vary along the span. This will also give rise to a situation which is similar to that in the lifting line theory, where trailing vortices are known to be distributed in the spanwise direction (horseshoe vortices), the rotational axis of the trailing vortices being in the direction of the flow. In view of the fact that the direction of the trailing vortices is perpendicular to the rotational axis of the shed vortices (which is in the direction of the span) and the symmetry at the mid-span, we assume that the perturbation velocity component in the flow direction is not directly affected by the trailing vortices. Indirectly the trailing vortices have an effect on the upwash field as discussed in the previous paragraph.

In view of the three-dimensionality mentioned above, the absolute value of the velocity perturbation may be influenced (with respect to the two-dimensional numerical calculation). To have a relevant comparison, we shall normalize both the measured and the calculated perturbations with their corresponding values at the trailing edge.

In the numerical calculation, we shall calculate the velocity perturbation with the strip assumption at the mid-span (assuming the airfoil is infinitely long in the spanwise direction, and is performing rigid body oscillation with the mid-span strip). This is justified in view of the symmetry of the configuration.

4.5.2 The Viscous Effect on Vorticity Convection

Consideration of the actual flow conditions, and the possible consequences on the measured velocity perturbation have been discussed in paragraph 4.5.1. We now proceed to the analysis of the velocity perturbations that come from both experimental measurement and numerical calculation. In the numerical calculations we adopt the strip argument at the mid-span. A proper definition of the mode of oscillation of this spanwise strip is based on the calibration of the airfoil as described in section 4.4.1.

The trailing edge has a unique importance in wing theory. It is at the trailing edge where the Kutta-Joukowski condition is applied. It is also in this neighbourhood where the shedding of vorticity occurs; the boundary layers join in the wake. For this reason, we pay attention to the behaviour of the velocity perturbation in this particular region. The peculiar maximum of the velocity perturbation at the trailing edge, observed in both the experimental traverse (figure 4.16) and the numerical calculation, to be shown later in figures 4.17 and 4.18, is intriguing. A comparison between the measured and the calculated magnitude of the maxima was made. The results are listed in table 4.2[†]. The general trend appears to be clear. At low reduced frequency, the discrepancy between the experiment and the linear calculation ($1-u_{\text{exp}}/u_{\text{cal}}$) is small. In view of the discussion in paragraph 4.5.1, the discrepancy can to certain extent be attributed to the effect of the trailing vortices due to the three-dimensionality. As the reduced frequency is increased, however, the discrepancy increases consistently. At the highest reduced frequency studied ($k=9.54$), the measured maximum perturbation amplitude at the trailing edge is about 60% of that predicted by the classical theory. The argument of 'trailing vortices effect' does not seem to be able to explain this increasing discrepancy corresponding to the growth of the reduced frequency.

Accompanying the harmonic oscillation of the airfoil, the distribution of the trailing vortices (due to the three-dimensionality) is also sinusoidal in the streamwise direction. A higher reduced frequency implies a shorter length of the trailing vortex waves. As a result, the congregation of the short trailing vortex waves would have a limited effect on the upwash field of the airfoil. This is in a way similar to the memory effect of the shed vortices in the spanwise direction (in that case the memory effect tends to be independent of the reduced frequency when k is about 1, cf. chapter 2). With such a formulation, it appears reasonable to interpret the reduction of the maximum perturbation at the trailing edge as due to the viscous effect of the flow, of which the convection of the shed vortices and the satisfaction of the Kutta-Joukowski condition

[†] The absolute value of the velocity perturbation amplitude depends on the strength of the excitation, i.e. the amplitude of the airfoil oscillation.

are two factors we can think of. The discussion of the first will come up later. We will address here the second, since it is consistent with the observation of other researchers, e.g. Chen and Ho [9], in experiments with other principles (measurements of trailing edge loading, trailing edge streamline, etc.).

Table 4.2 Comparison of the perturbation amplitude at the trailing edge.

k	u_{cal} (m/s)	u_{exp} (m/s)	u_{exp}/u_{cal}
1.88	0.047	0.042	0.89
2.74	0.13	0.11	0.75
3.58	0.12	0.09	0.85
4.9	0.13	0.11	0.85
5.38	0.089	0.092	1.03
5.54	0.22	0.16	0.73
7.25 (120 Hz)	0.21	0.14	0.66
7.25 (160 Hz)	0.21	0.13	0.66
9.54	0.19	0.11	0.58

Comparisons of streamwise traverses of the amplitude of velocity perturbation were made with the numerical calculations assuming constant convection velocity of U_0 , adopting the strip assumption as mentioned in paragraph 4.5.1. The results are shown in figure 4.17, in which the vertical coordinate stands for the perturbation amplitude, and the horizontal coordinate represents the streamwise distance from the trailing edge of the airfoil. Both the experimental traverse and the numerical calculation were made at a y elevation that is $0.1c$ from the centerline of the wake. For both the experimental and the computational results, the amplitudes of harmonic velocity perturbation were scaled with the corresponding maximum values at the trailing edge. For each reduced frequency, the streamwise distance was scaled with the corresponding half-wave-length, $\lambda/2$.

We first note the point they (measurement and calculation curves) have in common. It

is immediately clear that the curves from both experiments and numerical calculations have a general similarity in shape. Following an observer travelling in the streamwise direction, we notice that upon approaching the trailing edge, the perturbation attains a maximum value in that neighbourhood. It then decreases when the streamwise distance from the trailing edge becomes large, until a minimum is reached at some distance. This unique feature deserves an interpretation.

In chapter 2 we studied the induced normal velocity component in the immediate neighbourhood of a source layer. The magnitude of the normal velocity component is found to be half of the local strength of the source distribution (equation (2.28)). This is true also for the induced tangential velocity component in the immediate neighbourhood of a vortex layer, since in a two-dimensional case the complex potential of a source would be that of a vortex if it is turned by $\pi/2^\dagger$. Such an ideal measurement (in the immediate neighbourhood of a 'vortex sheet') is apparently not applicable in a real situation, since what we have is a vortex layer of finite thickness. In the present experiment the measurement points have a finite distance from the wake centerline which, in a far field view, represents the position of the abstraction of a discontinuity layer.

Apparently, the finite distance will introduce influences from the neighbouring vortex elements. This can be seen quite well in the numerical modelling. On the projection of the airfoil on the x-axis, $-c \leq x \leq 0$, it is distributed with bound vortices which vary with time. The positive half of the x-axis is occupied with the shed vortex wave of constant amplitude (assuming that the shed vorticity is convected with a constant velocity). Observing in the neighbourhood of the trailing edge with a certain distance from the

[†] This can be done by multiplying the complex potential of the source with i ($i = (-1)^{1/2}$). In such a way the potential function of the source becomes the stream function of the vortex, and the stream function of the source becomes the (negative) potential function of the vortex. From the orthogonality between the potential and stream function it is immediately clear that the normal velocity component of the source becomes the tangential component for the vortex.

plane $y=0$, one sees a half-infinite vortex wave and the bound vortices near the trailing edge. Due to this kind of non-uniformity in the vorticity distribution, the magnitude of the perturbation would depend on both the observation point's distance from the vortex sheet, and its streamwise position. This partially explains the behaviour of the amplitude of the velocity perturbation observed above.

Further downstream, however, the effect of bound vortices fade away so that one sees locally an infinite vortex wave on the x -axis[†]. In such a circumstance, the magnitude of the perturbation would be independent of streamwise position of the observation point. What matters is only the distance from the observation point to the vortex sheet. This is clearly demonstrated by the damping-out of the amplitude oscillation at a larger distance down stream of the trailing edge in the calculated curves (figure 4.17).

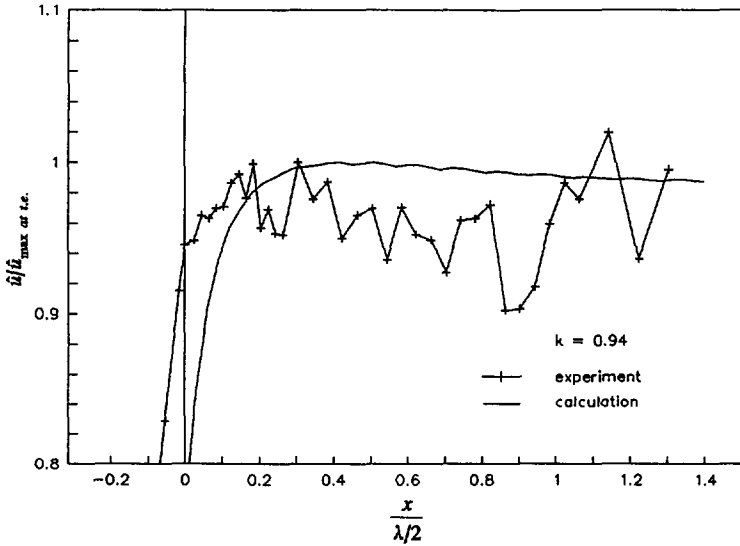


Figure 4.17 To be continued. For caption, see page 93.

[†] This depends on the observation point's distance from the vortex sheet. If the observation point is closer to the vortex sheet, then the 'fading away' is faster.

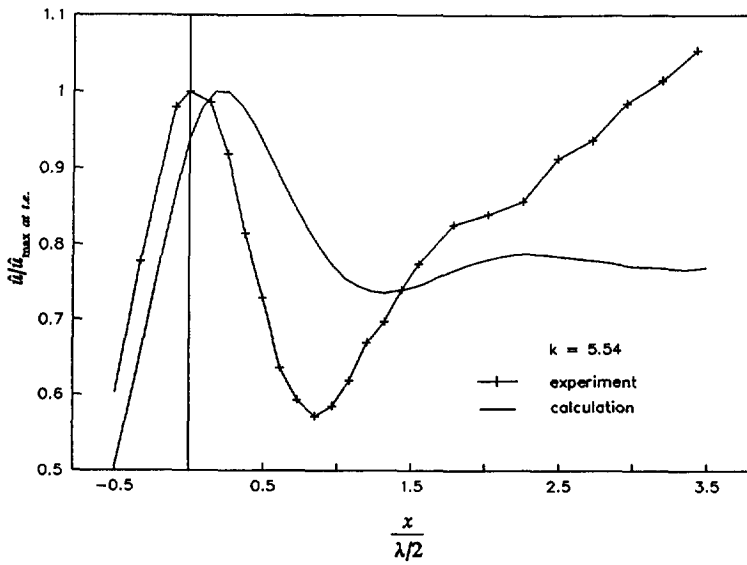
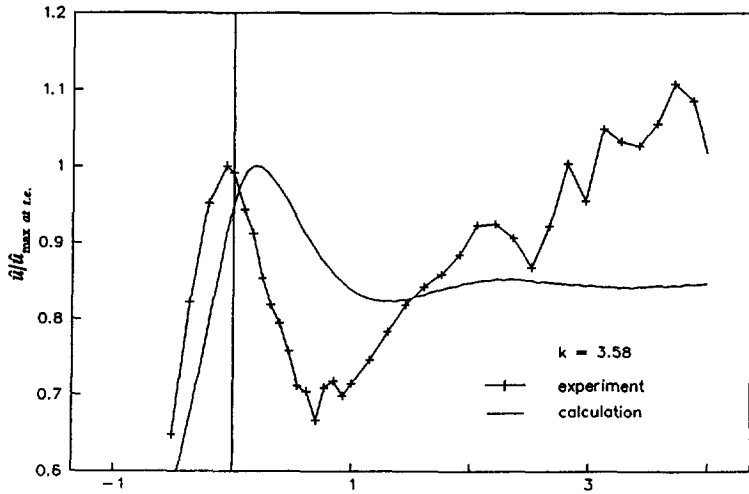


Figure 4.17 To be continued. For caption, see page 93.

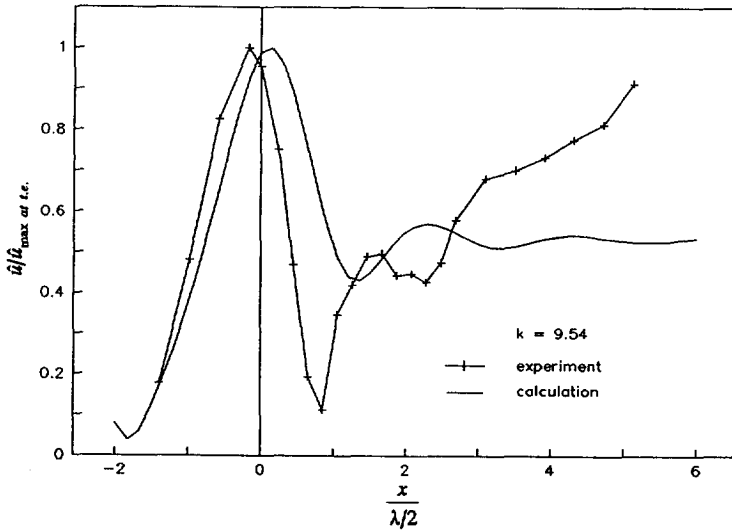
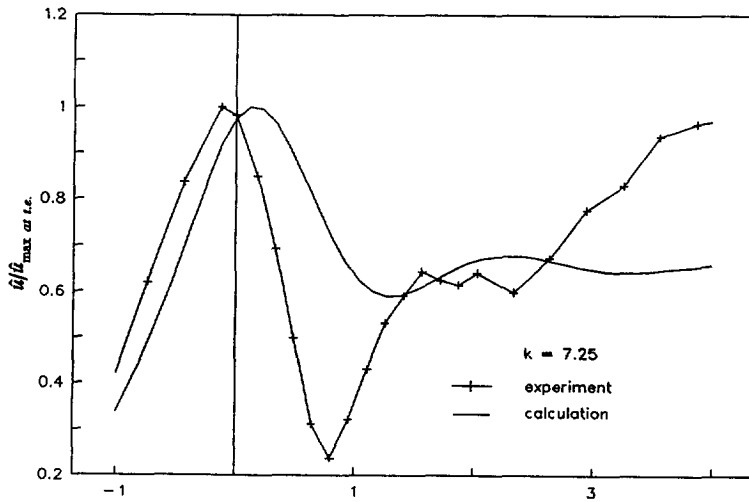


Figure 4.17 Comparison of the experimental and the calculated (assuming constant convection velocity) amplitude of velocity perturbation. Elevation of traversing, in both experiment and calculation, is at $y=10c\%$. Trailing edge of the airfoil is at $x=0$. $\lambda=U_0T$ is the wave length.

Referring still to figure 4.17, we now proceed to the analysis of the differences between the experimental and the calculated results. We notice three features that reflect the discrepancy between experiment results and the theoretical predictions assuming constant convection velocity, namely, 1). the experimental curves' increasing versus the calculated curves' approaching constant values; 2). the difference in the positions where the minima (the dip) of the perturbation amplitudes happen; 3). the difference in the depth of the dips measuring from the maxima at the trailing edge to the minima near the trailing edge. In what follows we shall discuss these separately.

4.5.2.1 The Difference in the Perturbation Behaviour at Larger Distance from the Trailing Edge

For the general behaviour of the curves shown in figure 4.17, numerical calculation predicts that after the occurrence of the minimum near the trailing edge, the amplitude of the velocity perturbation gradually approaches a constant value, though secondary oscillation is still observed in the range of our study. In the experiment, however, we observe in the same range of traversing the amplitude of perturbation shows a general increasing trend with the distance from the trailing edge. Corresponding to the secondary oscillations in the calculated results, we can still see comparable symptoms in the experimental curves, though they are somewhat submerged in the general increasing trend. In view of the discussion in section 4.4.3, this appears to be in agreement with the development of wake geometry. It is well recognized that as the distance increases the diffusion of momentum results in a thickening of the wake. For a traverse at constant elevation this implies that the hotwire probe comes gradually closer to the wake when travelling downstream. This results in an increasing amplitude with the distance in the measurement results (figure 4.14).

In view of the above discussion, we observe that the experimental and numerical results are in qualitative agreement. The similarity in the general behaviour of the two curves has a two-fold implication. It proves that the modelling assumed in the numerical

calculation is qualitatively correct. On the other hand, by such a judgement, the mechanism of the flow interaction is understood. Despite of this reassuring observation, there remain other clear discrepancies between the experimental and numerical results.

4.5.2.2 The Difference in the Position Where the Minima Occur

We notice in figure 4.17 that, systematically, with respect to the numerical prediction, the experimental curves are substantially shifted to the left, e.g. the minima of the velocity perturbation amplitude occur earlier than would be expected according to the numerical calculations (assuming constant convection velocity). So are the maxima of the perturbation amplitude at the trailing edge.

In order to explain this difference between the experimental and numerical results, we refer to figure 4.18.

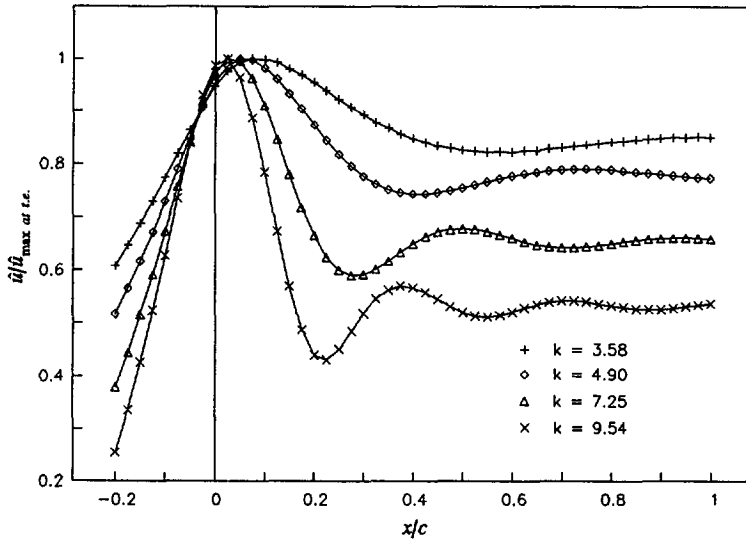


Figure 4.18 Calculated (constant convection velocity U_0) amplitude curves of velocity perturbation at different reduced frequencies. Trailing edge at $x=0$.

This figure shows the calculated perturbation amplitudes at different reduced frequencies. The vertical axis represents the perturbation amplitude scaled with the corresponding maximum value at the trailing edge. The horizontal axis represents the distance from the trailing edge, and is scaled with the chord length of the airfoil. We observe in this figure, that the curves with higher reduced frequency are shifted to the left (closer to the trailing edge) in a similar way to what appears in figure 4.17! From the discussion in section 4.4.3, we understand that the reduced frequency can in fact be interpreted as a parameter that represents the ratio of the chord length and the wave length of the shed vortices, i.e. $k \propto (\text{chord length}/\text{wave length})$. In other words, a larger reduced frequency corresponds to a shorter wave length. Therefore it can be concluded from figure 4.18 that corresponding to a shorter wave length, the amplitude curve of the perturbation is shifted more to the left, i.e. closer to the trailing edge. Therefore, observing the discrepancy in figure 4.17, we conclude that the wave length of the shed vorticity in an actual, viscous flow is shorter than what is assumed in the numerical calculation ($\lambda = U_0 T$). This is in fact equivalent to the statement that the shed vortices are not transported with the mean flow velocity U_0 , but that the convection is retarded.

4.5.2.3 The Difference in the Depth of the Dip

The third clear discrepancy between experimental and the calculated results based on classical theory is the amount of perturbation amplitude reduction, defined as $(u_{\max} - u_{\min})/u_{\max}$. In figure 4.17 we see that this discrepancy is consistent and quite appreciable. A similar feature is observed in figure 4.18, where we see that corresponding to shorter wave lengths (higher reduced frequency), the amount of amplitude reduction is larger. This is again a solid confirmation for the observation made earlier: in real flow the wave length of shed vortices is shorter than $\lambda = U_0 T$, or, the convection of the shed vortices is retarded with respect to the uniform flow velocity U_0 .

In figure 4.19 we plot the reduction of the perturbation amplitude as a function of the reduced frequency. We notice in this figure that though the amount of reduction in

experiment and calculation show the same behaviour of increasing with the reduced frequency, the rates of increase are appreciably different. It is clear that the reduction in the experimental results develops at a considerably faster rate than that predicted by the numerical calculation assuming constant convection velocity U_0 .

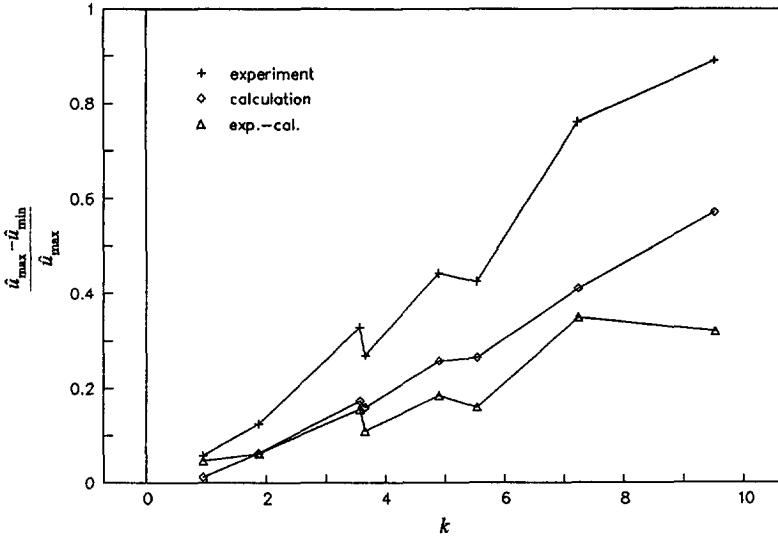


Figure 4.19 A comparison of the perturbation amplitude reduction.

Persistency of vorticity is well recognized. Therefore the extra amount of the amplitude reduction appears to suggest an interaction of vortex waves. In chapter 3 we conjecture that in view of the flow structure in the near wake, it is plausible that the convection of shed vorticity is conceived in a layered structure. In the outer part of the wake the velocity defect is less. So that the wave length of the shed vorticity would be not much different from $U_0 T$. We shall refer to this as the outer wave[†]. But in the inner part of the wake (near the wake centerline), the velocity varies strongly with the distance, so

[†] If one looks microscopically, there would be two such waves on the two outer edges of the wake. They are symmetric about the wake centerline in view of the antisymmetrical property of the lift problem (the velocity is antisymmetric, so that the unsteady part of the vorticity is symmetric). Therefore in what follows we shall make no distinction of these two.

that it is reasonable to expect that in this region the shed vortices would have a wave length which is shorter initially. As the distance from the trailing edge is increased, the length of the inner wave is gradually extended approaching U_0T . Associated with the unsteady motion of an airfoil in a viscous flow we then expect a two-wave structure for convection of the shed vortices.

It is clear that the measured curves shown in figure 4.17 consist of the contribution (vector sum) of the two vortex waves mentioned above. The inner wave, with its wave length varying along the wake, interferes with the outer wave, giving the extra amount of the amplitude reduction. To verify this conjecture, another set of numerical calculation was made to simulate the two-wave structure.

In this numerical procedure, the outer wave and its velocity perturbation in the flow field is calculated in the same way as described in the beginning of the present section (constant convection velocity U_0). For the inner wave, the principle of the numerical modelling is essentially the same as for the outer wave, only the convection velocity of shed vorticity is assumed to be a function of the distance from the trailing edge. It starts with zero value at the trailing edge, and gradually increases to the value of the undisturbed flow velocity. In such a way the inner vortex wave and its perturbation in the flow field can be calculated. For more details concerning the numerical procedure, the reader is referred to chapter 5. The velocity perturbation is obtained by performing vector summation of the contributions due to the two vortex waves. In view of what is shown in figure 4.19, we made the proportion of the waves adjustable. The results of this calculation are shown in figure 4.20, for cases with reduced frequency 3.58 and 5.54 respectively. For the case where the reduced frequency is 3.58, the inner wave is 20% of the outer wave in strength. For the case where the reduced frequency is 5.54, the inner wave is 40% of the outer wave in strength. From figure 4.20 it appears that the results of the two-wave model fit the experimental curve better concerning the reduction of perturbation amplitude. Also, the trend that the strength of the inner wave increases with increasing reduced frequency agrees qualitatively with what is shown in figure 4.19.

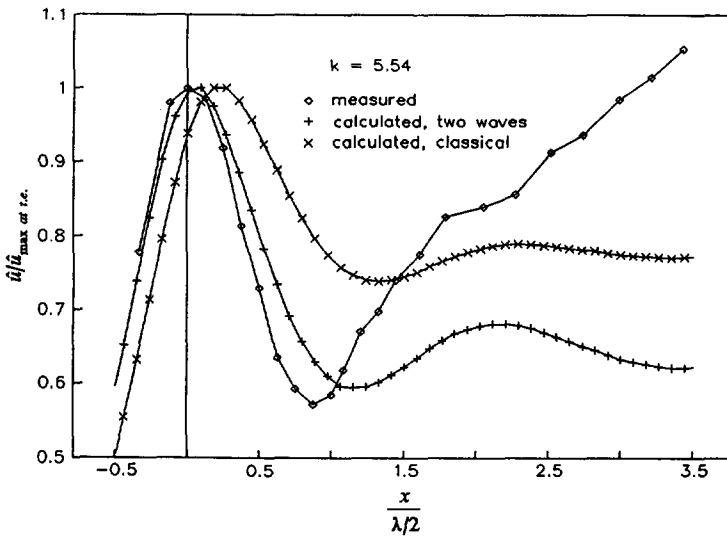
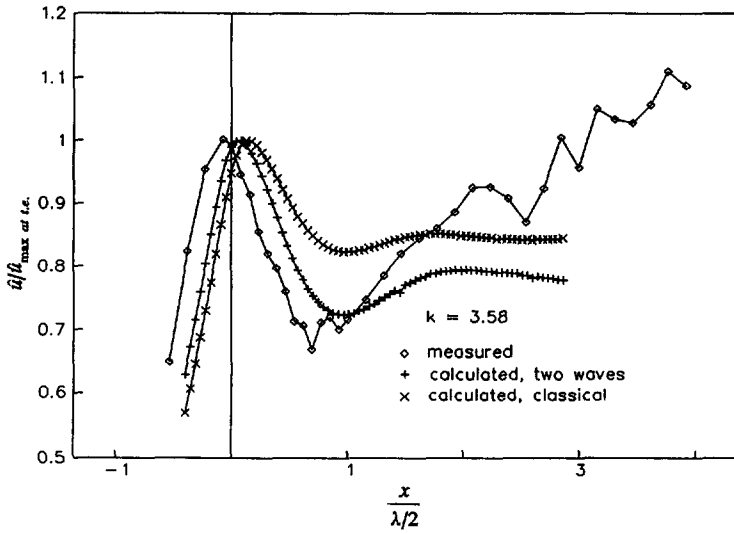


Figure 4.20 Simulating the amplitude reduction with the two-wave model.

From the numerical calculation we found that the perturbations due to the two waves are approximately in phase at the trailing edge. As the distance from the trailing edge is increased, the phase difference builds up. In the neighbourhood where the minima

occur the two run into counter phase (for $k=3.58$ case the counter phase happens closer to the trailing edge). This observation is in line with the partially destructive interference conjecture elaborated above.

Measurements of the mean velocity profile of the unsteady wake is also in agreement with the above observation. Shown in figure 4.21 are results from the mean velocity profile measurement of two unsteady wakes.

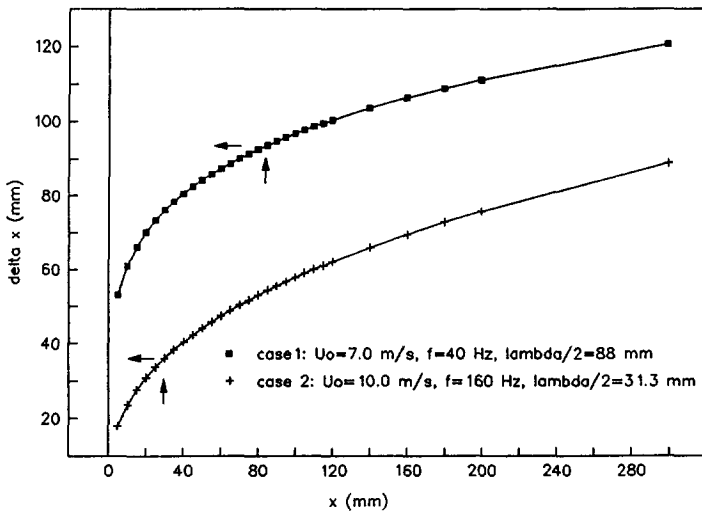


Figure 4.21 The outer wave overtakes the inner wave by half a wave length at a distance about $\lambda/2$ from the trailing edge. The vertical axis, denoted with δx gives the distance of overtaking.

In case 1, the uniform velocity is 7.0 m/s and the excitation frequency is 40 Hz, yielding a half-wave-length of 88 mm (in this neighbourhood the minimum occurs). In case 2, the velocity is 10.0 m/s, $f=160$ Hz, and $\lambda/2=31.25$ mm (in this neighbourhood the minimum occurs). It is clear from this figure that in each of the two cases, a particle with the uniform flow speed overtakes the particle with the centerline velocity by an amount of $\lambda/2$ in a distance which is about the half-wave-length (approximately

10% less, to be more precise) from the trailing edge (see Appendix D). In other words, at the distance of about 90% of $\lambda/2$ from the trailing edge, the vorticity at the centerline will run into counter phase with respect to the vorticity at the outer edge of the wake if they start in phase at the trailing edge.

4.6 Concluding Remarks

In this chapter we described an experimental study in the near wake range of an airfoil. The experiment was conducted at the open end of the M-tunnel in the Low Speed Laboratory of the Aerospace Engineering Department, Technical University Delft.

A steady wake measurement was made for the airfoil at zero angle of incidence. Good symmetry of the mean velocity, as well as the velocity fluctuation profile was observed. Two dimensionality was checked to be satisfactory.

The near wake is found to consist of two parts, namely, a potential wake and a viscous wake. The potential wake exists because of the perturbation due to the thickness distribution of the airfoil. Both the velocity defect and the velocity gradient are small here. The velocity deficiency in the potential wake is filled up at a faster rate. Comparison with numerical calculation shows a fair agreement.

For the inner viscous wake the self preservation of the mean velocity profile is reached at about $0.2c$ behind the trailing edge. The growth of the half-wake-width and the centerline velocity is in agreement with what Chen and Ho [9] observed in a closed wind tunnel.

For unsteady motion of an airfoil, it is identified in the present study that the process of the associated vorticity shedding is a linear one. This observation is relevant to the study of aeroelasticity problem in the sense that experimental studies can be related to

the theoretical ones by way of linear extrapolation.

The perturbation is strongly reduced frequency dependent. In the measured range, it is found that the perturbation is not very sensitive to the change of the Reynolds number.

For the investigation of the convection of shed vortices, a novel approach is devised. It integrates experimental measurement and numerical calculation. The modelling of the numerical calculation is based on the mechanism as discussed in chapter 2 in the main line, and is shown to be qualitatively correct. By comparing the experimental and the numerical calculation we extract the real physical information contained in the measured results.

Technically, this approach consists of three steps. First, the velocity perturbation outside of the wake is measured in the experiment. Then, corresponding numerical calculations are made, based on the principle as described in chapter 2 (for details of the numerical calculation one is referred to chapter 5). Finally, comparisons between experimental and numerical results are made and conclusions are drawn.

It is concluded from the present study that the shed vortices have a shorter wave length than assumed in the linear theory. In other words, the convection of the shed vortices is retarded.

Referring to the larger amount of the perturbation amplitude reduction observed in the experiment (with respect to the numerical result based on the classical theory of Theodorsen), it is inferred that shed vorticity convection in the near wake is conceived in a two-wave structure. The extra amount of reduction of the perturbation amplitude measured outside the wake may arise from the partially destructive interference of the two waves at about $\lambda/2$ distance from the trailing edge. Comparison with a two-wave simulation verifies this conjecture. The two-wave structure is also compatible with the near wake flow structure as discussed in chapter 3. Measurement of mean velocity profile of the unsteady wakes supports this interpretation.

Chapter 5

Numerical Studies

5.1 Introduction

The present chapter is directed at two objectives. In the first place, we are to provide a detailed description of the numerical modelling applied in the present chapter as well as in the reference calculation in chapter 4. Secondly, we are to present numerical studies of the kinematics of the flow associated with the unsteady motion of an airfoil. The study is accomplished with a vorticity distribution based panel method.

In the panel method, the governing equation represents the flow-tangency requirement on the boundary surface. Vortex shedding, accompanying the oscillation of the airfoil, is determined by imposing the Kutta-Joukowski condition in the form of smooth off-flow at the trailing edge, in conjunction with Kelvin's theorem of conservation of (total) circulation.

The distribution of the shed vorticity is another important factor to be determined, and whose significance is seen in the memory effect (cf. chapter2). In the present study, we examine two extreme cases. In the first case, the velocity of vorticity convection is assumed to be identical with the constant uniform flow velocity U_0 . This comes down to assuming that the vorticity is convected at the outer layers of the wake. In the second case we assume the velocity of shed vorticity convection to be a function of the streamwise distance from the trailing edge. In this case, the convection velocity starts with zero value at the trailing edge. It develops as the distance from the trailing edge is increased approaching the uniform flow velocity U_0 , corresponding to convection at the centerline of the wake.

It might be recalled that in the previous chapter, in order to verify the conjecture of the

two-wave structure in the shed vorticity convection we implemented a simple modelling (paragraph 4.5.2.3). In fact, the two-wave verification modelling is a synthesis of these two extreme cases. In the two-wave modelling, the two extreme cases were calculated separately. The induced perturbation in the flow field was calculated by taking the weighted vector sum of the contributions from the two. The weighting factor is inferred from figure 4.19.

As mentioned above, we are interested in the investigation of the kinematics, such as bound circulation, and the bound vorticity distribution. This is for several reasons. First of all, we noticed in chapter 4 that the importance of the kinematical study of the flow field follows from the role it played in the experimental investigation of shed vorticity convection in a viscous flow. In the second place, the kinematics is of intrinsic interest itself in view of the mechanism of the problem we are dealing with. Replacing the oscillating airfoil and the wake with a vortex sheet, we see that the distribution of the singularities is the origin of perturbation to the flow field. The distribution is not arbitrary. In the wake, it has to follow a pattern prescribed with equation (2.23) for constant velocity U_0 , and equation (2.24) for non-constant velocity $U(x)$. On the airfoil, the vorticity distribution is such that the induced (by both the bound and the shed vorticity) normal velocity component has to be identical with what is specified by equation (2.16), so that the boundary condition is satisfied. This study also appears to be necessary in view of the fact that in the analytical solutions of the classical theory (cf. chapter 2) the kinematics is concealed in the integrated results, i.e. the loadings. Moreover, the kinematics might also be relevant to the understanding of unsteady boundary layers on an oscillating airfoil.

5.2 The Panel Method

A panel method is a numerical method for solutions of linear potential problems. Essentially, it is a numerical implementation of the surface integral in the field theory. By virtue of Green's identity (appendix E), for problems governed by the Laplace equation (potential problem, therefore) the solution can be represented by an appropriate distribution of sources and doublets over the boundary surfaces. Once the distribution of the singularities is properly determined according to the boundary condition the potential flow is solved. In line with this, the first step of solving a potential problem is to seek a proper distribution of the singularities which satisfies the boundary conditions on the bound surface and at infinity. In what follows, the discussion appears to be for steady problems, but it can easily be extended to the unsteady problems.

In the numerical calculation, the profile contour is approximated with a number of line segments which are called *panels*. The distribution of singularities is to be determined piecewisely on each of the panels according to some prescribed manner. The distribution is determined so that taking account of the perturbation introduced by the singularities the flow-tangency condition on the solid boundary is satisfied at the collocation points on each of the panels.

In the two-dimensional case, a source distribution $q(x)$ over a segment, $a \leq x \leq b$, on the x -axis introduces a perturbation potential (cf. equation (2.24))

$$\phi(x, y) = -\frac{1}{2\pi} \int_a^b q(\xi) \ln \sqrt{(x-\xi)^2 + y^2} d\xi. \quad (5.1)$$

Corresponding to this, there is a discontinuity in the normal velocity component across the distribution. The jump of the discontinuity is $v^+ - v^- = q(x)$, where the superscripts $+$ and $-$ denote the upper and the lower side of the distribution respectively. The tangential velocity component is continuous across the distribution.

A distribution of doublets $q(x)^\dagger$ over $a \leq x \leq b$ on the x -axis has a potential in the space which can be written

$$\phi(x, y) = \frac{1}{2\pi} \int_a^b \frac{q(\xi)y}{(x-\xi)^2 + y^2} d\xi. \quad (5.2)$$

This gives rise to a discontinuity in the tangential velocity component across the distribution. The jump is $u^+ - u^- = \partial q / \partial x$. The normal velocity component is continuous across the distribution in this case.

In view of the perturbation the singularities introduce into the flow field, it is clear that the source distribution is relevant to the thickness problem in the thin airfoil theory (in fact, it results in the 'potential wake', as identified in chapter 4), while the doublet distribution is associated with the lift problem. In what follows we shall concentrate on the latter.

The property of the doublet distribution is strongly reminiscent of vorticity distribution for which perturbation velocity component is continuous in the normal direction, but discontinuous in the tangential direction. In fact it can be proved that the two are indeed equivalent. Consider the distribution of doublet $q(x)$ over $a \leq x \leq b$, on the x -axis. The potential as written in equation (5.2) can be integrated by parts to yield

$$\begin{aligned} \phi &= \frac{q(\xi)}{2\pi} \tan^{-1} \frac{y}{x-\xi} \Big|_a^b - \frac{1}{2\pi} \int_a^b \frac{\partial q}{\partial \xi} \tan^{-1} \frac{y}{x-\xi} d\xi \\ &= \frac{q(\xi)}{2\pi} \theta \Big|_a^b - \frac{1}{2\pi} \int_a^b \frac{\partial q}{\partial \xi} \theta d\xi, \end{aligned} \quad (5.3)$$

where $\theta = \tan^{-1}(y/(x-\xi))$ as sketched in figure 5.1.

[†] For simplicity of notation, we use here $q(x)$ also for the doublet distribution. It will not be confused with the source distribution since they are only temporal in the context.

It is clear that this is a potential due to two concentrated vortices $-q(a)$, $q(b)$ at $(a,0)$, $(b,0)$, and a distribution of vorticity $\gamma = \partial q / \partial x$ over $a \leq x \leq b$, $y=0$. So that we see that a doublet distribution can equivalently be replaced with a distribution of vortices.

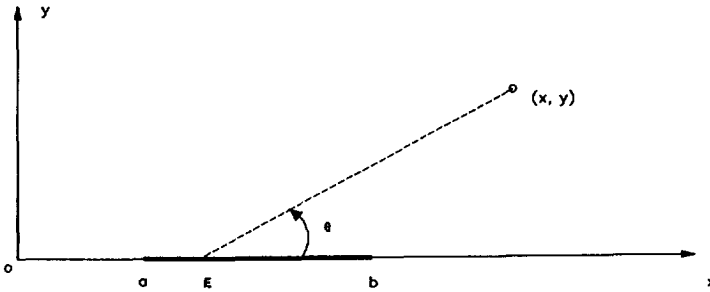


Figure 5.1 The spatial relation between the doublet distribution over $a \leq x \leq b$, $y=0$ and a field point at (x,y) .

As discussed in chapter 2, for the lift problem we are concerned with, the airfoil is replaced with a flat plate. We divide the plate into a number of panels on which the vorticity distribution is to be determined subject to the flow-tangency condition on the surface. The jump (discontinuity) of tangential velocity component across the distribution is just the local vorticity strength γ . The segment discussed above can be understood as one of the panels. The joint of two neighbouring panels is referred to as a node, or a nodal point. By properly choosing the vorticity distribution, the concentrated vortices at the nodes of the panels will cancel each other, except at the leading and the trailing edge. As is usual in the airfoil problem we shall allow the singularity at the leading edge, but remove the one at the trailing edge by applying a Kutta-Joukowski condition.

5.3 The Governing Equations and the Discretization

5.3.1 The Governing Equations

Formally, a potential problem is governed by the Laplace's equation. However, if we approach the problem from the Green's identity, we do not solve for the potential in the field directly. Instead, we seek for appropriate distribution of the singularities on the boundary according to the boundary conditions prescribed. In this connection, the equation that describes the boundary conditions becomes the governing equation. In the panel method approach of the unsteady airfoil problem, the conservation of circulation and the Kutta-Joukowski conditions enter also as the governing equation, making the problem determinate.

5.3.1.1 The Boundary Conditions

Let a Cartesian coordinate system (x,y) be chosen so that the x -axis is in the direction of the uniform flow with velocity U_0 . The y -axis is perpendicular to the mean flow and positive upwards. Velocity components of flow in the two directions are denoted with u and v respectively. We consider the flat plate performing a small amplitude[†] harmonic oscillation with its mean position on the x -axis. The leading edge is at $x=0$, and the trailing edge at $x=c$. Though the boundary condition has been derived in chapter 2, for the convenience of reference we recapitulate it here.

Let the instantaneous position of the plate be described by

$$y=Y(x,t), \quad \text{on } 0 \leq x \leq c. \quad (5.4)$$

[†] To be more precise, the amplitude does not need to be small in principle, as long as the product of the amplitude and the frequency is small with respect to U_0 . The requirement of small amplitude is more for the convenience of writing the boundary condition on the plane $y=0$.

The flow velocity in the normal direction of the plate must be equal to that of the plate itself at each moment. This can be written as $\mathbf{v}_f \cdot \mathbf{n} = \mathbf{v}_p \cdot \mathbf{n}$, where $\mathbf{n} = (-\partial Y / \partial x, 1)$ is the normal vector on the plate. The subscripts f and p stand for *flow* and *plate* respectively. Recognizing that the oscillation is of small amplitude, the velocity of the plate can be written $\mathbf{v}_p = (0, \partial Y / \partial t)$. The velocity of the flow is the sum of the uniform flow $(U_0, 0)$ and the perturbation (u, v) . So that the boundary condition on the plate can be written

$$\frac{\partial Y}{\partial t} = -(U_0 + u_f) \frac{\partial Y}{\partial x} + v_f . \quad (5.5)$$

Omitting the term that is of higher order small we have

$$v_f = \frac{\partial Y}{\partial t} + U_0 \frac{\partial Y}{\partial x} . \quad (5.6)$$

The restriction that the oscillation is small in amplitude allows equation (5.6) to be applied on $0 \leq x \leq c, y = 0$.

Since the singularities on the bound surface are basic solutions of the Laplace equation, their perturbation decays with increasing distance. The condition that the perturbation vanishes at infinity, leaving only the uniform flow, is automatically satisfied with the velocity potential $U_0 x$. Of course, in the neighbourhood of the vortex wake, which extends from the trailing edge to $(\infty, 0)$, this is not the case.

5.3.1.2 The Conservation of Circulation

Accompanying the oscillation of the plate, vortices are continuously shed into the wake. Observing the conservation of the total circulation in the whole flow field, the total circulation is independent of time. Therefore, the relation between the bound and shed vorticity can be written

$$\Gamma_b(t) = \Gamma_b(t + \delta t) + \delta \Gamma_w. \quad (5.7)$$

In equation (5.7) the subscripts b and w stands for *bound* and *wake* respectively.

5.3.1.3 The Kutta-Joukowski Condition

Vortex shedding accompanying the oscillation of an airfoil is determined by applying the Kutta-Joukowski condition at the trailing edge, in conjunction with the law of conservation of total circulation. The basic form of the Kutta-Joukowski condition is that flow from the two sides of the airfoil, upon joining at the trailing edge, passes smoothly into the wake. The essence of this phenomenological hypothesis is that a flow cannot go around a sharp corner, e.g. the sharp trailing edge in the present case, in such a way global separation of the flow is avoided. This being the case, the bound circulation round the airfoil is uniquely determined (cf. chapter2).

In mathematical terms, this implies

$$\gamma_b(c) = \gamma_w(c), \quad (5.8)$$

in which $\gamma_b(c)$ is the strength of bound vorticity at the trailing edge, and $\gamma_w(c)$ is the strength of the newly shed vorticity located adjacent to the trailing edge. For simplicity, in what follows we shall omit the subscript b for bound vorticity if no confusion will be introduced.

In the case where the flow is purely potential and without retardation, the wake is an infinitely thin sheet across which the streamwise velocity is discontinuous. When no retardation in shed vorticity convection is accounted for it can be proved that equation (5.8) implies another statement: the pressure difference at the trailing edge is zero (the zero loading hypothesis). The equivalence of the two hypotheses is demonstrated as follows.

For unsteady potential flow, Bernoulli's equation reads

$$p = -\rho \left(\frac{\partial \phi}{\partial t} + \frac{1}{2} V^2 \right) + f(t), \quad (5.9)$$

where $V = ((U_0 + u)^2 + v^2)^{1/2}$, and $f(t)$ is an arbitrary function of time only. Neglecting higher order small terms, such as u^2 and v^2 (they would tend to cancel anyway, in the calculation of pressure difference across a vortex sheet), Bernoulli's equation is linearized to be

$$p = -\rho \left(\frac{\partial \phi}{\partial t} + U_0 u \right) + f(t). \quad (5.10)$$

Denoting with subscript u and l for the *upper* and *lower* side respectively, we have for the pressure difference

$$p_l - p_u = \rho U_0 (u_u - u_l) + \rho \frac{\partial}{\partial t} (\phi_u - \phi_l). \quad (5.11)$$

Let the difference vanish at the trailing edge, it follows

$$U_0 (u_u - u_l) = -\frac{\partial}{\partial t} (\phi_u - \phi_l), \quad \text{at } x=c, \quad (5.12)$$

where it is recognized $u_u - u_l = \gamma$, per definition. $\phi_u - \phi_l = \left(\int u dx \right)_{y=0+, x=c} - \left(\int u dx \right)_{y=0-, x=c} = \Gamma$ is the bound circulation. So that the hypothesis of zero loading implies

$$U_0 \gamma(c) = -\frac{d\Gamma}{dt}. \quad (5.13)$$

Considering a small time interval δt , the bound circulation is changed by an amount $\delta \Gamma$. In view of the convection speed U_0 , the wake is extended by a length $U_0 \delta t$. If δt is small enough, it can be assumed that the shed vorticity is evenly distributed over this wake element, so that $\gamma_w = -\delta \Gamma / (U_0 \delta t)$. In view of equation (5.13), we see that the hypotheses of zero loading and smooth off-flow are equivalent, both require that

$\gamma(c) = \gamma_w$ (equation (5.8)).

For the case where convection of the shed vorticity is retarded, the two hypotheses are not equivalent on the level of the outer potential flow. In this case the shed vorticity over a wake element is $\gamma_w = -\delta\Gamma/(U_w\delta t)$, where U_w is the convection velocity which is different from U_0 . Obviously, $U_0\gamma(c) = U_w\gamma_w$ (zero loading requirement) and $\gamma(c) = \gamma_w$ (smooth off-flow requirement) cannot be satisfied simultaneously, if $U_w \neq U_0$. Based on physical consideration, we maintain the smooth off-flow hypothesis, i.e. $\gamma(c) = \gamma_w$, so that global separation of the flow may be avoided.

As noticed earlier, in classical theory (where there is no retardation), the wake is only a terminology that represents a sheet of tangential velocity discontinuity. It does not have a finite lateral dimension. On account of the fact that the density of the fluid is uniform, the wake has a vanishingly small mass per unit length in view of its lateral dimension. Therefore zero loading is a necessary requirement in this case. For, if otherwise, a discontinuity of the pressure across the 'wake' will necessarily result in an infinite acceleration, which is physically unacceptable.

Considering the retardation in shed vorticity convection we are implicitly confronted with an actual wake. In view of what is discussed in chapter 3, we understand that the reduction of the lateral dimension of the wake to infinitesimal is because its scale in this direction is of higher order small with respect to the relevant scale in the potential flow (the chord length c). To see what actually happens to the shed vortices we need to consider the boundary layer scale for the moment. With this scale we can see the finite lateral dimension of the wake and the velocity defect in it. In this case, if we require a shed vortex to move with velocity U_0 , it would be subject to a finite 'Kutta force' (and thus infinite acceleration). So it would have to move with the local velocity in the wake (which is less than U_0). This is for the same reason why in the classical theory it has to move with the uniform flow velocity. This is in fact a restatement of Kelvin's theorem (only it is applied at a finer, boundary layer scale); there can be no Kutta force if the relative velocity vanishes.

Turning back to the geometrical scale of potential flow, at which the present numerical calculation is performed, the issue of non-zero loading across the 'infinitely thin' wake encountered in the case of retarded shed vorticity convection should not worry us. Because we know that though the geometrical dimension of the wake is made to vanish in the lateral direction, it retains a finite mass per unit length in the flow direction, so that the infinite acceleration can be avoided[†].

5.3.1.4 The Integration

According to Kelvin's theorem, for uniform convection, vorticity in the wake $\gamma_w(x,t)$ is related to the bound circulation by (Ashley & Landahl [2])

$$\gamma_w(x,t) = -\frac{1}{U_0} \frac{\partial}{\partial t} \Gamma(c, t - \frac{x-c}{U_0}). \quad (5.14)$$

The denominator U_0 in this equation expresses the distribution of the shed vorticity, while the argument $t-(x-c)/U_0$ indicates that vorticity shed at time $t-(x-c)/U_0$ is observed at point $(x,0)$ at time t . The latter is in fact a Galilei transformation.

A vorticity distribution $\gamma(x,t)$ on $a \leq x \leq b$, $y=0$ will induce a velocity in the y -direction at a point $(x_0,0)$ in the following way (cf. chapter 2)

[†] If vortex elements in the wake move at the local velocity, then pressure variation in the lateral direction of the wake is continuous. Therefore, $\partial p/\partial y$ is bounded. The pressure difference across the wake would be proportional to δ , the thickness of the wake. The mass per unit length of the wake is also proportional to δ . In this sense, it can be observed that the mass per unit length of the wake is non-vanishing.

$$v(x_0, t) = \frac{1}{2\pi} \int_a^b \frac{\gamma(\xi, t)}{x_0 - \xi} d\xi. \quad (5.15)$$

In the present study, we assume that the harmonic oscillation $y = \hat{a}(x)e^{i\omega t}$ has been going on for so long that the vortex wake virtually extends to infinity. Taking into account of the perturbation of both the bound and the shed vorticity we have for the up-wash field at the plate

$$\hat{v}(x) = -\frac{1}{2\pi} \oint_0^c \frac{\hat{\gamma}(\xi) d\xi}{x - \xi} + \frac{i\omega \hat{\Gamma}}{2\pi U_0} \int_c^\infty \frac{\exp(-i\omega(x-c)/U_0)}{x - \xi} d\xi, \quad (5.16)$$

where \hat{v} , $\hat{\gamma}$, and $\hat{\Gamma}$ under the hat are the complex amplitudes of the up-wash, bound vorticity, and the bound circulation respectively. According to equation (5.6), we have for the boundary value problem the integral equation

$$\frac{\partial \hat{Y}}{\partial t} + U_0 \frac{\partial \hat{Y}}{\partial x} = -\frac{1}{2\pi} \oint_0^c \frac{\hat{\gamma}(\xi) d\xi}{x - \xi} + \frac{i\omega \hat{\Gamma}}{2\pi U_0} \int_c^\infty \frac{\exp(-i\omega(\xi - c)/U_0)}{x - \xi} d\xi, \quad (5.17)$$

in which the bound vorticity $\hat{\gamma}(x)$ is to be solved. Here, we observe that the Cauchy principal value integral represents the perturbation due to the bound vorticity. The second integral on the right hand side of equation (5.17) gives the perturbation due to the shed vorticity in the wake.

In line with the interpretation of equation (5.14), we can write the relation for the case in which convection of shed vorticity is non-uniform

$$\gamma_w(x, t) = -\frac{1}{U(x)} \frac{\partial}{\partial t} \Gamma(c, t - \int_c^x \frac{1}{U(\xi)} d\xi), \quad (5.18)$$

which satisfies equation (2.24) as is easily verified. Obviously, equation (5.18) reduces to equation (5.14) for constant convection where $U(\xi) = U_0$. Corresponding to this, the

integral equation governing the boundary value problem for non-uniform convection of vorticity is then

$$\frac{\partial \hat{Y}}{\partial t} + U_0 \frac{\partial \hat{Y}}{\partial x} = -\frac{1}{2\pi} \oint_0^c \frac{\hat{\gamma}(\xi) d\xi}{x-\xi} + \frac{i\omega \hat{\Gamma}}{2\pi} \int_c^\infty \frac{1}{x-\xi} \frac{\exp(-i\omega \int_c^\xi \frac{d\zeta}{U(\zeta)})}{U(\xi)} d\xi. \quad (5.19)$$

5.3.2 The Discretization

The governing equations were established in the last section. They are:

- the equation for conservation of circulation (equation (5.7));
- the equation for the Kutta-Joukowski condition (equation (5.8));
- the equation for the boundary condition (equation (5.17)/(5.19)).

At this stage these equations are exact with respect to the numerical approximations that are to follow. Equations (5.7) and (5.8) should be satisfied at each moment of the motion. Equations (5.17) and (5.19) should be satisfied on the whole boundary surface at each moment. To realize numerical calculation approximations need to be made in order to render the number of equations to a finite (manageable) amount. This is done by way of discretization. Appropriate equations should be satisfied at only a finite number of spatial points and/or time steps. The spatial points at which the equation for the boundary condition is satisfied are referred to as the *collocation points*.

5.3.2.1 The Panels

In numerical calculation, the plate is resolved into a number of N panels. The governing equation that ensures the boundary condition applies to each of these panels. Experience with analytical treatment of airfoil problems shows that the vorticity distribution has a

more complicated behaviour near the leading and the trailing edge (Ashley & Landahl [2]). To have a better resolution, the panels are so divided that they are finer near the two edges, but coarser on the mid-chord. This is done with a cosine scheme. The coordinate of the nodal points is

$$x_i = 1 - \cos\left(\frac{(i-1)\pi}{N}\right), \quad i = 1, 2, \dots, N+1. \quad (5.20)$$

5.3.2.2 The Process

We start the calculation at time $t=0$, when the plate is set into oscillation. Before this moment the plate is aligned in the uniform flow with zero angle of attack. As soon as the unsteady motion begins, bound circulation is built up and counter vortices are shed into the wake. In principle, a stationary state[†] can be reached only infinitely long after the onset of the unsteady motion. However, experience with calculations shows that after about 4 periods of oscillation the stationary state is practically established. Vortices farther down-stream in the wake have little influence on the flow field near the plate. The step length of time increment plays a role in the accuracy of the numerical calculation. It appears from calculation practice (van Duivenbode [35]) that when the length of the time step is 2.5% of the period, and the number of the panels is 40, the numerical results check the analytical solution (with $U=U_0$, as described in chapter 2) already satisfactorily. In the case where the convection of shed vortices is retarded, it is natural to expect that the vortex wave extends in a slower rate. In the actual calculation we consider that the stationary state is reached after 6 periods of oscillation.

[†] By stationary state we mean that despite the unsteady nature of the process, the characteristics of it—the amplitude and the phase angle of bound circulation here—is time independent.

5.3.2.3 The Distribution of Vorticity

The bound vorticity distribution $\hat{\gamma}(x)$ in equations (5.17) and (5.19) is an unknown function. We shall approximate it with numerical values at the nodal points. Over the panels, i.e. in between the nodal points, we assume a linear interpolation

$$\gamma_i(x_i) = \frac{\gamma_{i-1} + \gamma_i}{2} + \frac{\gamma_i - \gamma_{i-1}}{l_i} x_i, \quad (5.21)$$

in which l_i is the length of the panel (panel i) and x_i is the local coordinate with its origin at the middle of that panel. Such a distribution is generally valid for most of the panels except for the first one, because the velocity singularity at the leading edge results in a vorticity distribution singular like $x^{-1/2}$. For this reason we shall allow a distribution of vorticity in the form of $\gamma_s(x) = Ax^{-1/2}$, and let, in the linear distribution part, the vorticity strength be zero at $x=0$. So that we have for the bound vorticity distribution $\gamma = \gamma_l + \gamma_s$.

The distribution of the shed vorticity in the wake is assumed to be piecewisely constant over each of the wake elements. This is valid because the influence of the wake vorticity on the up-wash field is small with increasing distance (Giesing [14]), and also there are no collocation points for the wake elements where boundary conditions should be satisfied. In van Duivenbode [35] it is shown that it is the introduction of the singular distribution γ_s at the leading edge that plays an important role in improving the accuracy.

5.2.3.4 The Discretization of the Governing Equations

The conservation of circulation requires that the total circulation in the entire flow field must remain unchanged at each time step. Corresponding to equation (5.7) and the vorticity distribution discussed above, this can be written

$$\int_0^c \gamma(\xi, t) d\xi = \int_0^c \gamma(\xi, t + \delta t) d\xi + \gamma_w(t) \delta s_w. \quad (5.22)$$

The second term on the right hand side is the circulation of shed vorticity during a small time interval δt . While $\delta s_w = U(c, t) \delta t$ is the length of the first wake element just downstream of the trailing edge. Since we start the unsteady motion at zero angle of attack, the total circulation is zero, so that at each time step we have

$$\int_0^c \gamma(\xi, t + \delta t) d\xi = -\gamma_w(t) \delta s_w. \quad (5.23)$$

As mentioned earlier, the boundary condition is satisfied at the collocation point of each of the panels. Considering numerical stability the collocation points are chosen at the middle of each of the panels. In line with equation (5.17) (and also equation (5.19)), this can be written for each collocation point, according to the devised vorticity distribution

$$\begin{aligned} \frac{\partial Y}{\partial t} + U_0 \frac{\partial Y}{\partial x} = & -\frac{1}{2\pi} \int_0^c \frac{A/\sqrt{\xi}}{x_0 - \xi} d\xi - \frac{1}{2\pi} \oint_{x_i}^{x_{i+1}} \frac{\gamma(\xi) d\xi}{x_0 - \xi} \\ & - \frac{1}{2\pi} \sum_{j=1, j \neq i}^N \int_{x_j}^{x_{j+1}} \frac{\gamma(\xi) d\xi}{x_0 - \xi} + \frac{1}{2\pi} \sum_{k=1}^n \int_{c+(k-1)U\delta t}^{c+kU\delta t} \frac{\gamma_{w,k}}{x_0 - \xi} d\xi. \end{aligned} \quad (5.24)$$

In this equation, terms on the left hand side give the normal velocity at appropriate collocation point x_0 . The first term on the right hand side gives the normal velocity induced by the singular vorticity distribution. The second term represents the normal velocity induced by the linear vorticity distribution on the panel itself. The third term are the contributions due to linear vorticity on all the other panels on the airfoil $0 < x < c$. The last term gives the influence of the shed vorticity in the wake. For each of the terms influence factors can be written, corresponding to the vorticity strength at the nodal points (Appendix F). These will be used in forming the coefficient matrix for numerical calculation.

The form of the wake influence term is different from the ones in equations (5.17) and (5.19). This difference arises from the fact that in the analytical treatment the wake vorticity is considered to be frozen in the space, while in the numerical calculation the motion of the shed vortices is followed. They actually describe the same mechanism. Only in the numerical calculation the shed vortices must be relocated at each time step.

5.2.3.5 The Numerical Calculation

The flow chart of the numerical implementation is shown in figure 5.2. An important part of the calculation follows an algorithm as devised in van Duivenbode [35]. The equations to be solved are equation (5.24) for the boundary conditions at the collocation point of each of the panels, equation (5.22) for the conservation of the total circulation, and equation (5.8) for the Kutta-Joukowski condition. The prescribed boundary condition forms the free vector $\{b\}$ for the simultaneous equations. It is updated at each time step, to take account of the perturbation due to the old shed vorticity at the collocation points and the instantaneous oscillation of the plate. With the coefficient matrix being constant, the simultaneous equations are solved after the free vector $\{b\}$ is established. The bound circulation and the vortex shedding are accordingly determined. The shed vortices in the wake are then relocated according to the prescribed convection function before the free vector $\{b\}$ is updated.

The stationary state is considered to be reached after a number of periods of oscillation as discussed above. For calculation of the velocity perturbation in the space, the time has to be longer. Because in this case the influence of the shed vorticity in the far end of the wake may also be important depending on the position of the calculation point. This is controlled through the input. When the stationary state is reached, appropriate calculations such as the bound vorticity distributions, induced perturbation in the flow field, etc. are executed. This is performed for one period of the oscillation before the whole calculation is concluded.

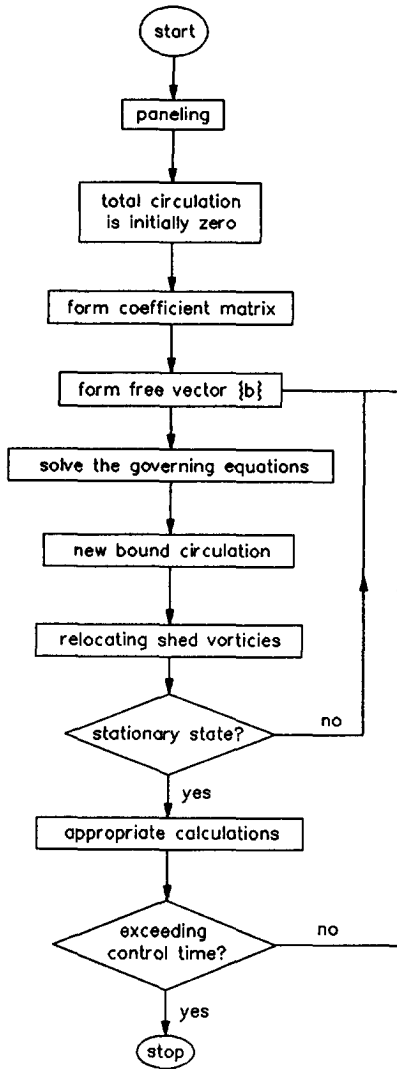


Figure 5.2 Flow chart of the numerical calculation.

5.4 Results and Discussion

In this section we present and discuss the calculated results. In the first 4 paragraphs we are concerned with the case where the convection of the shed vorticity is with the uniform flow velocity U_0 . In the last paragraph we shall deal with the case where the shed vorticity convection is retarded.

5.4.1 The 3/4 Chord Point

In section 2.4 it has been shown that the lift force due to circulation can be represented by the upwash at the 3/4 chord point of the plate

$$L_c = -2\pi\rho U_0 b C(k) v_{3c/4}. \quad (5.25)$$

For this reason, this particular point on the airfoil is referred to as the rear aerodynamic centre (Fung [13]). In terms of the aerodynamic response, the oscillation of an airfoil with a fixed pivot point can generally be decomposed into two elementary modes, namely, a heaving and a 'pure' pitching about the rear aerodynamic centre

$$\begin{aligned} v_{3c/4} &= \frac{\partial Y}{\partial t} \Big|_{3c/4} + U_0 \frac{\partial Y}{\partial x} \Big|_{3c/4} \\ &= -U_0 \hat{\alpha} e^{iU_0 k t} + \left(x_0 - \frac{3c}{4}\right) i U_0 k \hat{\alpha} e^{iU_0 k t}, \end{aligned} \quad (5.26)$$

where x_0 is the position of the pivot point measured from the leading edge, and k is the reduced frequency. The first term on the right hand side of equation (5.26) is the upwash due to the 'pure' heaving, and the second is the upwash at the 3c/4 point due to a pitching motion.

Apparently, the lift force exhibits a symmetry with respect to the $3c/4$ point[†] for different modes of pitching motion. In fact, though less apparent, this is true also for the bound circulation, as can be seen in figure 5.3.

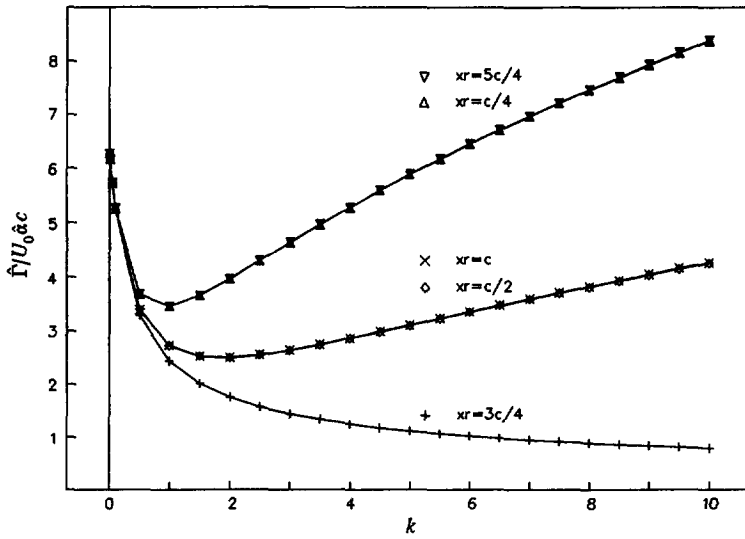


Figure 5.3a Amplitude of bound circulation for different modes of pitching oscillation. k is the reduced frequency.

In figure 5.3a, we notice that for two pitching motions when the pivot points are symmetrically located with respect to the rear aerodynamic centre, the amplitudes of the corresponding bound circulations are identical. In this figure they coincide perfectly, so the reader is reminded not to mistake them as one. The two curves on the upper part represent actually the bound circulation of four cases.

[†] Here, by symmetry we mean that if the pivot points of two pitch motions are symmetrical with respect to the $3c/4$ point, then the aerodynamic response of the two motions are also symmetrical with respect to the one for the 'pure' pitching, in terms of both amplitude and phase angle. This will become clearer in the following discussion.

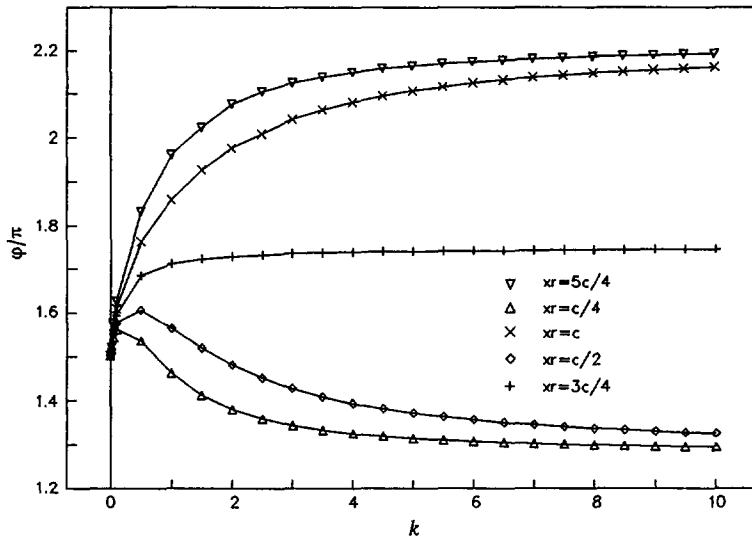


Figure 5.3b Phase angle of bound circulation for different modes of pitching oscillation. k is the reduced frequency.

In figure 5.3b, the phase angle is determined with reference to a harmonic wave which is $3\pi/2$ lagging behind the oscillation. In this figure we see that the bound circulation of two symmetrical pitching motions have the same amount of phase shift with respect to the phase angle of the circulation associated with the pitching motion about the $3c/4$ point. However they are on the different sides of the reference curve. At very low reduced frequency, the amplitudes of the circulation are seen to be nearly the one in the steady case, 2π , and they are essentially in phase with the oscillation of the plate.

It is also clear that the development of the bound circulation, as a function of the reduced frequency, depends on the mode of oscillation. For 'pure' pitching (pivot at $3c/4$), the bound circulation is decreasing monotonously with increasing reduced frequency. While for pitching about a pivot distinct from the rear aerodynamic centre, the bound circulation is seen to increase in higher reduced frequency range. This non-uniform behaviour of the amplitude curves can be explained by considering the upwash

at the rear aerodynamic centre for different modes of oscillation.

In equation (5.26) we observe that for oscillation pivoted at the $3c/4$ point, the upwash at the rear aerodynamic centre depends only on the instantaneous angle of incidence of the plate. With a given amplitude of oscillation, the amplitude of the upwash is constant for all reduced frequencies. In this case, the reduced frequency enters only as a parameter describing the harmonic oscillation of the plate. But for pitching with a pivot at other than the $3c/4$ point, the rear aerodynamic centre is itself performing an oscillation in the transverse direction. This, in addition to the instantaneous angle of incidence, gives rise to an upwash of heaving nature as represented by the second term on the right hand side of equation (5.26). The amplitude of upwash of this kind is proportional to the reduced frequency of the motion, so that in the high reduced frequency range this term is overwhelming. Thus, the development of the bound circulation in these circumstances is dominated by the augmentation of the upwash at the $3c/4$ point. In line with this, it appears clear that pure pitching is a proper case for studying the effect of the shed vorticity.

5.4.2 The Bound Circulation and the Related Force

The lift force acting on an airfoil can be calculated by integrating the pressure difference on its two sides, along the chord.

$$L = \int_0^c (p_l - p_u) dx, \quad (5.27)$$

where the pressure is determined with the linearized Bernoulli's equation. Inserting equation (5.10) into equation (5.27) we have for the lift force

$$L(t) = \rho U_0 \Gamma(t) + \rho \frac{\partial}{\partial t} \int_0^c \int_0^x \gamma(\xi, t) d\xi dx. \quad (5.28)$$

As discussed in chapter 2, the lift force on the airfoil arises generally from two origins, namely, the force which is related to bound circulation, and the force which is related to the apparent mass effect. These two kinds of forces have different natures. The apparent mass force arises from the acceleration of the fluid ($\partial\phi/\partial t \neq 0$) due to the solid body's unsteady motion. So that it is present only when the motion of the airfoil is time-dependent, even though the total circulation bound to the body might be zero. While for the circulation related force, the unsteadiness of the motion is not absolutely necessary. The lift force on a steadily moving airfoil is a good example. In this case, the second term on the right hand side of equation (5.28) vanishes because of the steadiness, with only the first term remaining (which vanishes also for the special case of a flat plate at zero angle of incidence).

In principle, the distribution of bound vorticity, $\gamma(x, t)$, can be decomposed into two parts, $\gamma = \gamma_1 + \gamma_2$, with, say, $\int \gamma_1 dx = 0$ and $\int \gamma_2 dx = \Gamma$. Clearly, the force due to the vorticity distribution γ_1 is related to the apparent mass effect as mentioned above, while the one associated with γ_2 is related to the bound circulation. Thus, the circulation related force has essentially two origins. The one represented by $\rho U_0 \Gamma$ comes in because the rectilinear motion of the airfoil with speed U_0 implies a stretching of a vortex ring[†] with such a rate, that the momentum in the flow is increased at a rate amounting to $\rho U_0 \Gamma$ (von Kármán & Burgers [36]). Consequently a reaction force from the flow is acting on the airfoil. The other part which is included in the time derivative term of equation (5.28) can be understood as due to the vortex shedding corresponding to the unsteady motion of the airfoil. In a far field point of view, the variation of the bound

[†] Imagine a wing with finite length of span. The bound vortex, the trailing vortex at the two ends of the span, and the starting vortex form a vortex ring. If the length of the span is infinitely stretched a two-dimensional situation is established.

circulation and the corresponding shed vortex comprise at each moment a vortex doublet. This vortex doublet introduces momentum to the flow field, so that a force is acting on the airfoil as the reaction of the flow.

This distinction is not made artificially. Instead, it has implications on the quasi-steady argument which simplifies the unsteady problem. This argument has two main features, namely, the shed vortices are instantly convected to infinity so that they have no effect on the upwash field, and the lift force is solely due to the instantaneous bound circulation, i.e. $\rho U_0 \Gamma$ (the last term in equation (5.28) drops off). In view of the different dependencies of the two forces on the operation parameters, it is clear that the quasi-steady argument is not uniformly valid for all the reduced frequencies as can be seen in figure 5.4.

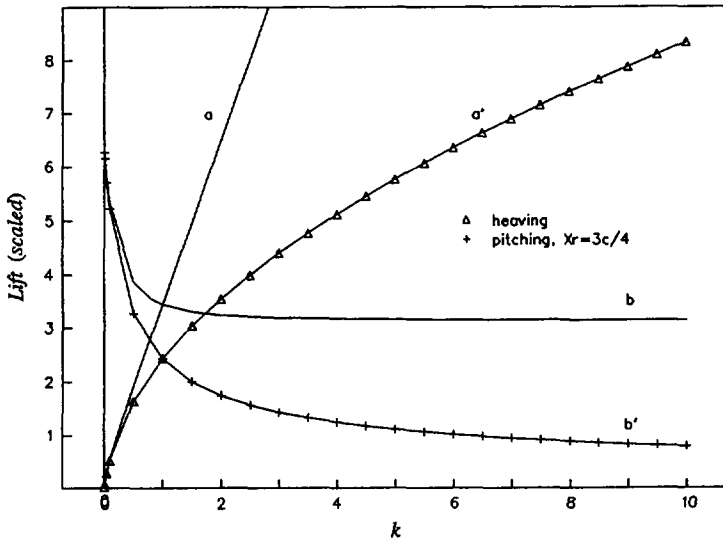


Figure 5.4 Amplitude of the circulation related forces (the values are scaled with $\rho U_0 \alpha$ for pitching, and $\rho U_0 a/c$ for heaving).

In figure 5.4 the amplitude of circulation related forces are shown as a function of the reduced frequency for the two 'pure' oscillations, namely, heaving and pitching about 3/4 chord point. In this graph, comparisons are made between the amplitude of the

force that is $\rho U_0 \Gamma$ (from the present numerical calculation, denoted with a' and b' for the two cases respectively) and the amplitude of total circulation related force (denoted with a and b for the two cases respectively), i.e.

$$\rho U_0 \Gamma(t) + \rho \frac{\partial}{\partial t} \int_0^c \int_0^x \gamma_2(\xi, t) d\xi dx.$$

The latter is calculated from equation (2.51). The force for pitching motion is scaled with $\rho U_0 \hat{\alpha}$, and the force for heaving motion is scaled with $\rho U_0 \hat{a}/c$, where $\hat{\alpha}$ and \hat{a} are the amplitudes of the pitching and heaving oscillation respectively.

It is clear that, corresponding to each specific mode of oscillation, the curves for comparison ($a \sim a'$, $b \sim b'$) are virtually reduced to one in the lower reduced frequency range. In the case of heaving motion the upwash is essentially zero when the reduced frequency is low ($\partial Y/\partial t + U_0 \partial Y/\partial x = \partial Y/\partial t \ll U_0$). The circulation due to the slow heaving is therefore vanishingly small. The situation is in fact that of a flat plate in an uniform flow with zero angle of incidence. For pitching motion of the airfoil, the circulation related force depends mainly on the upwash due to the instantaneous angle of incidence of the plate, as we have seen in the previous paragraph. Shedding of vorticity occurs, but the slow oscillation determines that the rate is low. So that in this case the circulation related force arises mainly from the extension of the vortex ring area. In this range, k up to 0.5, say, the quasi-steady argument is approximately valid.

As the reduced frequency is increased, the difference soon develops. This indicates that at the high reduced frequency the momentum introduced by vortex shedding becomes important. We also notice that at high reduced frequency the curves corresponding to the heaving motion behave quite differently from the ones for pitching. This difference is found to be due to the involvement of the reduced frequency in the upwash for the heaving motion as can be seen from equation (5.26). In fact, when the lift (or bound circulation) of the heaving motion is scaled with the reduced frequency, it becomes identical with that of the pure pitching as can be seen in figure 5.5.

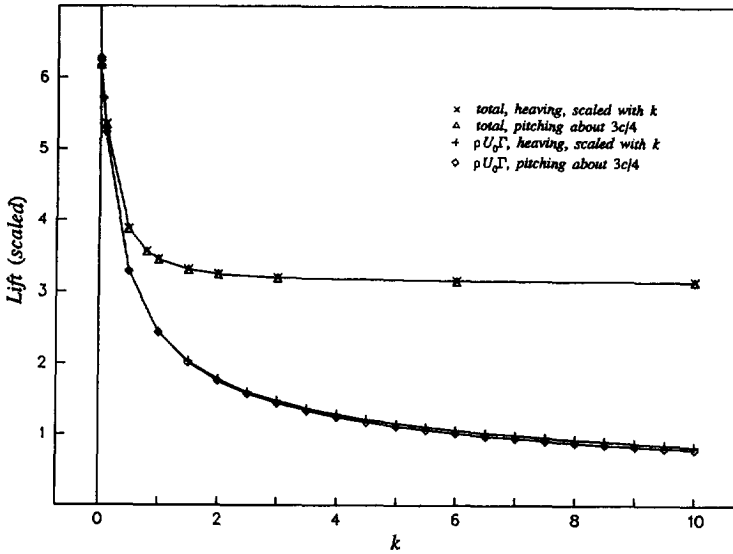


Figure 5.5 Circulation related forces for heaving are identical with those of pitching, when scaled with the reduced frequency k .

Pitching with another pivot is an intermediate case. When at low frequency, it is the pitching effect that dominates. At high reduced frequency the heaving effect becomes dominant (figures 5.3a and 5.4).

From the discussion above, it can be understood that it is the wave structure (represented by the reduced frequency $k = \omega c / 2U_0 \sim c / \lambda$) that determines the aerodynamic response on the airfoil. The specific mode of oscillation is not of direct relevance.

5.4.3 The Distribution of Bound Vorticity

The boundary layer is the location where vorticity is generated. When viewed with an outer flow scale the boundary layer is regarded as a vortex sheet attached to the solid surface. In the present case we have therefore two vortex sheets attached to the two sides of the plate. By virtue of the anti-symmetry in the lift problem, they can be replaced with one, $\gamma = u_u - u_l = 2u_u = -2u_l$.

For steady motion of a thin, uncambered airfoil it is found that the bound vorticity distribution approaches zero at the trailing edge with a behaviour $[(c-x)/c]^{1/2}$, when $x \rightarrow c$. This is referred to as the elliptic behaviour of vorticity distribution in the neighbourhood of the trailing edge (von Kármán & Burgers [36]). The loading at the trailing edge, $-\rho U_0 \gamma$, approaches zero likewise, satisfying the Kutta-Joukowski condition. The gradient of the pressure difference, however, presents a square root singularity $((c-x)^{-1/2})$ as $x \rightarrow c$. Therefore, the flow condition in this neighbourhood is expected to be more complicated.

For unsteady motion of the airfoil, the Kutta-Joukowski condition still requires that the loading at the trailing edge be zero if the shed vortices are convected with velocity U . But, apparently, the vorticity would not be zero like in the steady case, because of the vortex shedding due to the unsteady motion. In fact it is the balance of the two kinds of pressures, as discussed in the previous paragraph, that makes the loading zero, i.e.

$$\delta p(c) = -\rho U_0 \gamma(c) - \rho \frac{\partial}{\partial t} \int_0^c \gamma(\xi, t) d\xi = 0.$$

A question naturally arises: how is then the vorticity distributed in the neighbourhood of the trailing edge?

In figure 5.6 the calculated amplitude of the bound vorticity distribution from the mid-

chord to the trailing edge is shown[†]. The amplitude of vorticity distributions is scaled with $U_0 \hat{\alpha}$. It is seen that at very low reduced frequency (say, up to 0.05), the distribution qualitatively resembles that in the steady case. Only it is not zero at the trailing edge, indicating that there is a vortex shedding accompanying the unsteady motion. This, again, justifies the quasi-steady argument. However, as the reduced frequency is increased, the trend changes. Instead of decreasing, the distribution now increases upon approaching the trailing edge. The gradient ($\partial \hat{\gamma} / \partial x$) appears to increase with the reduced frequency.

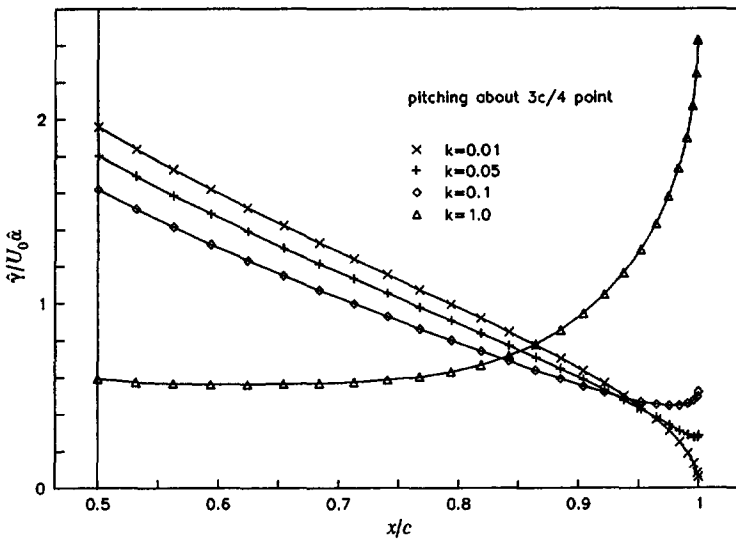


Figure 5.6 Amplitude of vorticity distribution near the trailing edge, for pitching about $3c/4$ point.

The increasing gradient of the vorticity in the x -direction implies that as the trailing edge is approached, there is an acceleration of the boundary layer on one side, and a deceleration on the other side of the plate. The situation alternates each half period of the oscillation. It is well known, on a viscous flow scale, deceleration of the boundary

[†] The singular behaviour of the vorticity distribution at the leading edge makes the scale of the complete graph so large that the distribution near the trailing edge is barely recognizable. For this reason we show only the part from mid-chord to the trailing edge.

layer flow may imply the possibility of its separation. Though potential flow theory can not answer the question as to what happens locally inside the boundary layer, this observation, in the scope of the outer flow scale, gives rise to some concern about the validity of the Kutta-Joukowski condition for oscillations at higher reduced frequencies at finite values of the amplitude of oscillation.

On account of the validity of the quasi-steady argument, it can be anticipated that the bound vorticity distribution would essentially be in phase over the major part of the chord for low reduced frequency oscillation. Near the trailing edge, some phase shift may be expected in view of the vortex shedding. The situation is not so clear when the reduced frequency is high. On the one hand the unsteadiness of the motion is stronger. On the other, bound circulation (therefore vortex shedding) is weaker. This can be clarified only with actual calculation. In figures 5.7a, b we show the phase curves of the bound vorticity ($\gamma_1 + \gamma_2$) at various reduced frequencies, for pitching oscillations about the mid-chord and the rear aerodynamic centre respectively.

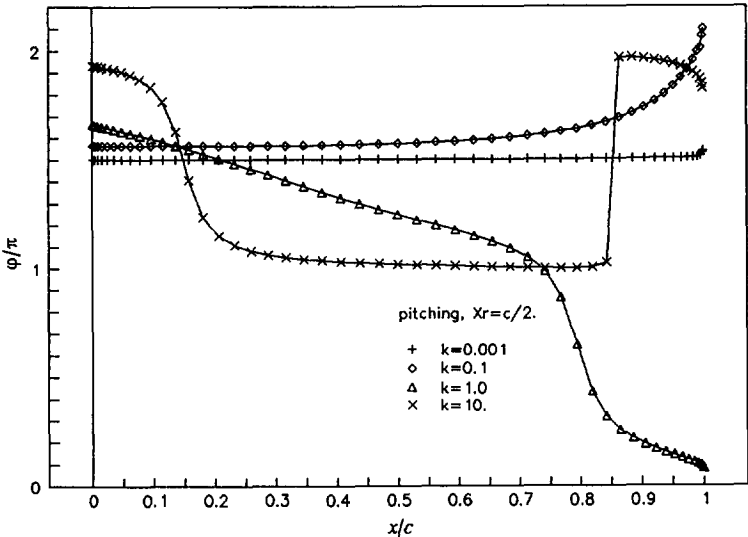


Figure 5.7a Phase curves of bound vorticity for pitching motion about mid-chord point.

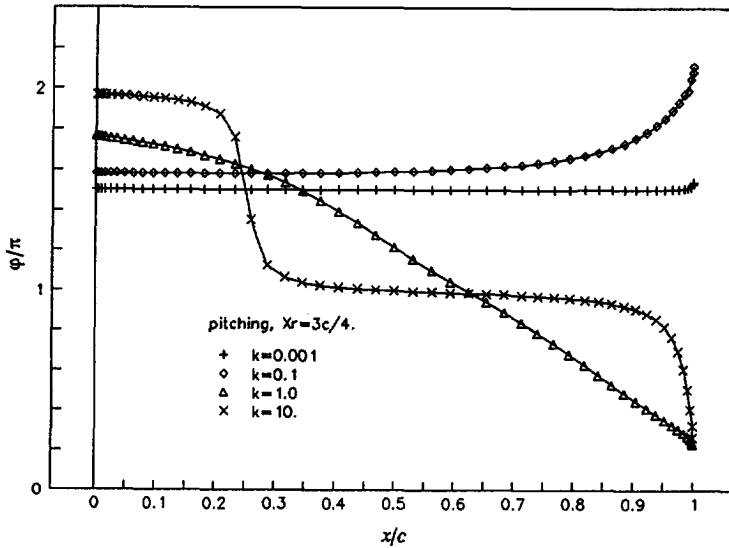


Figure 5.7b Phase curves of bound vorticity for pitching motion about $3c/4$ point.

It is clear from both of the two graphs that the phase shift shows a strong dependency on the reduced frequency. At very low reduced frequency the shift of phase angle is very much concentrated in the neighbourhood of the trailing edge as was expected. As the reduced frequency is increased the influence extends towards the leading edge. But the shift of the phase angle is still uniform along the chord generally ($k=0.1$). It ceases to be so at a moderate reduced frequency, $k=1$, say. Therefore it is reasonable to infer that it is the structure of the vortex wave which has an important influence on the aerodynamic response, since the reduced frequency can be interpreted as the wave length measured with the chord length.

It is interesting to note the peculiar behaviour of the phase angle of the vorticity distribution at high reduced frequency, $k=10$. In this circumstance, the bound vorticity appears to group itself locally along the chord, i.e. in some localized regions the vorticity is essentially in phase, while in between the regions there is a jump of π in the value of the phase angle. This jump necessarily implies a minimum in the amplitude of

the bound vorticity distribution at that locality as can indeed be seen in figure 5.8 where the amplitude curve of the distribution is displayed. Because the jump of the phase is not abrupt, the amplitude attains a small but non-zero value at the point of phase jump.

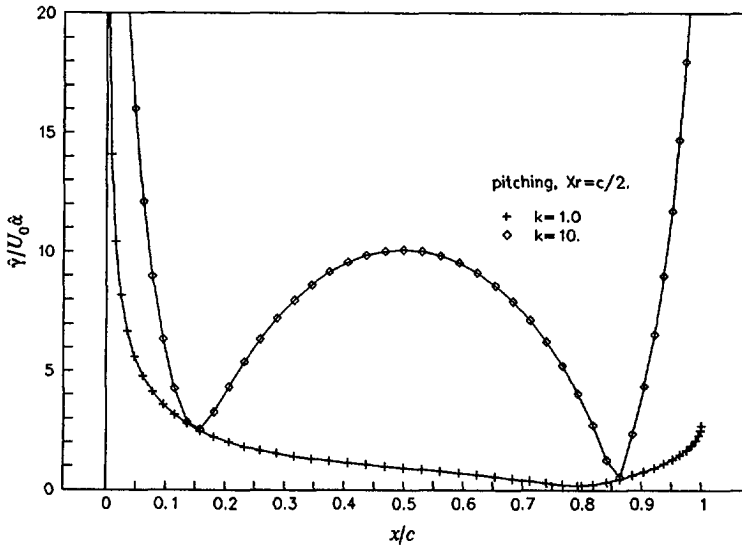


Figure 5.8 Amplitude curve of bound vorticity distribution for pitching motion about mid-chord point.

When a flat plate performs a heaving motion in an otherwise stagnant fluid, the total bound circulation is zero (though locally it is not), because of the symmetry of the flow. But the plate still experiences a force. This is the apparent mass force as mentioned earlier. The vorticity distribution at a certain moment for this motion is schematically shown in figure 5.9. It is seen that the bound vortices on the front and rear half of the plate are just in counter phase. When the plate heaves in an uniform flow parallel with its mean position, this symmetry does not exist. The Kutta-Joukowski condition enforces a vortex shedding at the trailing edge, and the flow carries the shed vortices away, so that bound circulation builds up in order that the total circulation (bound circulation and the circulation of the shed vortices) in the whole flow field is unchanged.

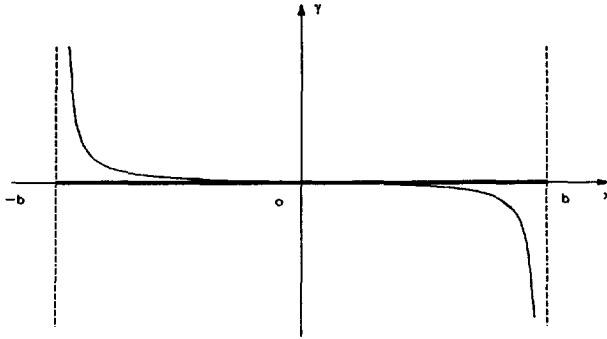


Figure 5.9 Schematic drawing of the bound vorticity distribution for a plate heaving in a stagnant fluid.

The reduced frequency can be interpreted in some other way. In view of its definition, $k = \omega c / 2U_0$, it can be written $k \sim (c/U_0)/T$, where T is the period of the oscillation. Obviously, c/U_0 is proportional to the inverse of the convection rate of the shed vorticity, and $1/T$ to the rate of its generation. Therefore, the reduced frequency can be understood as a ratio between the generation and convection rate of the shed vorticity. A small reduced frequency implies a more effective vorticity convection, while a larger one implies the converse. By high reduced frequency the shed vorticity appears to be more congested near the trailing edge in such a way that high concentration of vorticity is established at both the leading and trailing edge. Thus, the situation more resembles the case where the plate oscillates in a stagnant fluid. Comparison of figures 5.10 and 5.9 verifies this statement. In the preparation of figure 5.10, to demonstrate the effect more clearly, the reduced frequency is taken to be 100. In fact, a similar behaviour can already be observed at $k=10$.

Despite the general similarity, we see that at the trailing edge the strength of vorticity attains a finite value instead of approaching infinity as it would be in the stagnant fluid. Obviously, this is due to the Kutta-Joukowski condition imposed. It is also seen that the phase angle shifts locally at the trailing edge. On account of the anti-symmetrical distribution, it is apparent that in this mode of oscillation a major part of the force on

the plate is due to the apparent mass effect.

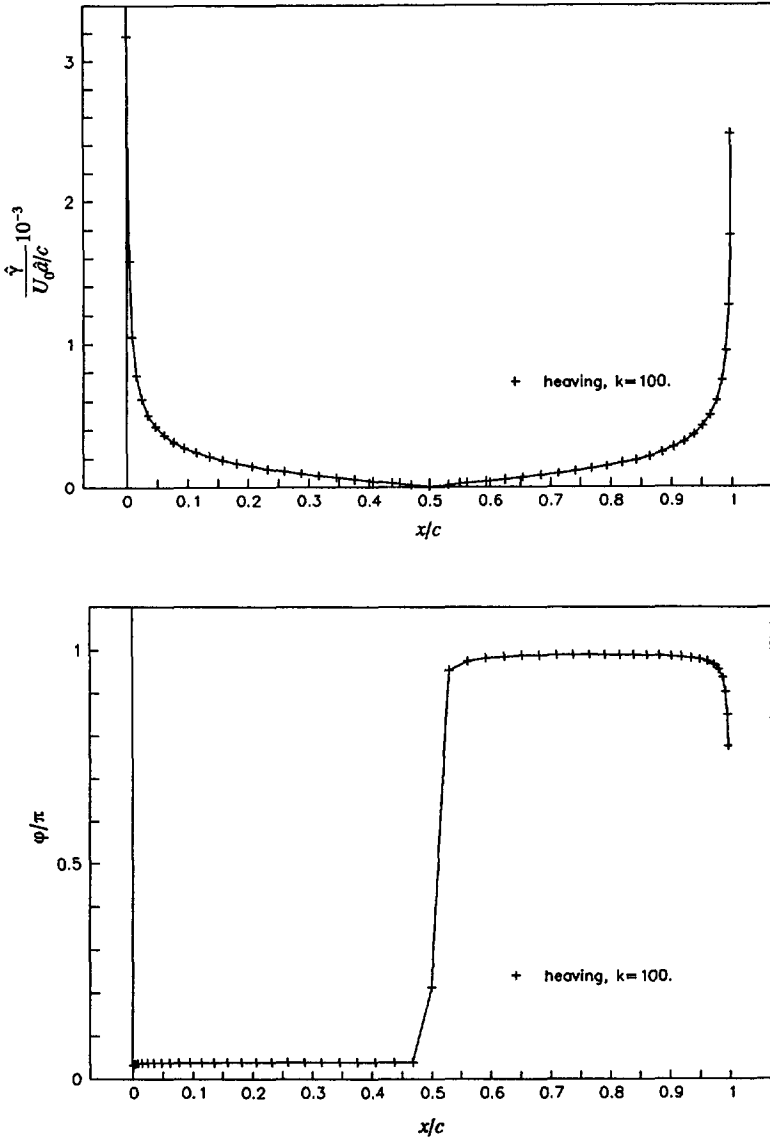


Figure 5.10 Amplitude and phase curves of bound vorticity for plate heaving in uniform flow.

5.4.4 The Perturbation Velocity in Space

The variation of bound vorticity, and the shed vortices in the wake induce an unsteady velocity perturbation in space. Conversely, the information concerning the distribution of bound and shed vortices is contained in the induced perturbation field. In line with this, we devised the experimental study as described in chapter 4. Despite of the qualitative agreement of the general features which confirm the mechanism of the theoretical modelling, discrepancies between the measured and the calculated results reveal the differences between the real physics and the theoretical model, whereupon we gain insight into the real flow. Theoretical modelling serves in this circumstance as a reference.

From a practical point of view, knowledge of the perturbation field is of interest for problems in which another airfoil is passing by in the neighbourhood of the oscillating airfoil, for instance the motion of helicopter blades, or the stabilizer of an airplane which is not very far from the wake of the main wing. In this case the following airfoil is subject to an unsteady flow field resulted from the foregoing one. The unsteady perturbation field is also interesting for certain experimental studies in unsteady aerodynamics. For instance, some of the researchers make use of the unsteady flow field induced by the shed vortices from either a cylinder or an oscillating airfoil upstream the one that is being studied (Commerford & Carta [10], Polling & Telionis [26]). The calculation of the perturbation field is of intrinsic interest itself, because it reveals some features unknown before. For details of the calculation, one is referred to Appendix G.

Shown in figures 5.11 and 5.12 are the amplitude and phase distribution of the streamwise perturbation velocity component resulted for pitching oscillations of a plate about its trailing edge for reduced frequency $k=1.0$ and 3.14 respectively. The convection velocity of the shed vortices is assumed to be $U=U_0=\text{const.}$

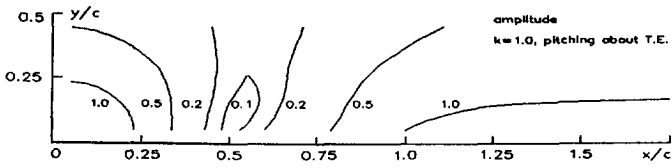


Figure 5.11a Amplitude distribution of the streamwise perturbation velocity component, $k=1.0$.

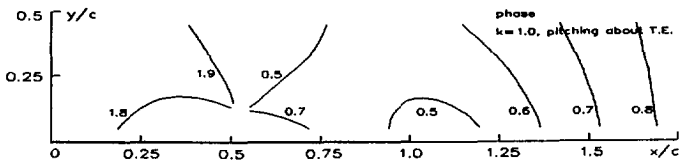


Figure 5.11b Phase distribution of the streamwise perturbation velocity component, $k=1.0$.

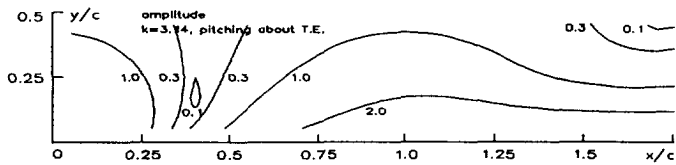


Figure 5.12a Amplitude distribution of the streamwise perturbation velocity component, $k=3.14$.

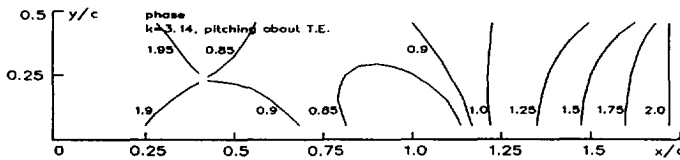


Figure 5.12b Phase distribution of the streamwise perturbation velocity component, $k=3.14$.

We notice from these figures that due to the interaction of the vorticity distributed on $y=0$, there exist a number of nodal points in space. These are the points at which the amplitude of the perturbation velocity is zero (figures 5.11a, 5.12a), and the phase angle is not resolvable (figures 5.11b, 5.12b).

Comparing figures 5.11 and 5.12, it emerges that the location of the nodal points apparently depends on the distribution of the bound vorticity and the vortex wave in the wake, in view that the difference for the two cases is only the magnitude of the reduced frequency. This can be seen more clearly in figure 5.13, for which we assume a concentrated vortex at the origin. The vortex is made to change its strength sinusoidally. Corresponding to this, we assume a vortex shedding in order to conserve the total circulation. The shed vorticity moves with an assumed velocity, so that the structure of the free vortex wave is prescribed. In this figure we observe that nodal points appear regularly in the streamwise direction, with distance of about a wave length in between. The pattern of the phase distribution becomes more regular farther downstream of the concentrated vortex, indicating that the influence of the concentrated vortex is diminishing, and what is felt locally is in fact an infinite vortex wave at $y=0$.

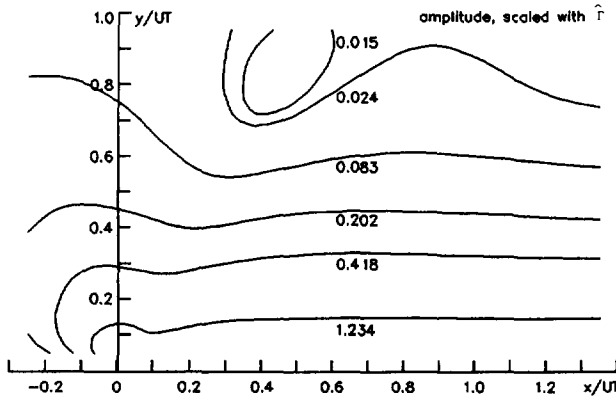


Figure 5.13a Amplitude distribution of the streamwise perturbation velocity component, concentrate vortex.

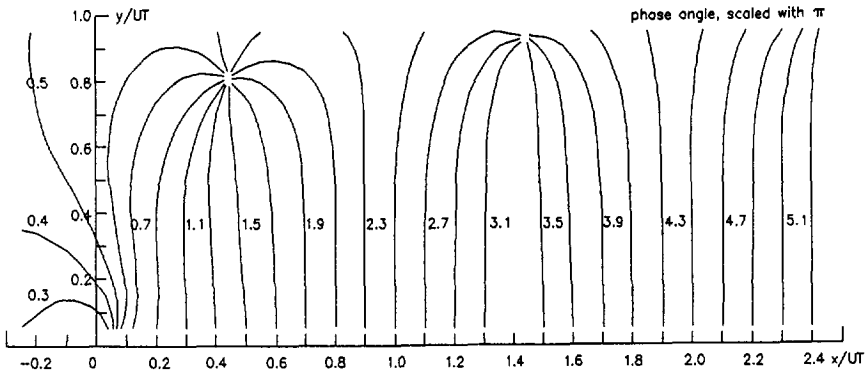


Figure 5.13b Phase distribution of the streamwise perturbation velocity component, concentrate vortex.

5.4.5 Modification due to Retardation of Vorticity Convection

In chapter 4, by comparing the measured perturbation structures with the ones calculated according to the classical theory described above, it was concluded that the convection of the shed vorticity is retarded (paragraph 4.5.2.2). It is further argued that the convection of the shed vorticity is conceived in a two-wave structure (paragraph 4.5.2.3). This is based on the observation of the systematic difference in the magnitude of the perturbation amplitude reduction between the measurement and the numerical calculation according to the classical theory. The essence of the argument is that, in view of the persistency of vorticity, the larger amount of the perturbation amplitude reduction in the experiment can only be explained by the interference of the vortex waves. The argument was verified with an artificially devised two-wave model which synthesises the perturbation due to the vortex waves of two agencies, namely, the uniform convection and the retarded convection as is the case in the present paragraph. We now proceed to calculate the part of the solution related to the inner wave.

The present paragraph must not be regarded as merely an appendix of chapter 4, however. It stands on its own right. Clearly, the retardation in shed vorticity convection would modify the memory pattern (cf. chapter2). We are interested to see what the retardation effect would be on the aerodynamic response. In the present calculation, convection velocity is assumed to be zero at the trailing edge. It develops with the increasing distance from the trailing edge, $U(x)/U_0 = 1 - (1 - B(x/c)^{1/2})^{-1}$, asymptotically approaching the uniform flow velocity. In the calculation presented here we take $B=5.6$, so that at one chord distance downstream of the trailing edge the velocity defect is recovered by about 80%.

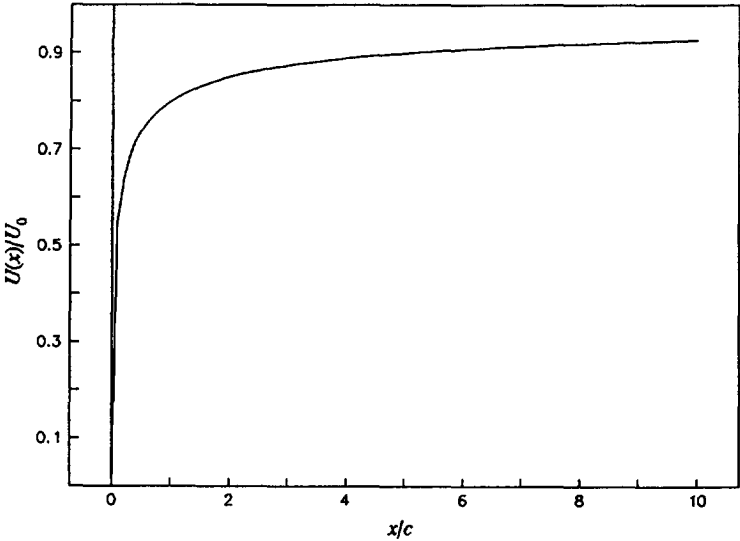


Figure 5.14 Development of the convection velocity as a function of the distance from the trailing edge.

Shown in figure 5.14 is a plot of the above mentioned velocity development as a function of the distance from the trailing edge.

The length of the wake element corresponding to the time increment δt is determined according to the velocity function with the iteration method of Newton.

To begin the discussion in this section, we point out that the symmetry as observed in paragraph 5.4.1 is also preserved in the case where convection of shed vortices is retarded. Having in mind that it is the upwash at the rear aerodynamic centre which determines the bound circulation, this is a rather straight forward consequence. For brevity, we do not show the graphs here. On the other hand, there are differences in other aspects. A pronounced one is that the bound circulation is appreciably affected by the retardation. In figure 5.15 the bound circulation is shown as a function of the reduced frequency for pitching about the $3c/4$ point, for cases of retardation and no-retardation respectively.

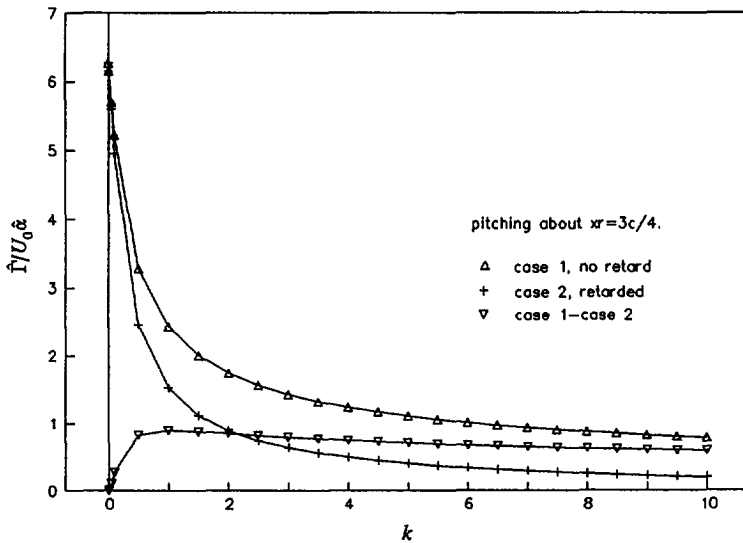


Figure 5.15 Comparison of the bound circulation amplitude.

Qualitative agreement is clear. Curves from both of the two cases behave in a similar way: with the same amplitude of oscillation, the bound circulation reduces with increasing reduced frequency, or in other words, it decreases with wave length in the wake. There is also quantitative difference, however, as is indicated by the curve with the inverted triangles (case 1-case 2). At very low reduced frequency, the differences are negligibly small. This is not difficult to understand. At lower reduced frequency the

wave length is relatively long with respect to the length scale in which the convection velocity has an appreciable growth, so that local retardation near the trailing edge (figure 5.14) does not change the wave structure much. Thus in this range of reduced frequency the retardation does not have its effect yet. Both of the two cases converge to the quasi-steady solution. The larger difference at higher reduced frequency can also be understood in line with this. But, the fact that the difference is approaching a constant in the high reduced frequency range seems to suggest that the uniform compression of the vortex wave[†] ($U=U_0=\text{const}$) and the non-uniform compression ($U=U(x)$) have different effects on the bound circulation.

Calculations were also made for the distribution of the bound vorticity. Modification to the distribution due to the retardation can be seen over the whole chord, though the general behaviour qualitatively resembles the ones for the no retardation case. The discrepancies of the results of the two cases depend on the reduced frequency. At low reduced frequency, in view of the larger convection rate with respect to that of the shedding, the perturbation due to the shed vortices is small. In this case the differences are observable mainly in the neighbourhood of the trailing edge. As the reduced frequency is increased, the difference in the convection has a more pronounced effect on the shed vorticity distribution. The results of the 'retardation' case now have larger differences from that of the no retardation case. This is in agreement with the observation made in the last paragraph. Figure 5.16 shows such an example.

In the discussion of bound vorticity distribution for uniform convection (paragraph 5.4.3), it was noticed that when a plate is heaving with higher reduced frequency, the situation is similar to the case in which it performs the same motion in a stagnant fluid. It was argued there that this is due to the inadequacy in the convection of the shed vorticity with respect to its generation at higher reduced frequency. Congestion of shed vorticity in the wake increases the vorticity at the trailing edge so that locally the

[†] By 'uniform compression' we mean that at higher reduced frequency the wave length is shortened.

situation is similar to the oscillation in a stagnant fluid. The consequence is the reduction in the total bound circulation. This interpretation is in accordance with the fact that total bound circulation decreases with increasing reduced frequency (figure 5.5).

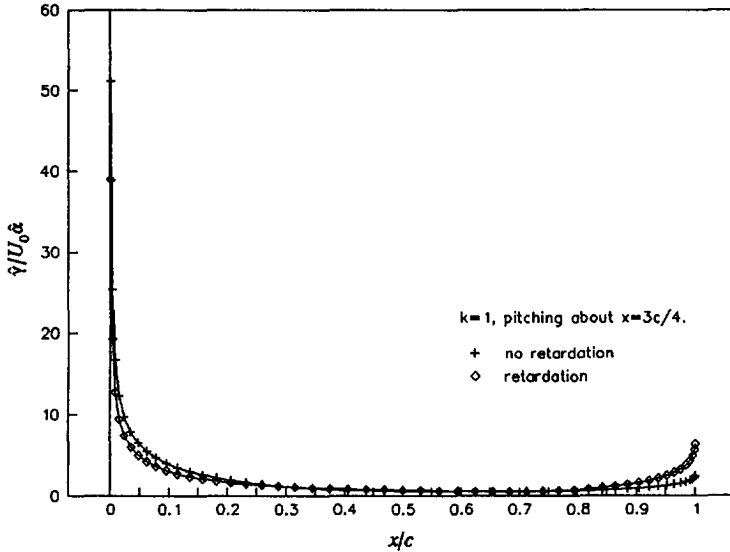


Figure 5.16 Amplitude of bound vorticity distribution for pitching about $3c/4$ point, $k=1$.

When convection of shed vorticity is retarded, in view of the Kutta-Joukowski condition ($\gamma(c)=\gamma_w$) and the behaviour of the convection function (figure 5.14) it is easy to infer that the effect explained in the paragraph above is strengthened. The very low convection velocity in the immediate neighbourhood of the trailing edge elevates the value of $\gamma(c)$, such that locally the flow appears to be even more stagnant. The statement can readily be checked by noticing figure 5.15, in terms of the global property.

To make the interpretation of local stagnation concrete, we point out here that the agreement is not only found in the global property. It is also to be found in the differential properties. In figure 5.17 are shown comparisons of amplitude and phase

angle of the bound vorticity distributions for heaving motion in retardation and no-retardation cases. The anticipation just made is clearly verified in these two graphs, both the amplitude and the phase angle of the bound vorticity distribution are more resembling those of the heaving in a stagnant fluid, as was shown in figure 5.9. The strength of vorticity does not approach infinity at the trailing edge because of the Kutta-Joukowski condition imposed there, but the retardation apparently enhances the strength of bound vorticity near the trailing edge.

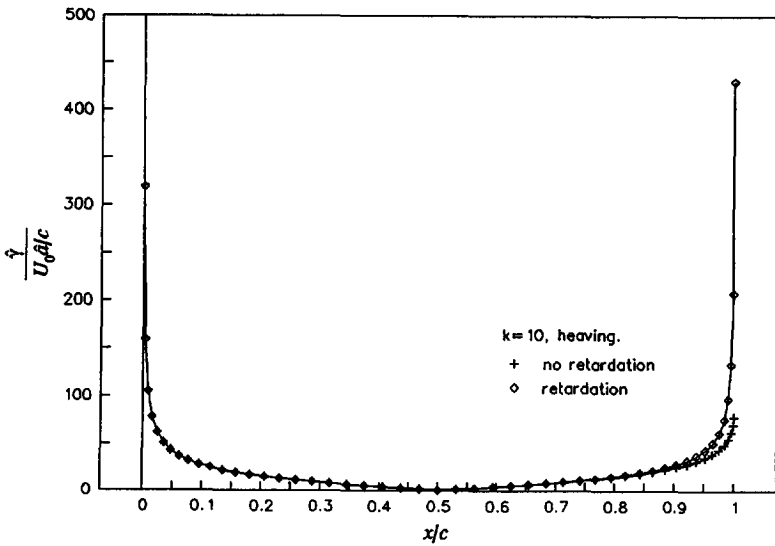


Figure 5.17a Comparison of the amplitude of bound vorticity distribution. heaving, $k=10$.

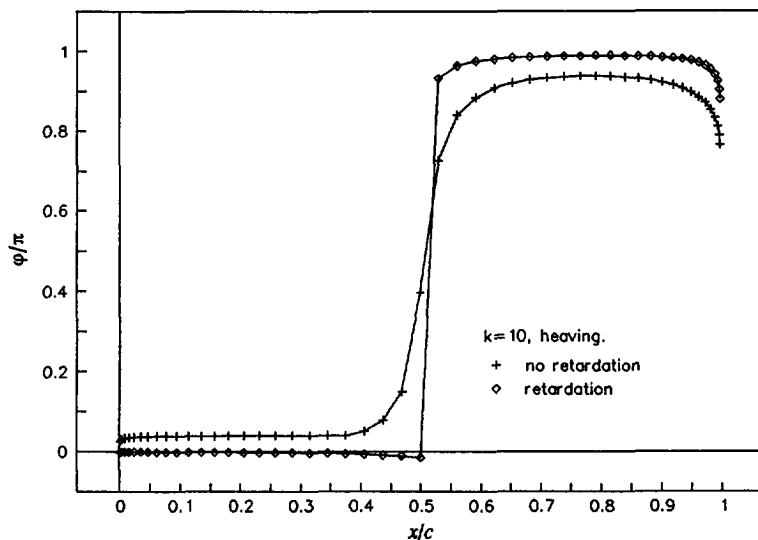


Figure 5.17b Comparison of the phase of bound vorticity distribution. Heaving, $k=10$.

5.5 Concluding Remarks

In this chapter a numerical study of the aerodynamic responses in terms of kinematics associated with the unsteady motion of an airfoil is presented. The objective is two-fold. In the first place, we elaborate the mechanism of the numerical modelling. Moreover, it serves as a reference for the numerical calculations performed in chapter 4. In the second half of this chapter the results of the numerical calculation are presented along with discussions.

The numerical study is accomplished with the vorticity distribution based panel method. Two extreme cases have been studied, namely, unsteady motion without retardation in shed vorticity convection and unsteady motion with retardation in the shed vorticity convection. In the second case the convection velocity corresponding to the centerline

velocity of the wake. The simple model used in chapter 4 for verifying the two-wave speculation is in fact a synthesis of these two. The weighting factor can be inferred from figure 4.19.

In the modelling of the case with retarded shed vorticity convection a confusing problem is encountered. The problem is namely that in view of the vanishingly small lateral dimension of the wake, it seems impossible that the shed vorticity in it would move with a velocity that is different from the mean flow velocity U_0 . The argument for this is that, if otherwise, the wake would be subject to a finite loading in the lateral direction, therefore an infinite acceleration would result on account of the infinitesimal mass per unit length of the wake, implied by its lateral dimension. This is not a trivial problem. It has been one of the arguments in objecting the retardation of the shed vorticity convection. In the present study, we argue that when concerning the convection of shed vorticity in a real flow, the wake should be viewed with the boundary layer scale. With this scale it is evident that a vortex element in the wake would have to move with the local velocity, just as a vortex element in the classical problem would have to move with velocity U_0 . In the potential scale, we argued that though the geometrical scale in the lateral direction reduced to infinitesimal, the mass remains to be finite, so that infinite acceleration due to the non-uniform convection could be avoided.

In the present study, the uniqueness of the $3/4$ chord point was demonstrated in terms of the symmetry of the bound circulation for pitching oscillation with respect to this point. For heaving motion, by scaling the bound circulation with the corresponding reduced frequency, it is shown that the development of the circulation, as a function of the reduced frequency, is identical with that of the pure pitching about the rear aerodynamic centre. This, from another aspect, confirms the unique importance of the upwash at the $3c/4$ point on the aerodynamic response.

From the observation made in the last paragraph, it is also understood that the structure of the vortex wave has a strong influence on the development of the bound circulation.

With the same strength of the upwash at the $3c/4$ point, shorter wave length (or larger reduced frequency) tends to inhibit the development of the bound circulation. The same is true also for the retardation case, only the inhibition is more severe. The mechanism of this phenomenon is revealed by the study of the bound vorticity distribution. It is found that insufficiency in shed vorticity convection leads to a situation similar to a plate oscillating in a stagnant fluid, so that the bound circulation is limited.

The bound vorticity distribution, in terms of both amplitude and phase angle, was found to vary with the reduced frequency. At lower reduced frequency it does not differ much from that in the steady case. This confirms the quasi-steady argument. At higher reduced frequency, the difference is drastic. Instead of decreasing upon approaching the trailing edge as in the steady case, the bound vorticity now increases. The gradient becomes larger with the reduced frequency. It is noticed that the positive gradient implies a flow deceleration on one side of the plate so that likely flow separation may occur at certain high reduced frequency. This might be relevant for unsteady experiments, where the amplitude is small but finite.

It is observed in the present study that, in a way, retardation in shed vorticity convection has a similar effect as short wave length by the no-retardation case. But the nonuniform vorticity convection strengthens the local stagnation effect. The bound vorticity distribution tends to be anti-symmetric about the mid-chord point for the heaving oscillation. It is observed that at the high reduced frequency range the bound circulation of the two cases approach different limits.

Velocity perturbation in space was calculated. The half-infinite vortex wave together with the bound vortex perturb the flow field so that some nodal points exist in the field. At the nodal point the amplitude of the velocity perturbation becomes zero and the phase angle is not resolvable. The distribution of the nodal points becomes regular farther away from the bound vortex, where the influence of the bound vortex is small and the vortex wave appears to be infinite. Besides these interesting features, this also has a close affiliation with the numerical modelling in chapter 4.

Chapter 6

Summary and Conclusions

The present study is directed at the investigation of the kinematics of flow associated with the unsteady motion of an airfoil. Though classical unsteady airfoil theory has been established since the 1930's and the mechanism of the problem is quite well understood, there appear to be two issues worth of further study. In the first place, the velocity of shed vorticity convection, assumed to be of the magnitude of the undisturbed uniform flow velocity in the classical theory, is arguable in view of the velocity defect in the wake. Secondly, the literature in the field of unsteady airfoil theory deals mainly with the aerodynamic loadings on the airfoil, corresponding to its unsteady motion. Having these integrated results, detailed information concerning the kinematics of the flow field is not made explicit. In the present study, we are concerned with the kinematics for two reasons. First, it plays an essential role in our experimental study of the shed vorticity convection (cf. chapter 4). Secondly, it is of intrinsic interest itself for the purpose of extending our knowledge in this field.

To study the shed vorticity convection, an experimental study has been conducted. As far as we know, this is the first attempt in this connection. Though Küssner proposed that the effect of the finite thickness of the airfoil[†] should be taken into consideration when studying the shed vorticity convection, this is still within the frame work of potential theory. The present study extends the scope by recognizing that the shed vorticity convection actually takes place within a viscous wake.

The experimental study is in itself novel in the method of approach. It consists of two parts, namely, experimental measurements and numerical calculations based on the

[†] This represents a 'potential wake' behind the airfoil, as identified in the experimental study in chapter 4.

classical theory[†], which serves as a reference. Specifically, we measured the velocity perturbation outside the wake traversing in the streamwise direction; and the corresponding numerical calculation was performed. The correctness of the numerical modelling is supported by its qualitative agreement with the measured results. By comparing quantitatively with the reference, the real physics contained in the experimentally measured results are extracted.

The numerical study described in chapter 5 is accomplished with a panel method based on vorticity distribution. The emphasis is placed upon the kinematics of the flow, in terms of the bound circulation, vorticity distribution and velocity perturbation in the space. Two limiting cases, namely, no-retardation and retardation (with wake centerline velocity) in shed vorticity convection, have been studied. For the model of nonuniform convection of the shed vorticity one encounters the problem concerning the lateral force on the wake and the application of the Kutta-Joukowski condition in a proper form. These were resolved in the present work based on physical arguments.

[†] With this, we mean that we base the mechanism of the numerical modelling on the classical theory. However, the velocity of the shed vorticity convection is in some cases different from the uniform flow velocity, U_0 , as assumed in the classical theory.

6.1 Conclusions

Vortices induce a perturbation velocity field in the flow. In the experimental study, the streamwise component of the perturbation velocity was measured. It is shown that the process of the vortex shedding accompanying the unsteady motion of an airfoil is a linear one, in terms of both additivity and homogeneity. This observation is important for the study of stability problems in the sense that experimental studies can be related to the theoretical ones by way of linear extrapolation.

Traversing in the streamwise direction shows that perturbations in the flow field are dependent on the reduced frequency, or, in other word, the structure of the vortex wave in the wake. It does not appear to be very sensitive to the Reynolds number in the range studied.

Having this observation, an experimental method was developed for the study of the convection of the shed vorticity. The streamwise component of the perturbation velocity is measured outside the wake and is compared with the corresponding numerical calculations. Qualitative agreements between the numerical results and those of experiment are observed. This confirms the correctness of the mechanism in the classical theory of Theodorsen. On the other hand, by studying the systematic discrepancies between results from the experimental measurement and the numerical calculation it is shown that the convection of the shed vorticity is retarded with respect to the uniform velocity U_0 used in Theodorsen's theory.

In the experimental study it is argued that convection of shed vorticity is effectively conceived in a kind of layered structure. Vortices in the outer layer are convected with a higher speed due to the small velocity defect in this region, while in the inner layer the convection is more retarded. The argument is supported with a simple two-wave model calculation. This observation is compatible with the triple-deck theory concerning the viscous flow structure in the near wake.

In the steady case, study of the near wake shows that, in addition to the usual viscous wake where the velocity defect and the gradients are large, there is an outer region where the corresponding quantities are substantially smaller. It is identified that this is in fact a potential non-uniformity due to the thickness of the airfoil which can be represented by a source/sink distribution along the camber line.

Numerical studies for the unsteady problems were made. The Kutta-Joukowski condition is taken in the form of smooth off-flow at the trailing edge. In the case of retarded convection of the shed vorticity a non-zero pressure difference across the infinitely thin vortex sheet might be expected on the level of potential flow. Seemingly, an infinite acceleration of the vortex sheet would result. But this is not the case. The model with retarded vorticity convection was conjectured on the following physical considerations. On the boundary layer flow scale, each vortex element would have to move with local velocity, leading to an effective retardation. On the potential flow scale, when considering the retardation effect, the mass of the wake needs to be taken into account, though the lateral dimension of the wake is vanishingly small here. In such a way, a finite pressure difference across it is allowable.

The uniqueness of the $3/4$ chord point is shown here in the sense that it is the upwash at this point that determines the development of bound circulation. It is also shown in the present study that, with the same magnitude of upwash at this point shorter wave length of the vortex wave inhibits the development of the bound circulation. This is also true for the case where convection of shed vorticity is retarded, only the non-uniform shortening of the wave length inhibits the bound circulation more severely. This is understood by studying the bound circulation. With heaving oscillation as an example, it is shown here that the shortening of the wave length (or local retardation) has the effect that the flow appears locally to be stagnant, so that the bound vorticity distribution is more antisymmetric about the mid-chord point. This, in effect reduces the total bound circulation.

Study of the bound vortex distribution near the trailing edge reveals some new features.

It is found, instead of reducing the magnitude, the bound vorticity strengthens upon approaching the trailing edge. The gradient is observed to increase with the reduced frequency. It is argued that this might have some consequence on the boundary layer flow near the trailing edge. The further implication of this may impair the validity of the Kutta-Joukowski condition above a certain reduced frequency. This is relevant to the experimental study where the amplitude is small but finite.

Calculation of the perturbation velocity in the flow field reveals some interesting features. Due to the interaction of the half-infinite vortex wave and the bound vortex a series of nodal points exist in space. At the nodal points the amplitude of the perturbation velocity becomes zero and the phase angle is not resolvable. At a larger distance from the bound vortex, its influence becomes smaller and the vortex wave appears to be infinite so that the distribution of the nodal points gets further away from the vortex sheet.

6.2 Recommendations

In the present study it is shown that convection of the shed vorticity is in fact retarded, and conceived in a kind of layered structure. A quantitative convection model is not established at this stage. In view of the practical application, further study on this would be of interest.

In view of the limited scope of the experiment, some specific recommendations can be made. In the present study, the range of Reynolds number was limited. The variation was in the same order of magnitude. To gain some insight into the Reynolds effect on the shed vorticity convection, further study which can account for a larger range of Reynolds number variation is desired.

In the present study, a symmetrical airfoil was used; the mean angle of incidence of which was zero. To generalize the research for practical interest, further study with

asymmetrical airfoil or non-zero mean angle of incidence is recommended. This would account for the vorticity convection in an airfoil dependent wake structure.

Studying the local flow structure at the trailing edge with the triple deck scales, some of the earlier researchers arrived at a global observation concerning the modification of the Kutta-Joukowski condition at the trailing edge. This observation is derived by considering the triple deck as a bulk which induces in the outer flow field a favourable pressure gradient. In the context of the layered vorticity convection hypothesis, it would be interesting to study how vortices behave in the different layers of the triple deck to accommodate the outer flow.

Appendix A.

A.1 The Velocity Components on the Boundaries in the Two Planes

From equation (2.11), we know that velocity magnitudes in the two planes are related with

$$\left| \frac{dw}{dz} \right| = \left| \frac{dw}{d\zeta} \right| \left| \frac{dz}{d\zeta} \right|, \quad (\text{A.1})$$

where z and ζ are related with the Joukowski transformation function, equation (2.9). We consider here the perturbation velocity in the two planes. On the solid boundary, where $r=b/2$, this is

$$|u-iv| = \sqrt{v_\theta^2 + v_r^2} \left| \frac{dz}{d\zeta} \right|_{r=\frac{b}{2}} = \frac{\sqrt{v_\theta^2 + v_r^2}}{|2\sin\theta|}, \quad (\text{A.2})$$

where v_θ and v_r are the tangential and radial velocity component in the ζ -plane. Conformal mapping preserves the angle which two vectors include, and scales the length of vectors uniformly. So that corresponding to velocity components u, v on the plate surface in the z -plane, we find the tangential and radial velocity component on the circle in the ζ -plane to be

$$\begin{aligned} v_\theta \Big|_{r=\frac{b}{2}} &= |u| |2\sin\theta|, \\ v_r \Big|_{r=\frac{b}{2}} &= |v| |2\sin\theta|. \end{aligned} \quad (\text{A.3})$$

A.2 Tangential Velocity Component on the Circle due to the Source-Sink Distribution

Referring to figure A.1, we proceed to calculate the tangential component of the perturbation velocity on the boundary $r=b/2$. Let a source element $q^+ d\phi b/2$ be at $(b/2, \phi)$, and a sink element $q^- d\phi b/2 = -q^+ d\phi b/2$ be at $(b/2, -\phi)$. At point P $(b/2, \theta)$ the source element will induce a velocity of magnitude

$$|dv^+| = \frac{1}{2\pi} \frac{q^+ \frac{b}{2} d\phi}{b \sin(\phi - \theta)/2}, \quad (\text{A.4})$$

and the sink element will give

$$|dv^-| = \frac{1}{2\pi} \frac{q^+ \frac{1}{2} b d\phi}{b \sin(\phi + \theta)/2}. \quad (\text{A.5})$$

Substituting equation (2.24) into equations (A.4) and (A.5), and with reference to figure A.1 we can calculate the tangential component due to this source-sink pair

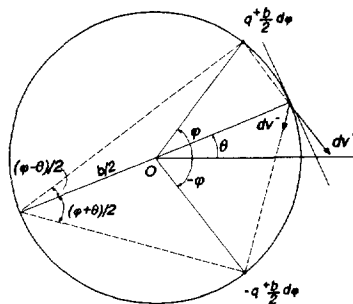


Figure A.1

$$\begin{aligned}
dv_{\theta} &= -|dv^+| \cos \frac{\varphi - \theta}{2} - |dv^-| \cos \frac{\varphi + \theta}{2} \\
&= \frac{4v_b \sin \varphi \frac{1}{2} b d\varphi}{2\pi b \sin(\varphi - \theta)/2} \cos \frac{\varphi - \theta}{2} - \frac{4v_b \sin \varphi \frac{1}{2} b d\varphi}{2\pi b \sin(\varphi + \theta)/2} \cos \frac{\varphi + \theta}{2} \\
&= -\frac{v_b \sin \varphi d\varphi}{\pi} \left(\frac{\cos(\varphi - \theta)/2}{\sin(\varphi - \theta)/2} + \frac{\cos(\varphi + \theta)/2}{\sin(\varphi + \theta)/2} \right) \\
&= \frac{2v_b \sin^2 \varphi d\varphi}{\pi(\cos \varphi - \cos \theta)}.
\end{aligned} \tag{A.6}$$

The tangential velocity component due to the source-sink distribution on the whole boundary is then

$$v_{\theta}(\theta, t) = \frac{2}{\pi} \int_0^{\pi} \frac{v_b(x, t) \sin^2 \varphi d\varphi}{\cos \varphi - \cos \theta}. \tag{A.7}$$

A.3 Tangential Velocity Component on the Circle due to a Vortex Pair

Referring to figure A.2, we calculate the tangential component of the perturbation velocity at a point P ($b/2, \theta$) on the circle.

$$v_\theta = \frac{\Gamma_0}{2\pi r_2} \cos(\varphi_2 - \theta) - \frac{\Gamma_0}{2\pi r_1} \cos(\varphi_1 - \theta)$$

$$= \frac{\Gamma_0}{2\pi} \left(\frac{r_2 \cos(\varphi_2 - \theta)}{r_2^2} - \frac{r_1 \cos(\varphi_1 - \theta)}{r_1^2} \right), \quad (\text{A.8})$$

where r_1 and r_2 can be calculated with the cosine-law

$$r_1^2 = \left(\frac{b^2}{4\xi} \right)^2 + \left(\frac{b}{2} \right)^2 - 2 \frac{b^2}{4\xi} \frac{b}{2} \cos\theta,$$

$$r_2^2 = \xi^2 + \left(\frac{b}{2} \right)^2 - 2\xi \frac{b}{2} \cos\theta. \quad (\text{A.9})$$

With the help of the two auxiliary lines in figure A.3, we observe that

$$r_1 \cos(\varphi_1 - \theta) = \frac{b}{2} - \frac{b^2}{4\xi} \cos\theta,$$

$$r_2 \cos(\varphi_2 - \theta) = \frac{b}{2} - \xi \cos\theta. \quad (\text{A.10})$$

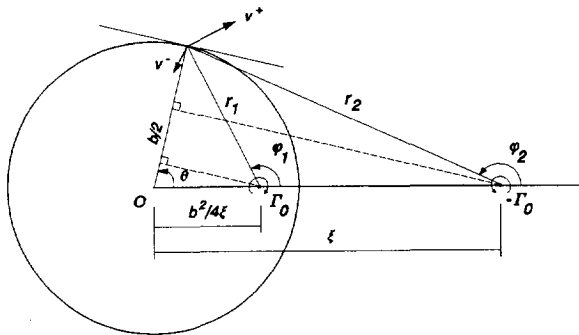


Figure A.2

Substitution of equations (A.9) and (A.10) yields

$$v_{\theta} = -\frac{\Gamma_0}{\pi b} \frac{\xi^2 - \left(\frac{b}{2}\right)^2}{\xi^2 + \left(\frac{b}{2}\right)^2 - \xi b \cos \theta}. \quad (\text{A.11})$$

Appendix B.

Derivation of the Vorticity Equation

The Navier-Stokes equation reads

$$\frac{\partial \mathbf{v}}{\partial t} + (\mathbf{v} \cdot \nabla) \mathbf{v} = -\frac{1}{\rho} \nabla p + \nu \nabla^2 \mathbf{v}. \quad (\text{B.1})$$

We recognize the vector identity

$$(\mathbf{A} \cdot \nabla) \mathbf{A} = (\nabla \times \mathbf{A}) \times \mathbf{A} + \nabla \left(\frac{1}{2} \mathbf{A}^2 \right). \quad (\text{B.2})$$

Therefore equation (B.1) can be written as

$$\frac{\partial \mathbf{v}}{\partial t} + (\nabla \times \mathbf{v}) \times \mathbf{v} + \nabla \left(\frac{\mathbf{v}^2}{2} \right) = -\frac{1}{\rho} \nabla p + \nu \nabla^2 \mathbf{v}. \quad (\text{B.3})$$

Taking curl on the two sides of equation (B.3), and denoting $\boldsymbol{\omega} = \nabla \times \mathbf{v}$, we have

$$\frac{\partial \boldsymbol{\omega}}{\partial t} + \nabla \times (\boldsymbol{\omega} \times \mathbf{v}) = \nu \nabla^2 \boldsymbol{\omega}. \quad (\text{B.4})$$

In arriving at equation (B.4), we recognized that the curl of a gradient is zero, i.e. **Curl Grad** $\phi = 0$.

$$\begin{aligned} \nabla \times (\boldsymbol{\omega} \times \mathbf{v}) &= (\mathbf{v} \cdot \nabla) \boldsymbol{\omega} - (\boldsymbol{\omega} \cdot \nabla) \mathbf{v} + \boldsymbol{\omega} (\nabla \cdot \mathbf{v}) + \mathbf{v} (\nabla \cdot \boldsymbol{\omega}) \\ &= (\mathbf{v} \cdot \nabla) \boldsymbol{\omega} - (\boldsymbol{\omega} \cdot \nabla) \mathbf{v}. \end{aligned} \quad (\text{B.5})$$

The third term on the right hand side of the first line vanishes because of the conservation of mass for incompressible flow, while the fourth term vanishes because

Div Curl $\mathbf{v}=0$. Hence we have

$$\frac{\partial \boldsymbol{\omega}}{\partial t} + (\mathbf{v} \cdot \nabla) \boldsymbol{\omega} = (\boldsymbol{\omega} \cdot \nabla) \mathbf{v} + \nu \nabla^2 \boldsymbol{\omega}, \quad (\text{B.6})$$

which in the two-dimensional case simplifies to

$$\frac{D\boldsymbol{\omega}}{Dt} = \nu \nabla^2 \boldsymbol{\omega}. \quad (\text{B.7})$$

Appendix C.

Design of the Airfoil.

The arrangement of the experiment was described in Chapter 4. Here we shall have a brief discussion on the construction of the airfoil.

In figure 4.1, it can be seen that the excitation to the flow is introduced by the oscillation of a NACA 0012 airfoil. The airfoil is driven by an exciter, whose characteristics is specified in Section 4.2. The power transmission is completed with a self-designed beam, and two piano threads ($\phi 0.2$ mm) which are clamped at the two ends of the beam, as well as the airfoil.

The airfoil was made of wood, in view of its favourable stiffness-to-weight ratio. Figure C.1 gives a top and a cross-sectional view of the airfoil. In order to reduce the mass (thus, the inertia force in the oscillation) the airfoil was made hollow. It is obvious that the moment of inertia of the cross section is not much reduced in such a way. The shaded area is made of Limba wood, and the unshaded of Balsa wood. The airfoil was made so that the fiber of the wood is in the spanwise direction. The surface is polished with celluloid lacquer.

The shaded box in the leading part of the airfoil is mean to sustain the shear force, the torque, and the bending in the in the spanwise direction. In the estimation of mechanical characteristics of the airfoil we consider only this box when the cross sectional property and the modulus are concerned. For mass distribution the other parts have also to be included.

For an uniform beam, its free vibration is described by the following equation

$$EI \frac{\partial^4 y}{\partial z^4} + m \frac{\partial^2 y}{\partial t^2} = 0, \quad (C.1)$$

where E is the modulus of elasticity, I the moment of inertia of the cross section of the beam, and m is the mass per unit length. z is in the axial direction. For the present problem, the box can be considered as a simple beam which has the frequency equation

$$\sin kL = 0, \quad (C.2)$$

here L is the length of the beam. k is defined as

$$k^4 = \frac{\omega^2 m}{EI}, \quad (C.3)$$

in which ω is the angular frequency of vibration. Solving the frequency equation, we get the frequency of the first bending mode

$$\omega_1 = \pi^2 \sqrt{\frac{EI}{mL^4}}. \quad (C.4)$$

Substitution with the proper numbers (see reference) in to equation (C.4), we estimate the first bending harmonic of the beam is about 150 Hz.

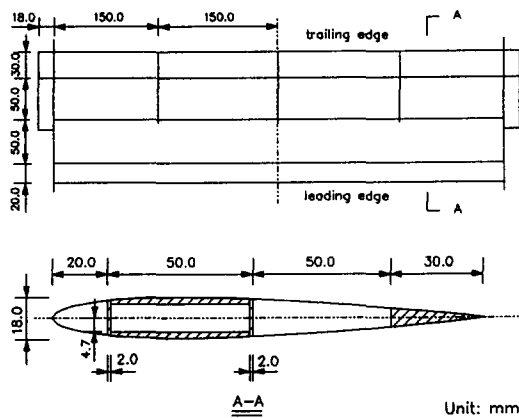


Figure C.1 Top and cross-sectional view of the airfoil.

Reference

- Abbot I.H. & von Doenhoff A.E. (1959). *Theory of Wing Sections*. Dover, New York.
- Sallenave, P. (1955). *Propriétés physiques et mécaniques de bois tropicaux de l'union Française*.

Appendix D.

The Mean Velocity in an Unsteady Wake

In Chapter 4, it is mentioned that in an unsteady wake a fluid particle with the centerline velocity takes about twice the time to reach a distance that is $\lambda/2$ behind the trailing edge than if it travels with the free stream velocity (fig. 4.19). This statement is made based on measurement of the mean velocity of two unsteady wakes. In what follows, we present the results of these two sets of measurement.

Case 1. $U_0=7.0$ m/s, $f=40$ Hz; $k=2.7$, $\lambda/2=88$ mm.

x (mm)	U_0/U_{\min}
6.6	2.70
16.6	1.79
26.6	1.55
46.6	1.37
166.6	1.16
366.6	1.10

We assume that the development of the centerline velocity, U_{\min} , follows the empirical relation

$$\frac{U_0}{U_{\min}} = 1 + \frac{C}{x^n}. \quad (\text{D.1})$$

In equation (D.1), C and n are constants to be determined with the measured data listed in the table on the left. It is found that for the given operation parameter they are

$$C=7.7, \quad n=0.8.$$

Therefore, in the present case the velocity can be described with

$$\frac{U_0}{U_{\min}} = 1 + \frac{7.7}{x^{0.8}}. \quad (\text{D.2})$$

We now consider the integration

$$\delta x = \int_0^{\lambda/2} \frac{U_0 - U_{\min}}{U_{\min}} dx, \quad (\text{D.3})$$

which is in fact the distance by which the particle with free stream velocity over-runs the one with centerline velocity, at $\lambda/2$ distance behind the trailing edge. Insert equation (D.2) into equation (D.3), it is calculated that $\delta x \approx 94$ mm, which is about the value of $\lambda/2$. This result means that particle with the free stream velocity takes about only half the time to arrive the half-wave-length distance, with respect to the time needed by the particle with centerline velocity.

In a similar way, we studied another case.

Case 2. $U_0 = 10.0$ m/s, $f = 160$ Hz; $k = 7.54$, $\lambda/2 = 31.25$ mm.

x (mm)	U_0/U_{\min}
5	2.40
15	1.71
25	1.52
55	1.32
75	1.26
105	1.20

The empirical formula is found to be

$$\frac{U_0}{U_{\min}} = 1 + \frac{3.74}{x^{0.61}}, \quad (\text{D.4})$$

upon which the over-run distance is calculated to be $\delta x \approx 36.7$ mm $\sim \lambda/2$. This leads to an observation which is consistent with what we made in case 1.

Appendix E.

Green's Identity

Observing the divergence theorem

$$\int_{\Omega} \nabla \cdot U d\Omega = - \int_A \mathbf{n} \cdot U dA, \quad (\text{E.1})$$

where Ω is a region in space, A the boundary of the region, and \mathbf{n} is the unit normal vector of A .

We define the vector U as

$$U = \phi \nabla \phi_s - \phi_s \nabla \phi, \quad (\text{E.2})$$

where ϕ is the velocity potential in Ω , and ϕ_s is the potential of a unit-strength source at point P . For two-dimensional problems, this is

$$\phi_s = \frac{1}{2\pi} \ln r, \quad (\text{E.3})$$

where r is the distance measured from P to the point at which U is to be evaluated. By the assumption of ϕ we know that $\nabla^2 \phi = 0$. If we exclude the singularity at P with a small circle A_ε , with radius ε , then in the remaining region Ω_ε we have $\nabla^2 \phi_s = 0$ since the potential of a source is a basic solution of the Laplace's equation. Making use of these, and taking divergence of equation (E.2) we find in the region Ω_ε

$$\nabla \cdot U = \nabla \phi \cdot \nabla \phi_s + \phi \nabla^2 \phi_s - \nabla \phi_s \cdot \nabla \phi - \phi_s \nabla^2 \phi = 0. \quad (\text{E.4})$$

It then follows in the region Ω_ε that

$$\int_{A+A_\varepsilon} \mathbf{n} \cdot (\phi \nabla \phi_s - \phi_s \nabla \phi) dA = - \int_{\Omega_\varepsilon} \nabla \cdot U d\Omega = 0. \quad (\text{E.5})$$

Therefore we have

$$\int_{A_\epsilon} \mathbf{n} \cdot (\phi \nabla \phi_s - \phi_s \nabla \phi) dA + \int_A \mathbf{n} \cdot (\phi \nabla \phi_s - \phi_s \nabla \phi) dA = 0. \quad (\text{E.6})$$

In the first integral on the left hand side of equation (E.6), we let $\epsilon \rightarrow 0$. Then the continuous function ϕ and $\nabla \phi$ approach their value at the point P respectively. So that in the limit we have

$$\int_{A_\epsilon} \mathbf{n} \cdot (\phi \nabla \phi_s - \phi_s \nabla \phi) dA = \phi_P \int_{A_\epsilon} \mathbf{n} \cdot \nabla \phi_s dA - \nabla \phi_P \cdot \int_{A_\epsilon} \phi_s \mathbf{n} dA, \quad (\text{E.7})$$

where the subscript P denotes the appropriate value at the point P.

Since ϕ_s is constant on the surface Ω_ϵ ($\phi_s = \ln \epsilon / 2\pi$) it can be taken outside the second integral. Then we recognize that

$$\int_{A_\epsilon} \mathbf{n} dA = 0. \quad (\text{E.8})$$

So that the second term on the right hand side of equation (E.7) vanishes. The integral in the first term is the outflux of a unit strength source. So that its value is unity. Hence we have the Green's identity

$$\phi_P = \int_A [(\mathbf{n} \cdot \nabla \phi) \phi_s - \phi (\mathbf{n} \cdot \nabla \phi_s)] dA. \quad (\text{E.9})$$

At an earlier stage ϕ_s was introduced as the potential of a unit strength source at P. But because it depends only on the distance between P and dA on the boundary A, it can also be regarded as the potential of unit strength at dA , evaluated at P. So that the first integral is in fact the potential of a source distribution on the boundary A, whose strength is the magnitude of the local normal velocity component of fluid on the boundary.

We notice that the dot product of a direction vector and the gradient of a source potential is the potential of a doublet oriented in the direction of the vector. Therefore the second integral in equation (E.9) is identified as the potential of a doublet distribution on the boundary surface A , with axis in the direction of \mathbf{n} and the strength of the local flow potential ϕ .

Appendix F.

Induced Velocity at a Collocation Point due to the Vortex Elements

In the numerical calculation, vorticity distribution, both on the plate and in the wake, is based on line segments assigned certain length. A segment with vorticity distribution on it is called a vortex element. For a bound vortex element, the strength at its two ends are to be determined, while on the segment a linear interpolation is assumed. For shed vorticity in the wake, a vortex element is assumed to have a constant strength. We shall show here the normal perturbation velocity component at the collocation points (the mid-point of a certain panel, in the present study) due to the different vortex elements.

F1. Normal Perturbation Velocity Component due to the Singular Distribution of the Bound Vorticity

In this case the vorticity distribution is described by $\gamma = A/x^{1/2}$, $0 \leq x \leq c$. It induces a perturbation velocity in the normal direction at point $(x_0, 0)$

$$v(x_0, 0) = \frac{1}{2\pi} \int_0^c \frac{A/\sqrt{x}}{x_0 - x} dx. \quad (\text{F.1})$$

With variable substitution $x = t^2$, this can easily be integrated to give

$$v(x_0, 0) = -\frac{A}{2\pi\sqrt{x_0}} \ln \left| \frac{\sqrt{x_0} + \sqrt{c}}{\sqrt{x_0} - \sqrt{c}} \right|. \quad (\text{F.2})$$

F2. Normal Perturbation Velocity Component due to the Linear Distribution of the Bound Vorticity on a Panel

With reference to the coordinate system shown in figure F.1, linear distribution of bound vorticity on a panel can be described with

$$\gamma(x,0) = \frac{\gamma_l - \gamma_r}{l} x + \frac{x_r \gamma_l - x_l \gamma_r}{l}, \quad (F.3)$$

where the subscripts l and r stand for leading and rear end of the panel, respectively. $l = x_r - x_l$, is the length of the panel. It induces a normal component of velocity at $x=0$ according to

$$v = \frac{1}{2\pi} \int_{x_l}^{x_r} \frac{\gamma(x)}{x} dx. \quad (F.4)$$

Insert (F.3) into (F.4), and integrate we have

$$v = \frac{1}{2\pi} \left(\gamma_r - \gamma_l + \frac{x_r \gamma_l - x_l \gamma_r}{x_r - x_l} \ln \left| \frac{x_r}{x_l} \right| \right). \quad (F.5)$$

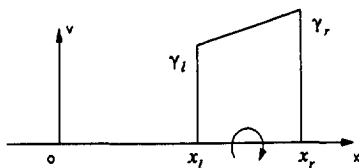


Figure F.1

It is clear that the vortex element induces at it own collocation point a normal velocity as well, if $\gamma_l \neq \gamma_r$. Noting that $x=0$ is addressed at the mid-point (the collocation point) of each of the panels, $x_l = -l/2$, $x_r = l/2$. Insert these into equation (F.5) we have $v = (\gamma_r - \gamma_l) / 2\pi$.

F3.Normal Perturbation Velocity Component due to a Wake Vortex Element

The vortex element of shed vorticity induces velocity at the collocation points in the same way, only $\gamma_r = \gamma_l = \gamma^i$ in this case. The superscript i indicates the i^{th} wake element.

$$v = \frac{\gamma^i}{2\pi} \ln \frac{x_r^i}{x_l^i}. \quad (\text{F.6})$$

Appendix G.

The Perturbation Velocity in Space

Referring to figure G.1, a vortex element $\gamma d\xi$ at $(\xi, 0)$ induces a perturbation velocity component in the x-direction at a point (x, y) as follows.

$$\begin{aligned} u &= \frac{1}{2\pi} \frac{\gamma(\xi)d\xi}{\sqrt{(x-\xi)^2+y^2}} \sin\theta \\ &= \frac{y}{2\pi} \frac{\gamma(\xi)d\xi}{(x-\xi)^2+y^2}. \end{aligned} \tag{G.1}$$

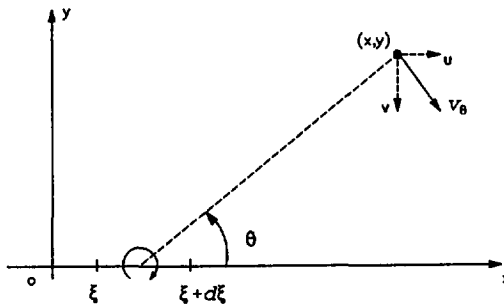


Figure G.1

Corresponding to the computational scheme in chapter 5, we consider the contribution due to the singular bound velocity, linear bound vorticity, and the shed vorticity distribution.

G.1 Induced x-wise Velocity Component due to the Singular Vorticity Distribution $\gamma = A/x^{1/2}$.

In line with equation (G.1), the perturbation velocity component in the x-direction can be written

$$\begin{aligned} u &= \int_0^c \frac{y}{2\pi} \frac{\gamma(\xi)d\xi}{(x-\xi)^2+y^2} \\ &= \frac{Ay}{2\pi} \int_0^c \frac{d\xi}{[(x-\xi)^2+y^2]\sqrt{\xi}}. \end{aligned} \quad (G.2)$$

Introducing variable substitution $\xi = t^2$, we obtain

$$\begin{aligned} u &= \frac{Ay}{2\pi} \int_0^{\sqrt{c}} \frac{2tdt}{t[(x-t^2)^2+y^2]} \\ &= \frac{Ay}{\pi} \int_0^{\sqrt{c}} \frac{dt}{x^2+y^2-2xt^2+t^4}. \end{aligned} \quad (G.3)$$

Let $x^2+y^2=r^2=B$, $-2x=C$, $1=D$, we have

$$u = \frac{Ay}{\pi} \int_0^{\sqrt{c}} \frac{dt}{B+Ct^2+Dt^4}. \quad (G.4)$$

Apparently,

$$C^2-4BD=4x^2-4(x^2+y^2)=-4y^2 \leq 0. \quad (G.5)$$

In view of equation (G.5), equation (G.3) then yields (see reference)

$$u = \frac{Ay}{4\pi Dq^3 \sin \alpha} \left(\sin \frac{\alpha}{2} \ln \frac{t^2+2qt \cos \frac{\alpha}{2} + q^2}{t^2-2qt \cos \frac{\alpha}{2} + q^2} + 2 \cos \frac{\alpha}{2} \tan^{-1} \frac{t^2-q^2}{2qt \sin \frac{\alpha}{2}} \right) \Bigg|_0^{\sqrt{c}}, \quad (G.6)$$

where

$$\begin{aligned}
 q &= \sqrt[4]{\frac{B}{D}} = \sqrt[4]{x^2+y^2} = \sqrt{r}, \\
 \cos\alpha &= -\frac{C}{2\sqrt{BD}} = -\frac{2x}{2\sqrt{x^2+y^2}} = -\frac{x}{r}, \\
 \sin\alpha &= \sqrt{1-\cos^2\alpha} = \frac{y}{r}, \\
 \sin\frac{\alpha}{2} &= \sqrt{\frac{1-\cos\alpha}{2}} = \frac{1}{\sqrt{2}} \frac{\sqrt{r-x}}{\sqrt{r}}, \\
 \cos\frac{\alpha}{2} &= \sqrt{\frac{1+\sin\alpha}{2}} = \frac{1}{\sqrt{2}} \frac{\sqrt{r+x}}{\sqrt{r}}.
 \end{aligned}$$

Substitute these into equation (G.6) and rearrange, we obtain

$$u = \frac{A}{4\sqrt{2}\pi r} \left(\sqrt{r-x} \ln \frac{c+\sqrt{2c}\sqrt{r+x}+r}{c-\sqrt{2c}\sqrt{r+x}+r} + 2\sqrt{r+x} \tan^{-1} \frac{c-r}{\sqrt{2c}\sqrt{r-x}} + \pi\sqrt{r+x} \right). \quad (G.7)$$

G.2 Induced x-wise Velocity Component due to Linear Bound Vorticity Distribution on a Panel.

Consider linear bound vorticity distribution on the i th panel

$$\gamma(x) = \frac{\gamma_{i+1} - \gamma_i}{x_{i+1} - x_i} x + \frac{x_{i+1}\gamma_i - x_i\gamma_{i+1}}{x_{i+1} - x_i}, \quad (G.8)$$

where x is measured in the coordinate system as shown in figure G.2.

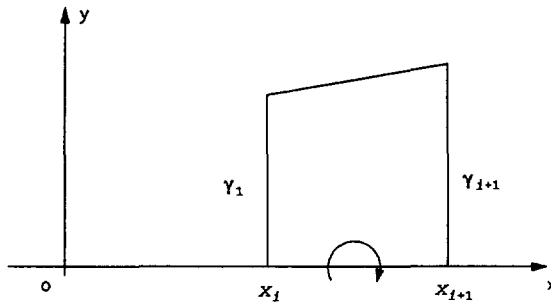


Figure G.2

In line with equation (G.1), the x-wise perturbation velocity component due to this vorticity distribution is

$$\begin{aligned} u &= \int_{x_i}^{x_{i+1}} \frac{y}{2\pi} \frac{\gamma(\xi) d\xi}{(x-\xi)^2 + y^2} \\ &= \frac{y}{2\pi} \left(\frac{\gamma_{i+1} - \gamma_i}{x_{i+1} - x_i} \int_{x_i}^{x_{i+1}} \frac{\xi d\xi}{(x-\xi)^2 + y^2} + \frac{x_{i+1}\gamma_i - x_i\gamma_{i+1}}{x_{i+1} - x_i} \int_{x_i}^{x_{i+1}} \frac{d\xi}{(x-\xi)^2 + y^2} \right). \end{aligned} \quad (G.9)$$

The second integral is standard. It yields an arctangent function. For the first integral, we introduce the variable substitution $\xi - x = t$. By doing so we have

$$\begin{aligned}
\int_{x_i}^{x_{i+1}} \frac{\xi d\xi}{(\xi-x)^2+y^2} &= \int_{x_i-x}^{x_{i+1}-x} \frac{t+x}{t^2+x^2} dt \\
&= \frac{1}{2} \int_{x_i-x}^{x_{i+1}-x} \frac{d(t^2+x^2)}{t^2+y^2} + x \int_{x_i-x}^{x_{i+1}-x} \frac{dt}{t^2+y^2} \\
&= \frac{1}{2} \ln \frac{(x_{i+1}-x)^2+y^2}{(x_i-x)^2+y^2} + \frac{x}{y} \left(\tan^{-1} \frac{x_{i+1}-x}{y} - \tan^{-1} \frac{x_i-x}{y} \right). \quad (G.10)
\end{aligned}$$

Substitute this into equation (G.9), with rearrangement, we have

$$\begin{aligned}
u &= \frac{\gamma_{i+1}}{2\pi(x_{i+1}-x_i)} \left[\frac{y}{2} \ln \frac{(x_{i+1}-x)^2+y^2}{(x_i-x)^2+y^2} + x \left(\tan^{-1} \frac{x_{i+1}-x}{y} - \tan^{-1} \frac{x_i-x}{y} \right) \right. \\
&\quad \left. - x_i \left(\tan^{-1} \frac{x_{i+1}-x}{y} - \tan^{-1} \frac{x_i-x}{y} \right) \right] \\
&\quad - \frac{\gamma_i}{2\pi(x_{i+1}-x_i)} \left[\frac{y}{2} \ln \frac{(x_{i+1}-x)^2+y^2}{(x_i-x)^2+y^2} + x \left(\tan^{-1} \frac{x_{i+1}-x}{y} - \tan^{-1} \frac{x_i-x}{y} \right) \right] \\
&\quad - x_{i+1} \left(\tan^{-1} \frac{x_{i+1}-x}{y} - \tan^{-1} \frac{x_i-x}{y} \right)]. \quad (G.11)
\end{aligned}$$

G.3 Induced x-wise Velocity Component due to Shed Vorticity Distribution.

The strength of shed vorticity is constant over each of the individual wake elements. For element i , we can write

$$\begin{aligned}
u &= \int_{x_i}^{x_{i+1}} \frac{y}{2\pi} \frac{\gamma_i d\xi}{(\xi-x)^2+y^2} \\
&= \frac{\gamma_i}{2\pi} \left(\tan^{-1} \frac{x_{i+1}-x}{y} - \tan^{-1} \frac{x_i-x}{y} \right). \quad (G.12)
\end{aligned}$$

Reference

Gradshteyn and Ryzhik, Table of Integrals, Series, and Products. Academic Press.
1980.

List of Major Symbols

A list of major symbols that appear frequently in the text is given here. In the first column the symbols are listed. In the second column the usual meaning of the symbols is described. The third column gives the dimension of the symbol, if there is any. Temporal symbols are not listed. They are defined in the text where they occur.

b	semi-chord length of an airfoil.	[L]
c	chord length of an airfoil.	[L]
C(k)	Theodorsen's function.	
F(k)	real part of the Theodorsen's function.	
G(k)	imaginary part of the Theodorsen's function.	
i	unit imaginary number. $i = -1^{1/2}$.	
k	reduced frequency. $k = \omega b / U_0$.	
L	characteristic length.	[L]
p	pressure.	[M][L] ⁻¹ [T] ⁻²
q	strength of a source/sink layer per unit length.	[L][T] ⁻¹
Re	Reynolds number.	
t	time.	[T]
T	period of oscillation.	[T]
u'	velocity fluctuation (chapters 3 and 4).	[L][T] ⁻¹
u _*	friction velocity (chapter 3). $u_* = (\tau_t / \rho)^{1/2}$.	[L][T] ⁻¹
U	time averaged streamwise velocity component.	[L][T] ⁻¹
U ₀	uniform flow velocity at infinity (assumed in i direction).	[L][T] ⁻¹
v	velocity perturbation, general velocity field (chapter 3). $\mathbf{v} = u\mathbf{i} + v\mathbf{j} + w\mathbf{k}$, reduces to $u\mathbf{i} + v\mathbf{j}$ in two-dimensional case.	[L][T] ⁻¹
v _b	normal velocity component of fluid particle in contact with a boundary surface.	[L][T] ⁻¹
V	velocity field (chapter 2). $\mathbf{V} = U_0\mathbf{i} + \mathbf{v}$.	[L][T] ⁻¹
w(z)	complex potential. $w = \phi + i\psi$.	[L] ² [T] ⁻¹

x, y, z	Cartesian coordinate system.	[L]
$Y(x, t)$	function describes the contour of a two-dimensional airfoil.	[L]
z	complex number. $z = x + iy$.	[L]
α	angle of incidence.	
γ	circulation of a vortex sheet, per unit length.	[L][T] ⁻¹
Γ	circulation. $\Gamma = \oint \mathbf{v} \cdot d\mathbf{x}$.	[L] ² [T] ⁻¹
δ	boundary layer thickness.	[L]
ζ	complex number. $\zeta = \xi + i\eta$.	[L]
λ	vortex wave length. $\lambda = U_0 T$ (assuming uniform convection velocity).	[L]
μ	coefficient of viscosity.	[M][L] ⁻¹ [T] ⁻¹
ν	kinematic viscosity. $\nu = \mu / \rho$.	[L] ² [T] ⁻¹
ξ, η	coordinates in the complex ζ -plane. dummy argument for integration.	[L]
ρ	density of fluid.	[M][L] ⁻³
ϕ	velocity potential. $\mathbf{grad} \phi = \mathbf{v}$.	[L] ² [T] ⁻¹
φ	angle, phase angle.	
ψ	stream function. $\mathbf{grad} \psi = v\mathbf{i} - u\mathbf{j}$.	[L] ² [T] ⁻¹
ω	angular frequency of oscillation.	[T] ⁻¹
ω	rotation. $\omega = \mathbf{curl} \mathbf{v}$.	[T] ⁻¹

Bibliography

- [1]. Abbott I.H. & von Doenhoff A.E. (1959). *Theory of Wing Sections*. Dover, New York.
- [2]. Ashley H. & Landahl M. (1965). *Aerodynamics of Wings and Bodies*. Addison-Wesley, Reading, Massachusetts.
- [3]. Bendat J.S. and Piersol A.G. (1971). *Random Data: Analysis and Measurement Procedures*. Wiley-Interscience.
- [4]. Bisplinghoff R.L., Ashley H. and Halfman R. (1955). *Aeroelasticity*. Addison-Wesley, Reading, Massachusetts.
- [5]. Bogucz E.A. & Walker J.D.A. (1988). *The Turbulent Near Wake at a Sharp Trailing Edge*. J.Fluid Mech., Vol. 196.
- [6]. Brown S.N. & Cheng H.K. (1981). *Correlated Unsteady and Steady Laminar Trailing edge Flows*. J.Fluid Mech., Vol. 108.
- [7]. Brown S.N. & Daniels P.G. (1975). *On the Viscous Flow about the Trailing Edge of a Rapidly Oscillating Plate*. J.Fluid Mech., Vol. 67.
- [8]. Brown S.N. & Stewartson K. (1970). *Trailing Edge Stall*. J.Fluid Mech., Vol. 42.
- [9]. Chen S.H. & Ho C.M. (1987). *Near Wake of an Unsteady Symmetric Airfoil*. J.Fluids and Structures, Vol. 1.
- [10]. Commerford G.L. & Carta F.O. (1979). *Unsteady Aerodynamic Response of a Two-dimensional Airfoil at High Reduced Frequency*. AIAA J., Vol. 12.
- [11]. Crighton D.G. (1985). *The Kutta Condition in Unsteady Flow*. Ann.Rev.Fluid Mech., Vol. 17.
- [12]. Daniels P.G. (1978). *On the Unsteady Kutta Condition*. Q.J.Mech.appl.Math. Vol. XXXI, Pt. 1.
- [13]. Fung Y.C. (1969). *An Introduction to the Theory of Aeroelasticity*. Dover, New York.

- [14]. Giesing J.P. (1966). *Nonlinear Two-dimensional Unsteady Potential Flow with Lift*. AIAA paper, No. 66-968.
- [15]. Goldstein S. (1930). *Concerning Some Solutions of the Boundary Layer Equations in Hydrodynamics*. Proc.Cambridge Phil.Soc., Vol. 26, Pt. 1.
- [16]. Greidanus J.H. (1949). *Low Speed Flutter*. J.Aeronaut.Sci. Vol. 16.
- [17]. Küssner H.G. *Non-stationary Theory of Airfoils of Finite Thickness in Incompressible Flow*. Manual on Aeroelasticity, Vol. 2, AGARD.
- [18]. Landau L.D. & Lifshitz E.M. (1959). *Fluid Mechanics*. Course of Theoretical Physics, Vol. 6, Pergamon Press.
- [19]. Melnik R.E. & Chow R. (1975). *Asymptotic Theory of Two-dimensional Trailing edge Flows*. NASA SP-347.
- [20]. Messiter A.F. (1970). *Boundary-layer Flow Near the Trailing Edge of a Flat Plate*. SIAM J.appl.Math., Vol. 18.
- [21]. Messiter A.F. (1983). *Boundary-layer Interaction Theory*. Trans.ASME, Vol. 50.
- [22]. Meyer R.E. (1983). *A View of the Triple Deck*. SIAM J.appl.Math. Vol. 43.
- [23]. Miller J.A. (1976). *A Simple Linearized Hotwire Anemometer*. J. of Fluids Engineering, Transaction of ASME.
- [24]. Milne-Thomson L.M. (1968). *Theoretical Hydrodynamics*. 5th ed. Macmillan & Co Ltd, London.
- [25]. Moran J. (1984). *An Introduction to Theoretical and Computational Aerodynamics*. John Wiley & Sons, New York.
- [26]. Polling D.R. & Telionis D.P. (1986). *The Response of Airfoils to Periodic Disturbances—The Kutta Condition*. AIAA J., Vol. 24.
- [27]. Prandtl R. & Tietjens O.G. (1957). *Applied Hydro- & Aeromechanics*. Dover, New York.
- [28]. Press W.H., Flannery B.P., Teukolsky S.A., and Vetterling W.T. (1989). *Numerical Recipes in Fortran*. Cambridge Univ.Press, Cambridge.
- [29]. Schlichting H. (1979). *Boundary Layer Theory*. 7th ed. McGRAW-HILL Book Company.

- [30]. Steketee J.A. (1975). *Lecture Note Aero II*. (in Dutch), Delft.
- [31]. Stewartson K. (1968). *On the Flow Near the Trailing Edge of a Flate Plate*. Proc.Roy.Soc., Vol. 306, Pt. A.
- [32]. Stewartson K. (1969). *On the Flow Near the Trailing Edge of a Flate Plate II*. Mathematika, Vol. 16.
- [33]. Tennekes H. & Lumley J.L. (1972). *A First Course in Turbulence*. MIT Press.
- [34]. Theodorsen Th. (1935). *General Theory of Aerodynamic Instability and the Mechanism of Flutter*. NACA Report No. 496.
- [35]. van Duivenbode E. (1988). *Numerical Solutions for Flows Past Two-dimensional Oscillating Airfoils*. (in Dutch), Master Thesis, Delft.
- [36]. von Kármán Th. & Burgers J.M. (1934). *Aerodynamic Theory*. (edited by Durand), Vol. II, Julius Springer, Berlin.

Abstract

The present study deals with the investigation of the kinematics of the flow associated with the unsteady motion of an airfoil. Though classical unsteady airfoil theory has been established since the 1930's, there appear to be at least two issues worth of further study. In the first place, the convection velocity of shed vorticity, assumed to have the value of the undisturbed uniform flow velocity in the classical theory, is debatable in view of the velocity defect in the wake. Secondly, from an aerodynamic point of view, the kinematics of the flow field is not clearly revealed in the existing literature since it is concealed in the integrated result of aerodynamic loading. These two aspects constitute the basic subject of the present study.

Aimed at the first question, an experimental study has been conducted. The experimental study consists of two parts, i.e. measurements and numerical calculations which serve as a reference for the interpretation of the experimental results. In the experiments, the velocity perturbations outside the wake are measured, and are compared with the ones obtained from numerical calculations based on the classical theory. It is concluded, from these comparisons, that the convection of the shed vorticity is appreciably retarded. It is suggested that the convection of the shed vorticity may be suitably described as a kind of two-wave structure, which is compatible with the triple-deck theory, applied to describe the viscous flow structure in the near wake. Spectral analysis of the velocity perturbation shows that the process of vortex shedding associated with the unsteady motion of the airfoil is linear.

The numerical study has been carried out with a vorticity based panel method. It focuses on the flow kinematics in terms of the bound vorticity distribution and the velocity perturbation in space, associated with the unsteady motion of the airfoil. Two limiting cases of the shed vorticity convection have been studied, namely, no-retardation and pure retardation (convection follow the centerline velocity of the wake), have been studied. The numerical study is not isolated, but serves as reference for the numerical part of the experimental study. By itself, it reveals several new features of the kinematics of the flow field.

Samenvatting

Dit proefschrift beschrijft het onderzoek naar de kinematica van de stroming om een niet stationair bewegend draagvlak. Alhoewel de klassieke theorie met betrekking tot niet stationair bewegende draagvlakken dateert van de jaren 30, zijn er tenminste twee punten die verdere studie rechtvaardigen. Ten eerste, de convectie snelheid van de afgevoerde wervels, waarvan men in de klassieke theorie aanneemt dat deze gelijk is aan de snelheid van de ongestoorde stroming, is discutabel met het oog op het snelheids defect in het zog. Ten tweede, vanuit een aerodynamisch oogpunt gezien is de kinematica van het stromingsveld niet volledig beschreven in de bestaande literatuur omdat het impliciet zit in de aerodynamische belasting. Bovengenoemde punten vormen de basis van de onderhavige studie.

Met betrekking tot het eerste punt, is een experimentele studie uitgevoerd. Deze bestaat uit twee onderdelen te weten metingen en numerieke berekeningen die dienen als een referentie voor het interpreteren van de metingen. In het experiment zijn de verstoringen van de snelheid buiten het zog gemeten en deze zijn vergeleken met berekeningen op basis van de klassieke theorie. Uit deze vergelijking is geconcludeerd dat de convectie van de afgevoerde wervels aanzienlijk is geretardeerd. Gesteld wordt dat de convectie van de afgevoerde wervels beschreven kan worden met behulp van een soort twee golven structuur vergelijkbaar met de zgn. triple-deck theorie welke wordt gebruikt voor het beschrijven van de visceuze stroming in het nabije zog. Spectraal analyse van de snelheids verstoringen laat zien dat het proces van het afvoeren van wervels van een niet stationair bewegend draagvlak lineair verloopt.

Het numerieke gedeelte is uitgevoerd met behulp van een op wervels gebaseerde panelen methode. Hierbij is de aandacht gericht op de kinematica van de stroming in termen van de gebonden wervel verdeling en de ruimtelijk snelheids verstoringen om een niet stationair bewegend draagvlak. Twee limiet gevallen van de convectie van de afgevoerde wervels zijn bestudeerd, namelijk, geen retardatie en pure retardatie (convectie met de center lijn snelheid van het zog). De numerieke studie staat niet op zichzelf maar dient als een referentie voor het numerieke gedeelte van de experimentele studie. Het laat een aantal nieuwe facetten van de kinematica van de stroming zien.

Acknowledgements

Presented here are the results of my research work during the period from October 1987 to September 1992, in the group of Theoretical Aerodynamics, Department of Aerospace Engineering, Delft University of Technology, the Netherlands. I here acknowledge my gratitude to all the people who have contributed to the completion of it.

First of all, I should like to thank dr.ir. R. Coene who directly supervised my research work during the whole period. Dr. Coene's deep physical insight, extensive knowledge, and devoted enthusiasm to science have greatly inspired me. Through daily contact with him in the past period I have learnt much--in every sense. I also appreciate Mw. Coene's non-complaining about my occupying her husband's so much time in discussing the scientific matters in the evening hours.

I wish to acknowledge my gratitude to prof. dr.ir. Steketee for his general supervision on the study. His stringency in every details has been proven beneficial for the present work, and surely will be so in my future career. I should like to thank Mw. Steketee, who has made the working atmosphere so pleasant in the later stage of the reduction, when the discussion found place at her home.

I am indebted to all the members in the Low-Speed Wind Tunnel Laboratory of the department, for their kind help in the experimental part of the work. Especially, I should like to thank ir. Wubben for making the convenient computer controlled sampling programme available, ing. Deken for his assistance in the instrumentation, and ir. Passchier for his valuable suggestions.

Finally, my thanks are extended to all the members in the Theoretical Aerodynamics group, whose enthusiasm and friendship have made my work there so pleasant. Particularly, I should like to acknowledge my thanks to my fellow research assistants: Frans de Jongh, Andy van Esch, Jan van der Heijden, and Bart Wolles.

Curriculum Vitae

The author was born in Penlai, Shandong province, China, on 20 October 1962. In 1979, he graduated from Jimei Secondary School, Fujian province, China.

In 1979, he started his study in Harbour Engineering at the Department of Civil Engineering, Dalian University of Technology (formerly known as Dalian Institute of Technology), Liaoning province, China. He graduated in 1984 with a Bachelor's degree in the direction of structural engineering. After the graduation, he studied English in Shanghai Foreign Language Institute, Shanghai, China, for a year.

In 1985, he came to the Netherlands. After an intensive course in Dutch language for four months, he started his study at the Department of Civil Engineering, Delft University. In 1987, he graduated with a *ingenieur* degree in the direction of hydrodynamics.

In the same year he joined the Theoretical Aerodynamics group, Department of Aerospace Engineering, Delft University of Technology, as a research assistant for further study for a Ph.D degree. The research work conducted during the period from 1987 to 1992 leads to this dissertation.

Presently, the author is working at Fokker Aircraft Company, the Netherlands, on Dynamics and Loads.